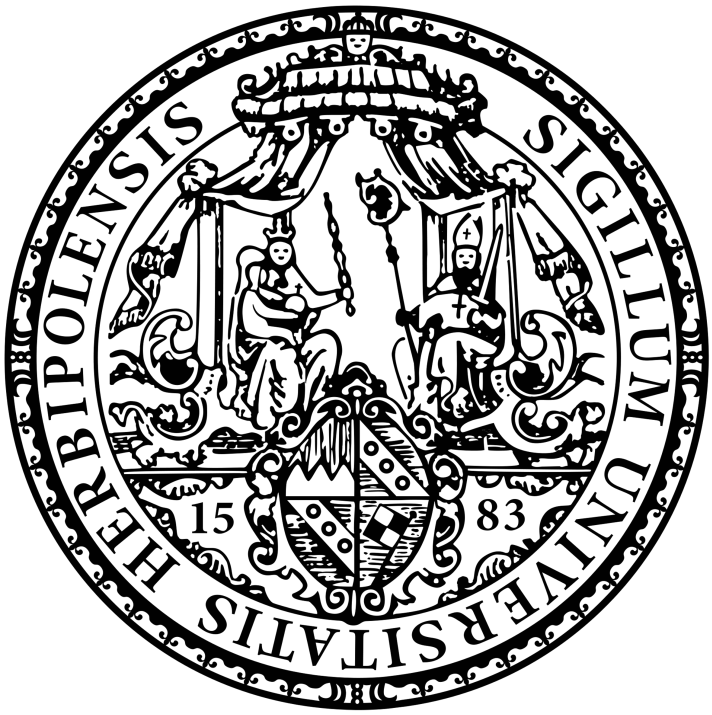

Systemic and local mechanisms of small fiber pathology in female patients with fibromyalgia syndrome

Systemische und lokale Mechanismen der Kleinfaserpathologie bei Patientinnen mit Fibromyalgie Syndrom

Doctoral thesis for a doctoral degree

at the Graduate School of Life Sciences,

Julius-Maximilians-Universität Würzburg,

Section Neuroscience

submitted by Christoph Erbacher

born in Aschaffenburg

Date of delivery: 30.06.2022

Submitted on: ……..……..

Members of the Promotionskomitee:

Chairperson: Prof. Dr. Markus Sauer

Primary Supervisor: Prof. Dr. Nurcan Üçeyler

Supervisor (Second): Prof. Dr. Christian Wegener

Supervisor (Third): Prof. Dr. Christian Stigloher

Supervisor (Fourth): Prof. Dr. Claudia Sommer

Date of Public Defence: ……..……

Date of Receipt of Certificates: …….

“The past is written, but the future is left for us to write, and we have powerful tools; openness, optimism, and the spirit of curiosity.”

-Jean-Luc Picard

Affidavit

I hereby confirm that my thesis entitled “Systemic and local mechanisms of small fiber pathology in female patients with fibromyalgia syndrome” is the result of my own work. I did not receive any help or support from commercial consultants. All sources and / or materials applied are listed and specified in the thesis.

Furthermore, I confirm that this thesis has not yet been submitted as part of another examination process neither in identical or in similar form.

_____ _____

Place, Date Signature

Eidesstattliche Erklärung

Hiermit erkläre ich an Eides statt, die Dissertation “ Systemische und lokale Mechanismen der Kleinfaserpathologie bei Patientinnen mit Fibromyalgie Syndrom” eigenständig, d.h. insbesondere selbstständig und ohne Hilfe eines kommerziellen Promotionsberaters angefertigt und keine anderen als die von mir angegebenen Quellen und Hilfsmittel verwendet zu haben.

Ich erkläre außerdem, dass die Dissertation weder in gleicher noch in ähnlicher Form bereits in einem anderen Prüfungsverfahren vorgelegen hat.

_____ _____

Ort, Datum Unterschrift

Contents

1. List of Figures and Tables

Introduction

Chapter 1

Chapter 2

2. Abbreviations

aa	amino acid
AChE	acetylcholinesterase
ACR	American College of Rheumatology
ADAM15	ADAM metallopeptidase domain 15
ADS	Allgemeine Depressionsskala
Ago2	argonaute 2
ATM	ATM serine/threonine Kinase
ATP	adenosine triphosphate
BDNF	brain derived neurotrophic factor
BMP3	bone morphogenetic protein 3
BMPR2	bone morphogenetic protein receptor 2
CCND1	cyclin D1
CCND2	cyclin D2
CDKN1A	cyclin dependent kinase inhibitor 1A
CDKN1B	cyclin dependent kinase inhibitor 1B
CholinomiRs	microRNAs regulating cholinergic transcripts
ChR2	channelrhodopsin-2
CHRNA4	cholinergic receptor nicotinic alpha 4 subunit
CHRNB2	cholinergic receptor nicotinic beta 2 subunit
CNS	central nervous system
CoC	co-culture
CPM	counts per million
ct	threshold cycle
Ctx	cholera toxin subunit B
Cx43	pore protein connexin 43
DAPI	4',6-diamidino-2-phenylindole
dCO	disease control
DE	differential expression
DGCR8	drosha–DiGeorge syndrome critical region gene 8
DTNB	5,50-dithiobis-2-nitrobenzoic acid
ECM	extracellular matrix
EIF5A	eukaryotic translation initiation factor 5A

EP300	E1A binding protein P300
ExM	expansion microscopy
FDR	false discovery rate
FIQ	Fibromyalgia Impact Questionnaire
FMS	fibromyalgia syndrome
FOXO1	forkhead box O1
GCPS	Graded Chronic Pain Scale
GO:BP	gene ontology for biological processes
hCO/CTR	healthy control
HNRNPL	heterogeneous nuclear ribonucleoprotein L
ICC	immunocytochemistry
IENF	intraepidermal nerve fiber
IENFD	intraepidermal nerve fiber density
IF	immunofluorescence
IGF1R	insulin like growth factor 1 receptor
IHC	immunohistochemistry
IL6ST	interleukin 6 cytokine family signal transducer
INSR	insulin receptor
iPSC	induced pluripotent stem cells
LDA	linear discrimination analysis
LDs	linear discrimination components
LR-White	London resin-white
MAP2K7	mitogen-activated protein kinase kinase 7
MAPK1	mitogen-activated protein kinase 1
MD	major depression
MDM2	MDM2 proto-oncogene
miR	microRNA
mRNA	messenger RNA
n.a.	not applied
ncRNA	non-coding single stranded RNA molecules
NCU	neuro-cutaneous unit
NGFR	nerve growth factor receptor
NGS	next-generation sequencing
NK	natural killer cell

NPSI	neuropathic pain symptom inventory
NR1D2	nuclear receptor subfamily 1 group D member 2
NRS	numeric rating scale
NT	neutrophil
nt	nucleotide
OD	optical density
PBMC	peripheral blood mononuclear cells
PBS	phosphate buffered saline
PCA	principal component analysis
PCs	principle components
PD	parkinson's disease
PGP9.5	protein gene product-9.5
png	portable network graphic
PNS	peripheral nervous system
PPMI	Parkinson`s Progression Markers Initiative
PRKAA1	protein kinase AMP-activated catalytic subunit alpha 1
qRT-PCR	quantitative real-time PCR
QST	quantitative sensory testing
RBC	red blood cells
RISC	RNA-induced silencing complex
RNA-seq	RNA-sequencing
ROI	region of interest
RORA	RAR related orphan receptor A
RPL13A	ribosomal protein L13a
RT	room temperature
SEM	scanning electron microscopy
SFN	small fiber neuropathy
SFP	small fiber pathology
SG	stress granule
SIM	structured illumination microscopy
SLC6A4	Solute Carrier Family 6 Member 4
SNORD	small nucleolar RNA
SOD2	superoxide dismutase 2
srAT	super-resolution array tomography

SRSF6	serine and arginine rich splicing factor 6
SSS	symptom severity scale
STX1A	syntaxin 1A
SYP	synaptophysin
SYT1	synaptotagmin 1
TBE	tris-borated buffer
TGFB1	transforming growth factor beta 1
tif	tagged image file
TRBP	transactivating response ribonucleic acid-binding protein 2
tRF	tRNA fragment
tRNA	transfer RNA
TRPV1	transient receptor potential cation channel subfamily V member 1
UPDRS	Unified Parkinson Disease Rating Scale
VN	vagus nerve
WBC	white blood cells
WGA	wheat germ agglutinin
WPI	Widespread Pain Index

3. Abstract

Fibromyalgia syndrome (FMS) is a largely heterogeneous chronic pain syndrome of unclear pathophysiology, which lacks objective diagnostics and specific treatment. An immune-related shift towards a pro-inflammatory profile is discussed at a systemic level. Small fiber pathology (SFP) and local participation of non-neuronal skin cells like keratinocytes in cutaneous nociception are potential peripheral contributors. Small RNAs, particularly microRNAs (miRs) and newly described tRNA fragments (tRFs) act as posttranscriptional key regulators of gene expression and may modulate systemic and peripheral cell pathways. On cellular level, the exact mechanisms of keratinocyte-intraepidermal nerve fiber (IENF) interaction in the skin are insufficiently understood.

Via small RNA sequencing and quantitative real-time PCR, we investigated miR and tRF signatures in whole blood cells and skin biopsy-derived keratinocytes of female FMS patients versus healthy controls. We applied gene target prediction analysis to uncover underlying cellular pathways affected by dysregulated small RNAs. Altered FMS small RNAs from blood were compared with their expression in disease controls, i.e. Parkinson`s patients and patients with major depression and chronic pain. Association of SFP with small RNAs was investigated via correlation with clinical parameter. To explore keratinocyte-nerve fiber interactions with high relevance for SFP and cutaneous nociception, we adapted a super-resolution array tomography (srAT) approach and expansion microscopy (ExM) for human skin samples. Further, we created a fully human 2D co-culture model of primary keratinocytes and induced pluripotent stem cell derived sensory neurons.

Blood miR deregulation indicated systemic modulation of immune processes exerted by CholinomiRs and by miRs targeting the FoxO signaling pathway. Short sized tRFs were associated with mRNA metabolism and splicing. This supports the hypothesis of an inflammatory/autoimmunity component in FMS. Expression of blood small RNAs in FMS were discriminative against disease controls, highlighting their potential as objective biomarker. Blood small RNAs were predominantly upregulated and correlations between miR and clinical parameter reflected rather pain in general than SFP.

In FMS keratinocytes, a downregulation of miRs and tRFs was evident. Pathways for adenosine monophosphate-activated protein kinase (AMPK), adherens junction, and focal adhesion were predicted to be affected by miRs, while tRFs may influence proliferation, migration, and cell growth. Similar to blood miRs, altered miRs in keratinocytes correlated mostly with widespread

pain and pain severity parameter. TRFs were partially associated with more severe IENF loss. Small RNAs in FMS keratinocytes may modulate pathways that define how keratinocytes interact with each other and with IENF.

These interactions include nerve fiber ensheathment, a conserved epithelial mechanism, which we visualize in human epidermis and a fully human co-culture model. Additionally, we revealed plaques of connexin 43, a pore forming protein involved in intercellular communication, at keratinocyte- nerve fiber contact sites. Objective quantification of these morphological findings in FMS and other diseases with SFP may inherit diagnostic value similar to IENF density.

We provide evidence for distinct miR and tRF signatures in FMS with implications for systemic immune regulation and local cell-cell interaction pathways. In the periphery we explored novel keratinocyte-nerve fiber interactions relevant for SFP and cutaneous nociception.

4. Zusammenfassung

Das Fibromyalgie Syndrom (FMS) umfasst ein sehr heterogenes chronisches Schmerzsyndrom mit ungeklärter Pathophysiologie, ohne objektive Diagnostik und gezielt wirkende Behandlungsmöglichkeiten. Auf systemischer Ebene wird eine entzündungsfördernde Verschiebung von Immunprozessen diskutiert. In der Peripherie stellen die Kleinfaserpathologie (SFP) und Beteiligungen nicht-neuronaler Hautzellen, beispielsweise Keratinozyten, an kutaner Nozizeption potenziell beitragende Faktoren dar. Kleine RNAs, vor allem microRNAs (miRs) und die kürzlich beschriebenen tRNA Fragmente (tRFs) agieren als posttranskriptionelle Schlüsselregulatoren der Genexpression und könnten daher systemische und periphere Zellprozesse modulieren. Die genauen zellulären Mechanismen bei der Interaktion von Keratinozyten mit intraepidermalen Nervenfasern (IENF) in der Haut sind nur unzureichend verstanden.

Mittels Sequenzierung von kleinen RNAs und quantitativer Real-Time PCR untersuchten wir miR und tRF Signaturen in Vollblutzellen und in durch Hautbiopsie gewonnene Keratinozyten von FMS Patientinnen im Vergleich zu gesunden weiblichen Kontrollen. Um zugrundeliegende Zellprozesswege aufzudecken, die von der Deregulierung kleiner RNAs betroffen sind, verwendeten wir Vorhersageprogramme für regulierte Gene. In FMS verändert vorliegende kleine RNAs im Blut verglichen wir mit ihrer Expression in Krankheitskontrollen, d.h. Parkinson Patientinnen und Patientinnen mit schwerer Depression und chronischem Schmerz. Die Beziehung zwischen SFP und kleinen RNAs wurde mittels der Korrelation mit klinischen Parametern untersucht. Zur Erforschung von Keratinozyten-Nervenfaser Interaktionen, mit großer Relevanz für SFP und kutane Nozizeption, adaptierten wir eine superauflösende Array-Tomographie (srAT) Methodik und Expansionsmikroskopie (ExM) für humane Hautproben. Außerdem entwickelten wir ein rein humanes 2D Ko-Kultur Zellmodell, bestehend aus primären Keratinozyten und sensiblen Neuronen, die aus induzierten pluripotenten Stammzellen generiert wurden.

MiR Deregulierungen in Blut wiesen auf systemische Modulierung von Immunprozessen hin, ausgeübt durch CholinomiRs und miRs, die auf den FoxO Signalweg einwirken. Die tRFs mit kurzer Fragmentlänge waren mit mRNA Metabolismus und Splicing verknüpft. Diese Ergebnisse unterbauen die Hypothese einer entzündungsfördernden/autoimmunen Komponente in FMS. Die Expression kleiner RNAs aus FMS Blut war unterschiedlich zu Krankheitskontrollen, was ihr Potenzial als objektive Biomarker hervorhebt. Kleine RNAs im

Blut waren überwiegend erhöht exprimiert und Korrelation zwischen miRs und klinischen Parametern spiegelten eher Schmerzen im Allgemeinen wider als SFP.

In Keratinozyten von FMS Patientinnen war eine Herunterregulierung von miRs und tRFs ersichtlich. Der Signalweg der Adenosinmonophosphat aktivierten Proteinkinase (AMPK), sowie Adherens Junction und Fokale Adhäsion waren prognostiziere Prozesse unter Einfluss von miRs. Ähnlich wie bei den Blut miRs, korrelierten veränderte miRs in Keratinozyten vor allem mit der Verbreitung des Schmerzes über den Körper und der Schmerzintensität. TRFs waren teilweise mit einem höheren Verlust an IENF verknüpft. Kleine RNAs in Keratinozyten von FMS Patientinnen könnten jene Prozesse modulieren, die festlegen, wie Keratinozyten miteinander und mit IENF interagieren.

Diese Interaktionen beinhalten den konservierten Mechanismus der Nervenfaserumhüllung, den wir in humaner Epidermis und einem komplett humanen Ko-Kultur Modell auflösen konnten. Zusätzlich zeigten wir Anhäufungen von Connexin 43, einem an interzellulärer Kommunikation beteiligten porenformenden Protein, an Keratinozyten-Nervenfaser Kontaktstellen. Eine objektive Quantifizierung dieser morphologischen Befunde in FMS und weiteren Erkrankungen mit SFP könnte einen diagnostischen Wert vergleichbar mit dem der IENF Dichte innehaben.

Wir liefern Belege für klare miR und tRF Signaturen in FMS mit Bedeutung für systemische Immunregulation und lokale Zell-Zell Interaktionsprozesse. In der Peripherie erkundeten wir neueartige Keratinozyten-Nervenfaser Interaktionen relevant für SFP und kutane Nozizeption.

5. Introduction

5.1. Fibromyalgia syndrome

Fibromyalgia syndrome (FMS) is a widespread chronic pain syndrome accompanied by additional symptoms such as fatigue, depression, and sleep disturbance (Häuser et al., 2008) with high prevalence, both across Europe (2.5%) and worldwide (2.7%) (Queiroz, 2013). Disease prevalence is increasing with age and women are predominantly affected (Branco et al., 2010), however, men may be underdiagnosed (Muraleetharan et al., 2018). First descriptions of FMS by Guillaume de Baillou reach back to the 16th century (Perrot, 2012). In the 19th and early 20th century, the terms 'fibrositis', 'myositis', and 'muscular rheumatism' were used to describe FMS, due to the predominant musculoskeletal origin of pain and the absence of deformation seen in joint rheumatism (Wang et al., 2015). Still, heterogeneity of symptoms and symptom severity, along with absence of pathological findings in muscular or fibrous tissue precluded diagnosis and classification. The first standardized criteria for symptom-based diagnosis were provided by a multi-disciplinary committee and was termed American College of Rheumatology (ACR) 1990 Criteria. These criteria were based on chronic widespread pain and tenderness at ≥11 out of 18 so called "tender points" (Wolfe et al., 1990) which were perceived painful upon pressure with 4 kg/cm^2. It is of note that these ACR 1990 criteria were defined for research purposes. A revision of the ACR 1990 criteria took place 20 years later, resulting in the "preliminary" 2010 ACR criteria, where the "tender point" concept was replaced by a Widespread Pain Index (WPI) and the regularly accompanying symptoms of FMS such as cognitive impairment, fatigue, unrefreshing sleep, or headache were included reflected by the Symptom Severity Scale (SSS) (Wolfe et al., 2010). The 2016 revision serve as the current "gold standard" for diagnosis with inclusion of generalized pain, reflected by pain in at least 4 of 5 body regions, as a new criterion (Wolfe et al., 2016).

The pathophysiological mechanisms underlying FMS are still largely unknown and no objective diagnostic biomarkers exist. As a consequence, no specific treatment is available, generating high socioeconomic costs and great social and psychological burden for patients and treating physicians (Spaeth, 2009, Annemans et al., 2009, Schmidt-Wilcke and Diers, 2017). Current national (Eich et al., 2017) and international (Ablin et al., 2013, Fitzcharles et al., 2013) guidelines recommend multimodal therapy approaches to relieve FMS symptoms. If non-pharmacological treatment options remain insufficient, the antidepressants amitriptyline and duloxetine, and the anticonvulsant pregabalin are commonly prescribed analgesic drugs that

can be used off-label, since no specific medication is licensed for the treatment of FMS symptoms in Europe (Kia and Choy, 2017).

Although FMS pain is mostly described as being muscular, systematic and comprehensive studies did not support a major role of muscle pathology in FMS (Simms et al., 1994, Simms, 1998). In the central nervous system (CNS), various alterations were reported when comparing FMS patients with healthy controls, including increased substance P and decreased serotonin levels in blood and cerebrospinal fluid, higher activity in sensory regions of the brain, cerebral hypoperfusion, impairment of the dopaminergic system, and regional decrease of grey matter volume (Russell, 1996, Bandak et al., 2013, Aster et al., 2022). However, only few findings were consistent between studies and might rather reflect general processes of chronic pain adaption (Schweinhardt et al., 2008, May, 2011, Sundermann et al., 2019).

In addition to the CNS, evidence is emerging for peripheral factors that may modulate FMS symptoms. Subpopulations of immune cells such as T-cells or monocytes might be involved in aberrant cytokine production, influencing symptom severity (Banfi et al., 2020, Merriwether et al., 2021) and associated autoimmune processes leading to this suspected pro-inflammatory state are discussed (Paiva et al., 2008, Buskila and Sarzi-Puttini, 2008). However, other studies found only weak associations of autoantibodies and FMS (Kötter et al., 2007, Suk et al., 2012). Numerous studies reported elevated pro-inflammatory cytokine expression, chemokines, lipid mediators, or high levels of reactive oxygen species in blood and immune cells of FMS patients compared to healthy controls (Benlidayi, 2019). However, these alterations often affected small patient subgroups, were inconsistent across studies, or did not allow functional correlations with patients` symptoms (Üçeyler et al., 2011, O'Mahony et al., 2021). A current concept of FMS proposes peripheral factors that initiate or maintain a centralized pain state (Cohen, 2017). Thus, deciphering these factors is paramount for deriving specific diagnostics and effective treatment strategies.

5.2. Small fiber pathology

One mind-changing major finding in the last decade was the functional and morphological impairment of small nerve fibers in subgroups of FMS patients (Üçeyler et al., 2013, Serra et al., 2014, Oaklander et al., 2013). A higher degree of small fiber impairment as reflected by a generalized reduction of skin innervation was associated with higher pain intensity and FMS symptom severity (Evdokimov et al., 2019). Small fiber pathology (SFP) may manifest as sensory deficits assessed via quantitative sensory testing (QST) or morphological alterations

indicated by reduced skin innervation (Devigili et al., 2008, Devigili et al., 2019). Accordingly, SFP was present in every second FMS patient (Grayston et al., 2019) implying an objective morphologic manifestation with potential relevance to FMS pathophysiology. SFP is commonly associated with small fiber neuropathy (SFN), describing a subtype of peripheral neuropathies, predominantly affecting thinly myelinated Aδ- and unmyelinated C-fibers (Lacomis, 2002), also referred to as intraepidermal nerve fibers (IENF). These IENF represent sensory nerve endings that sense and transmit noxious and thermal stimuli from the skin towards the spinal cord and ultimately to the brain (Lumpkin and Caterina, 2007). SFN can induce paresthesia and stabbing or burning pain typically in a glove and stocking pattern. SFN is categorized as acquired, hereditary, and idiopathic. Acquired SFN can arise from diabetes, drug abuse, or chemotherapy. Hereditary SFN emerges e.g. via gene variants in neuronal ion channels leading to altered excitability of small nerve fibers. In idiopathic SFN, a definite cause remains to be determined (Lauria et al., 2012). SFN diagnosis is based on patients` pain history and, after exclusion of polyneuropathy, the assessment of small nerve fibers. Although primarily associated with musculoskeletal pain, FMS patients often additionally report pain characteristics typical for SFN (Koroschetz et al., 2011). Therefore, SFP is increasingly recognized in FMS (Ghasemi and Rajabally, 2020, Grayston et al., 2019) and might represent one major peripheral factor involved in pain chronification and centralized pain state generation.

5.3. Cutaneous nociception as peripheral pain generator

Cutaneous nociception is a newly emerging concept linked to SFP that describes the contribution of the skin to pain (Stucky and Mikesell, 2021). Peripheral sensory neurons innervating the skin via small fibers have traditionally been presumed as the exclusive receivers and transducers of external stimuli. However, non-neuronal cells are increasingly recognized in cutaneous signal transduction (Denda et al., 2007). Keratinocytes are the main cell population of the epidermis and actively contribute to sensory transduction of various external stimuli of chemical, mechanical, or thermal origin, indicated by *in vitro* cell culture studies (Koizumi et al., 2004, Mandadi et al., 2009, Sondersorg et al., 2014, Moehring et al., 2018). In mice, nocifensive behavior was elicited upon specific chemical activation of keratinocyte transient receptor potential cation channel subfamily V member 1 (TRPV1) and by selective channelrhodopsin-2 (ChR2) expression and activation in keratinocytes (Baumbauer et al., 2015, Pang et al., 2015). Adenosine triphosphate (ATP) is suspected as an essential signaling molecule released by keratinocytes after chemical, mechanical, and thermal stimulation and

disruption of ATP signaling leads to deficient behavioral responses in mice (Moehring et al., 2018, Sadler et al., 2020). Vesicles, hemichannels, or gap junctions may represent complementary systems for keratinocyte ATP secretion and ATP release may be stimulus-dependent (Barr et al., 2013, Sondersorg et al., 2014, Maruyama et al., 2018). Recently, synapse-like structures were described at the keratinocyte-IENF interface via synaptophysin (SYP), synaptotagmin 1 (SYT1), and syntaxin 1A (STX1A) labeling (Talagas et al., 2020b). Further, neurite ensheathment by epidermal cells was described in model organisms such as *D. melanogaster* and *D. rerio* (O'Brien et al., 2012, Kim et al., 2012) and is also assumed in human skin (Talagas et al., 2020a). In *D. melanogaster*, ensheathment limits dendrite branching, stabilizes existing fibers and may modulate their sensitivity (Jiang et al., 2019). Due to the high conservation up to mammals, similar functions of IENF ensheathment are proposed and may be a preferential site for skin cell–nerve fiber cross talk. Investigating this communication and potential miscommunication under pathological conditions will help to better understand a range of diseases with SFP as a hallmark, including FMS.

5.4. Small RNAs as promising FMS biomarker

About 90% of the human genome is transcribed to RNA, yet only 2% contains protein coding messenger RNA (mRNA). Short non-coding single stranded RNA molecules (ncRNA), also termed small RNAs, are characterized by their size (cutoff at 200 nucleotides) and include microRNAs (miRs) and tRNA fragments (tRF) (Hombach and Kretz, 2016). Within the last decades, the role of miRs as posttranscriptional regulators of mRNA transcript levels has been established (Vishnoi and Rani, 2017) with profound implications for many diseases (Lu et al., 2008). Some studies previously reported alterations of miRs in FMS, but no robust biomarker was found yet (Cerdá-Olmedo et al., 2015, Masotti et al., 2017, Braun et al., 2020). Functions and relevance of tRFs are only beginning to unveil, but include translational repression, regulation of cell proliferation, and cellular stress response (Shigematsu et al., 2014). Therefore, pathological changes of miRs and tFRs may both explain alterations in FMS gene expression e.g. in immune or skin cells, subsequently modifying their cellular activity, but could also serve as objective biomarkers.

5.4.1. MiRs

MiRs are small ncRNA of approximately 22 nucleotide (nt) length, ubiquitously expressed across eukaryotic lineages (Bushati and Cohen, 2007). The first miR was discovered in 1993, as an endogenous regulator of genes that control developmental timing in *C. elegans*.(Lee et al., 1993)

Over the last decades, this led to the discovery of hundreds of distinct miR species in dozens of organisms, and the conclusion that nearly all mRNA transcripts and processes can be regulated by miRs (Bushati and Cohen, 2007). MiRs can derive from coding gene regions (exons), however, they are predominantly encoded in intragenic regions (introns) and are transcribed by polymerases II/III. The resulting pri-miRNA is cleaved by the Drosha–DiGeorge syndrome critical region gene 8 (DGCR8) complex within the nucleus and the processed pre-miRNA exported via Exportin-5–Ran-GTP into the cytoplasm. Then, Dicer and transactivating response ribonucleic acid-binding protein 2 (TRBP) excise the mature miR strand from the pre-miR hairpin. The mature miR enters the RNA-induced silencing complex (RISC) together with argonaute 2 (Ago2) proteins and guide RISC to silence target mRNAs by mRNA degradation or translational repression (Winter et al., 2009).

5.4.2. TRFs

Recently, a novel class of small regulatory RNAs was reported, deriving from transfer RNAs (tRNAs) (Pederson, 2010). These tRFs are much more heterogenous in length, ranging from 18-50 nt, depending on their region of origin. TRFs are thought to be involved e.g. in sequestering of RNA binding proteins, stress granule (SG) formation, repression of transposons, and miRNA-like post-transcriptional repression of mRNA (Su et al., 2020, Krishna et al., 2021). They can be grouped according to their original tRNA region (5`-tRF, 3`-tRF, i-tRF, and tRF-halves), according to the tRNA origin (mitochondrial, nuclear), or by the corresponding amino acid (aa) the parent tRNA encodes for (Loher et al., 2017). A comparison of the maturation pathways of miRs and tRFs is given in Figure 1.

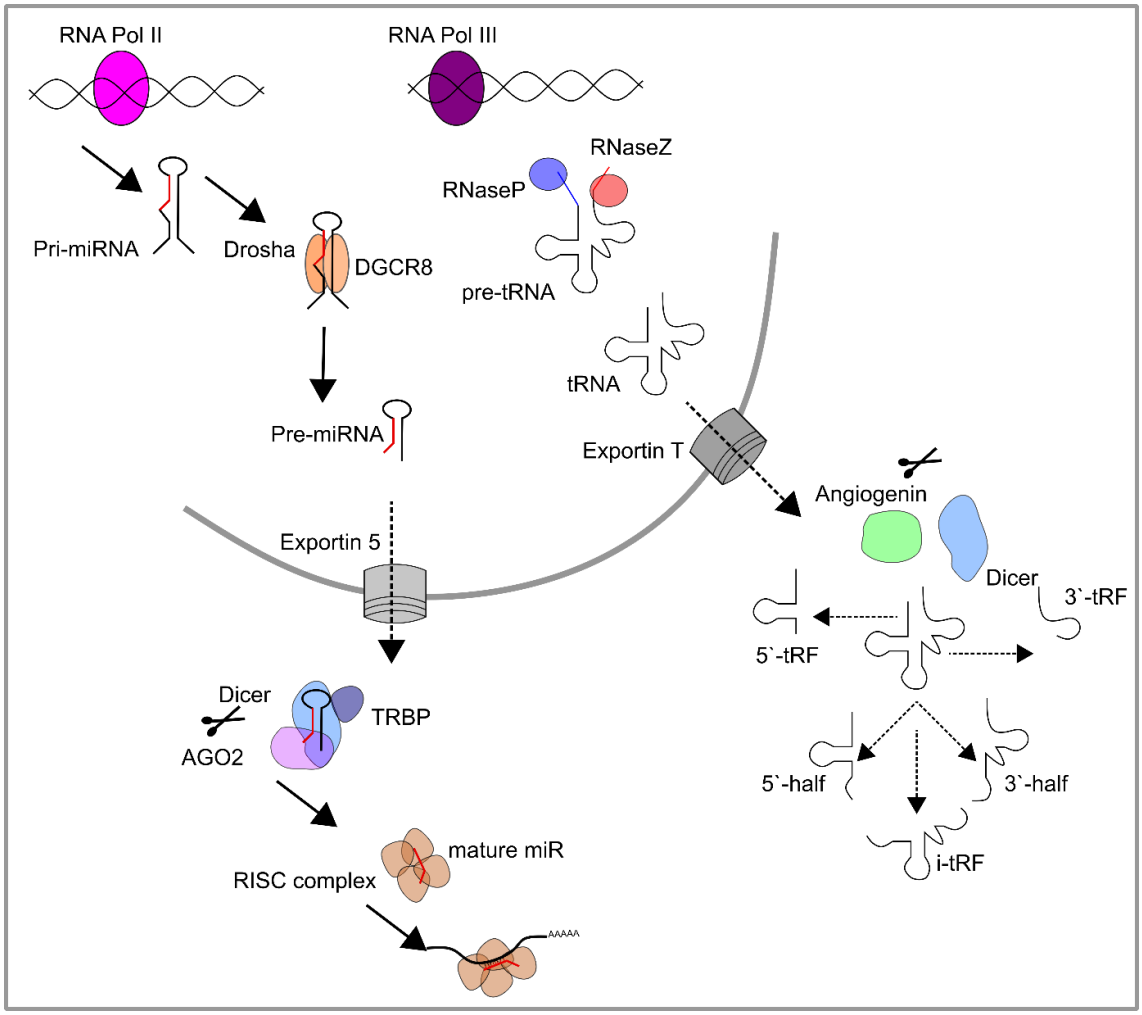

Figure 1. MiR and tRF biogenesis pathways. Pri-miRNA is synthesized primarily via RNA polymerase II, while pre-tRNAs are generated by RNA polymerase III. Pri-miRNA is further processed by DGCR8 into pre-miRNA prior to release via exportin 5 from the nucleus to the cytoplasm. RNase P and RNase Z convert pre-tRNA to mature tRNA, which is exported from the nucleus by exportin T. Within the cytoplasm, Dicer, AGO2, TRBP are required for mature miR generation. Finally, the RISC complex together with mature miR strands bind to complementary mRNA, leading to translational repression or mRNA degeneration, by partial base pairing or perfect pairing, respectively. For tRF generation, Dicer and Angiogenin enzymatic cleave mature tRNAs into different fragements, varying by their length and tRNA region, mostly 5`- and 3`-halves, 5`- and 3`-tRFs and i-tRFs. Abbreviations: AGO2, argonaut2; miR, microRNA; RISC, RNA-induced silencing complex; TRBP, transactivating response ribonucleic acid-binding protein 2; tRF, tRNA derived fragment; tRNA, transfer RNA; mRNA, messenger RNA.

5.5. Aims of the study

A large subgroup of FMS patients displays SFP characterized by neuropathic pain and skin denervation. Keratinocytes residing in the epidermis are sensory transducers that are in intimate contact with IENF. On molecular level, small RNAs modulate the gene expression of cells, including immune cells and keratinocytes. Therefore, we hypothesized:

1) Female FMS patients inherit distinct systemic (blood) and local (keratinocyte) small RNA expression signatures regulating gene expression of downstream targets.

2) Small RNAs signatures in FMS correlate with clinical parameter and SFP

3) Morphological principles of keratinocyte-IENF crosstalk can be deciphered on ultrastructural level in *ex vivo* human skin and *in vitro* via human cell culture models.

We tested these hypotheses in the following three studies, according to the outline in Figure 2. We applied small RNA sequencing for analysis of miRs and tRFs from peripheral blood and primary keratinocytes, with subsequent qRT-PCR validation of small RNAs and gene targets. Further, we performed morphological investigations of keratinocyte-nerve fiber interactions in the epidermis and a fully human 2D co-culture system at ultrastructural level.

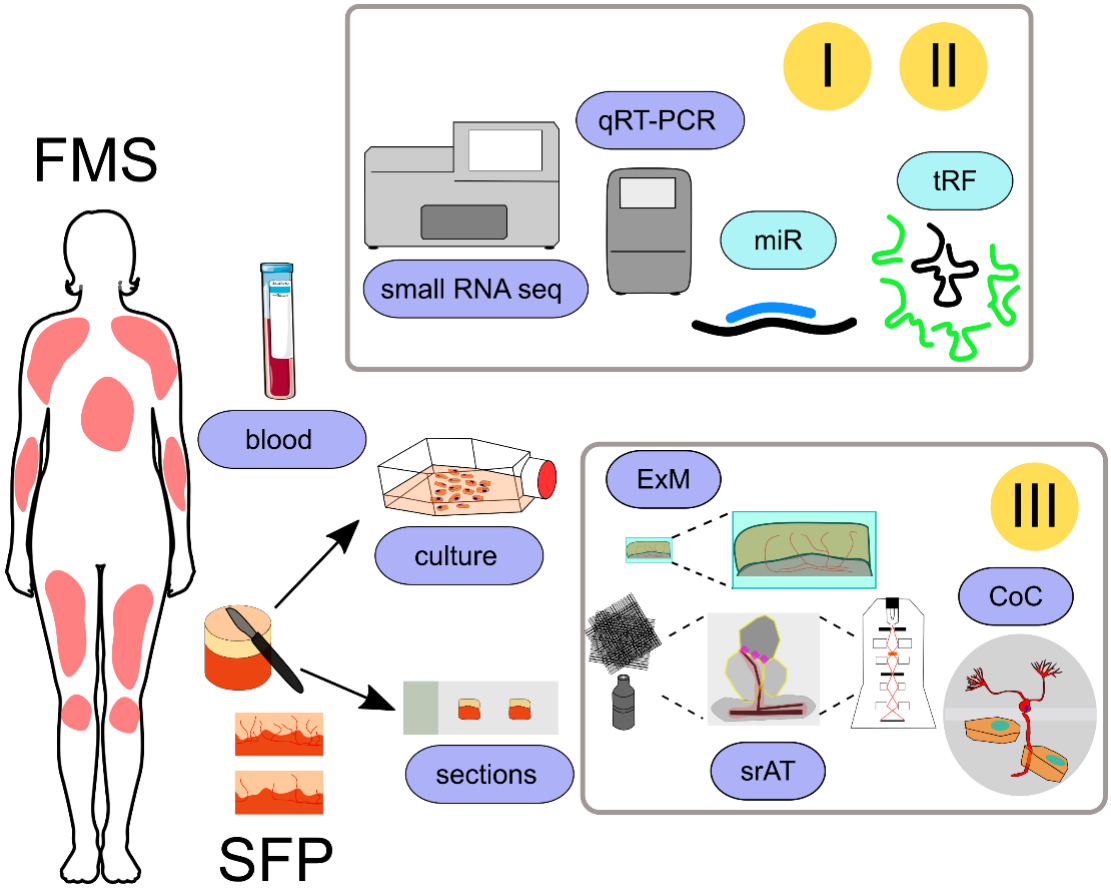

Figure 2. Graphical Outline. Skin punch biopsies from FMS and CTR were acquired for cultivation of primary keratinocyte lines and for histological tissue sections. RNA extracted from keratinocyte cultures and from whole blood, withdrawn from FMS and respective controls was analyzed via small RNA-seq and qRT-PCR (Chapter I, II). Tissue sections from healthy controls were used for super-resolution imaging via ExM and srAT and cultured keratinocytes and iPSC derived sensory neurons applied for CoC (Chapter III). Abbreviations: CoC, co-culture; ExM, expansion microscopy; FMS, fibromyalgia syndrome; iPSC, induced pluripotent stem cell; miR, microRNA; qRT-PCR, quantitative real-time PCR; RNA-seq, RNA sequencing; SFP, small fiber pathology; srAT, super-resolution array tomography.

6. Main methods overview

This section gives a short introduction into the main methods applied. The detailed information for materials and methods are given within each respective chapter.

6.1. Biomaterial acquisition

6.1.1. Blood

For analysis of systemic blood small RNA alterations, peripheral venous blood was drained from participants and collected via Tempus™ Blood RNA Tubes. Via these tubes, all cells are directly lysed and RNA is stabilized for several years, granting the advantage of a direct RNA expression snapshot (Duale et al., 2014) without the risk of introducing expression changes during cell extraction (Baechler et al., 2004). Furthermore, to minimize factors unrelated to the disease, blood was drawn in the morning after overnight fasting and subjects were instructed to restrain from heavy meals and extensive physical activity on the day before.

6.1.2. Skin tissue and primary cells

Skin punch biopsies represent a minimally invasive diagnostic technique to obtain skin tissue sections (Mangus et al., 2020) and derive primary cell lines such as keratinocytes and fibroblasts from patients and healthy study participants (Normand and Karasek, 1995). In SFN and currently discussed for FMS, the determination of the IENF density (IENFD) via immunolabeling of skin tissue sections represents an objective criterion of small fiber impairment (Egenolf et al., 2021, Evdokimov et al., 2019). Primary cell cultures and their gene expression can reveal novel insights for underlying pathologies in SFP (Evdokimov et al., 2020, Kress et al., 2021) or utilized for *in vitro* investigations of skin cell processes and interactions via skin models (Karl et al., 2019). Here, we used primary upper thigh keratinocyte cell lines for analysis of small RNA transcriptomic changes in FMS. Further, we investigated skin sections, keratinocytes, and sensory neurons differentiated from induced pluripotent stem cells all obtained from skin punch biopsies of the study participants. These preparations served to study principle keratinocyte-nerve fiber interactions *ex vivo* and *in vitro*.

6.2. RNA expression analysis

6.2.1. Quantitative real time polymerase chain reaction

Quantitative real time polymerase chain reaction (qRT-PCR) represents the most common method for detection and comparison of RNA expression levels across different samples and study groups (VanGuilder et al., 2008). The method relies on reverse transcription of RNA samples and subsequent PCR with specific primers against the transcript of interest and a

fluorescent reporter released or activated after each DNA replication step. While SYBR green-based methods rely on fluorescenct intercalation of SYBR Green I within double stranded DNA, TaqMan probes contain a fluorescent reporter that is being quenched until it is released when the reporter probe is incorporated in a new generated strand (Arikawa et al., 2008).

The ΔΔct method represents the most frequently used method for the comparison of relative gene expression (Pfaffl, 2007). First, the (fluorescence) detection threshold cycle (ct) of all samples and targets are determined. Then, subtraction of the ct from a 'endogenous control' target results in Δct values. The endogenous control must not be altered across the investigated groups. To compare consecutive experiments, Δcts from samples are subtracted from the Δct of a 'calibrator' sample run on every plate. The final ΔΔct are transposed to $2^{\wedge\text{-}(\Delta\Delta ct)}$ to receive the fold gene expression of the respective samples.

6.2.2. Small RNA sequencing

Small RNA sequencing refers to application of next-generation sequencing (NGS) for quantitative analysis with a size selection step for enrichment of short RNA species like miRs, snoRNA, piRNA, and tRFs (Giraldez et al., 2018). This can be achieved via gel-electrophoresis of total RNA or cDNA and subsequent purification of desired gel regions (Podnar et al., 2014). Several commercial NGS approaches exist, for example pyrosequencing via beads and sequencing by ligation chemistry, which are based on emulsion PCR, or sequencing by synthesis, relying on bridge PCR (Su et al., 2011). Here, the latter is used via an Illumina platform (llumina, San Diego, CA, USA) and described in more detail. First, synthesized cDNA with ligated forward and reverse adaptors is hybridized via complementary binding of the adaptor sequence. In a next step, the respective free adaptor end binds to a neighboring free complementary adaptor sequencing, thereby "bridging" the cDNA fragment. Afterwards, a polymerase synthesizes a new strand starting at the glass surface bound adaptor sequence. These bridging PCR steps are repeated in order to create clusters containing the same nucleotide sequence. Finally, these clusters provide sufficient density to record fluorescence peaks, being emitted after each step of incorporation of a new nucleotide labeled with fluorescent dyes (different for each nucleobase) during new strand generation by a polymerase (Bronner et al., 2014). The most striking difference to qRT-PCR is the simultaneous coverage of all RNAs present in a sample and measurements of total counts for each identified sequence (Liu et al., 2011).

6.3. Microscopy

6.3.1. Diffraction-limited microscopy

Phase contrast microscopy utilizes small discrepancies in the refractive index of a sample, e.g. cellular organelles and the surrounding aqueous phase. Via amplification or attenuation of the resulting wave front phases, bright and dark areas of the biological sample structures are created (Burch and Stock, 1942). Phase contrast imaging is ideal for live imaging of cultured cells, without any additional labeling of cellular components. Fluorescent labeling via antibodies directed against antigens, suitable specific toxins, or small molecules can be applied for specific detection and localization of usually not observable small cellular components, like membranes and proteins (Kuzmenkov and Vassilevski, 2018, Beutner, 1961). The fluorophores are excited by defined wavelengths and emit light on a right-shifted spectrum (Lichtman and Conchello, 2005). Immunocytochemistry (ICC) is applied in fixed cells, while immunohistochemistry (IHC) refers to immunoreaction of tissue samples (Brandtzaeg, 1998).

6.3.2. Structured illumination microscopy (SIM)

Structured illumination microscopy (SIM) represents a strategy for improvement of conventional widefield, mostly epifluorescence microscopy. Various forms of SIM have emerged. In principle, a grid is integrated within the light path, between light source and sample (Karadaglić and Wilson, 2008). Depending on the grid regime, e.g. lines or a lattice, several images are generated while the grid shifts. This results in the generation of Moiré fringes and allows discrimination of in-focus information, which is more strongly modulated by the grid, from out-of-focus information. After imaging, an algorithm processes the imprinted pattern information of the raw images to generate a refined output image (Langhorst et al., 2009). The attainable resolution underlies several factors, like grid structure, number of shifts and rotation, and subsequent processing capacities.

For example, the Zeiss Apotome (Zeiss, Oberkochen, Germany) with a simple line grid allows removal of axial out-of-focus information, resulting in quasi confocal output images (Bauch and Schaffer, 2006). More sophisticated setups like the Zeiss Elyra S.1 SIM (3DSIM), or Zeiss Lattice SIM (both Zeiss, Oberkochen, Germany) reach super-resolution defined as exceeding the light diffraction limit first described by Ernst Abbe, via determination of the origin of fluorescent light emission point, improving the resolution by a factor of 2 compared to widefield

microscopy (Wu and Shroff, 2018). This approach is suitable for a large range of applications, e.g. fluorescently labeled cell cultures or tissue sections.

6.3.3. Super-resolution array tomography (srAT)

srAT represents a correlative light and electron microscopy approach, combining the flexibility of specific immunofluorescence labeling against a variety of antigens with the ultrastructural context reflected by the electron density within a sample (Micheva and Smith, 2007). Super-resolution in this approach is achieved via three intertwined methods. Sectioning of samples in e.g. 100-nm consecutive sections defines a 100-nm axial (z) resolution. Lateral (x, y) resolution is improved for light microscopy by application of SR-SIM (Markert et al., 2016). Additionally, scanning electron microscopes (SEM) rely on electrons instead of photons as carrier of localization information, which possess much lower wave lengths and allow a lateral resolution of ~1 nm (Begemann and Galic, 2016). Therefore, this approach is ideal for determination of cellular interactions, co-localization and morphological properties in dense tissue with small sized cellular extensions, like IENF in the epidermis.

6.3.4. Expansion microscopy (ExM)

ExM represents a super-resolution imaging method based on immunofluorescence labeling. However, instead of improving the localization accuracy via elaborate microscope techniques, the biological samples are incorporated into a gel matrix and subsequently enlarged by gel swelling via water (Wassie et al., 2019). Diverse protocols for sample preparation and gel composition are currently developed allowing a factor of 4-20x enlargement of various specimens, while the ratio of label density, fluorescence retention, and preservation of isometric swelling determine the maximal magnification (Faulkner et al., 2020). ExM achieves super-resolution microscopy at standard widefield microscope setups and resolution can be further improved by using microscope based super-resolution approaches like SR-SIM.

7. Manuscripts

7.1. Chapter I: Distinct CholinomiR Blood Cell Signature as a Potential Modulator of the Cholinergic System in Women with Fibromyalgia Syndrome

Distinct CholinomiR Blood Cell Signature as a Potential Modulator of the Cholinergic System in Women with Fibromyalgia Syndrome

Christoph Erbacher[1], Shani Vaknine [2,3], Gilli Moshitzky [2,3], Sebastian Lobentanzer[4,†], Lina Eisenberg[2,3], Dimitar Evdokimov[1], Claudia Sommer[1], David S. Greenberg[2,3], Hermona Soreq[2,3,‡], Nurcan Üçeyler [1,*,‡*]

[1]Department of Neurology, University of Würzburg, 97080 Würzburg, Germany

[2] The Edmond & Lily Safra Center for Brain Sciences, The Hebrew University of Jerusalem, Jerusalem 9190401, Israel

[3]The Alexander Silberman Institute of Life Sciences, The Hebrew University of Jerusalem, Jerusalem 9190401, Israel

[4]Department of Pharmacology, College of Pharmacy, Goethe University, 60438 Frankfurt am Main, Germany

[†] Current address: Faculty of Medicine, Heidelberg University Hospital, Institute for Computational Biomedicine, Heidelberg University, 69120 Heidelberg, Germany

[‡] These authors contributed equally to this work.

Published in

Cells 2022, 11(8), 1276; https://doi.org/10.3390/cells11081276

April 9, 2022

cells

MDPI

Article

Distinct CholinomiR Blood Cell Signature as a Potential Modulator of the Cholinergic System in Women with Fibromyalgia Syndrome

Christoph Erbacher [1], Shani Vaknine [2,3], Gilli Moshitzky [2,3], Sebastian Lobentanzer [4,†], Lina Eisenberg [2,3], Dimitar Evdokimov [1], Claudia Sommer [1], David S. Greenberg [2,3], Hermona Soreq [2,3,‡] and Nurcan Üçeyler [1,*,‡]

[1] Department of Neurology, University of Würzburg, 97080 Würzburg, Germany; erbacher_c@ukw.de (C.E.); d_evdokimov@yahoo.de (D.E.); sommer@uni-wuerzburg.de (C.S.)
[2] The Edmond & Lily Safra Center for Brain Sciences, The Hebrew University of Jerusalem, Jerusalem 9190401, Israel; shani.vaknine@mail.huji.ac.il (S.V.); gilli.moshitzky@mail.huji.ac.il (G.M.); lina.eisenberg@mail.huji.ac.il (L.E.); david.greenberg1@mail.huji.ac.il (D.S.G.); hermona.soreq@mail.huji.ac.il (H.S.)
[3] The Alexander Silberman Institute of Life Sciences, The Hebrew University of Jerusalem, Jerusalem 9190401, Israel
[4] Department of Pharmacology, College of Pharmacy, Goethe University, Max-von-Laue-Str. 9, 60438 Frankfurt am Main, Germany; sebastian.lobentanzer@uni-heidelberg.de
* Correspondence: ueceyler_n@ukw.de; Tel.: +49-931-201-23542
† Current address: Faculty of Medicine, Heidelberg University Hospital, Institute for Computational Biomedicine, Heidelberg University, Im Neuenheimer Feld 267, 69120 Heidelberg, Germany.
‡ These authors contributed equally to this work.

check for updates

Citation: Erbacher, C.; Vaknine, S.; Moshitzky, G.; Lobentanzer, S.; Eisenberg, L.; Evdokimov, D.; Sommer, C.; Greenberg, D.S.; Soreq, H.; Üçeyler, N. Distinct CholinomiR Blood Cell Signature as a Potential Modulator of the Cholinergic System in Women with Fibromyalgia Syndrome. *Cells* **2022**, *11*, 1276. https://doi.org/10.3390/cells11081276

Academic Editor: Ángel A. Núñez

Received: 28 February 2022
Accepted: 6 April 2022
Published: 9 April 2022

Publisher's Note: MDPI stays neutral with regard to jurisdictional claims in published maps and institutional affiliations.

Abstract: Fibromyalgia syndrome (FMS) is a heterogeneous chronic pain syndrome characterized by musculoskeletal pain and other key co-morbidities including fatigue and a depressed mood. FMS involves altered functioning of the central and peripheral nervous system (CNS, PNS) and immune system, but the specific molecular pathophysiology remains unclear. Anti-cholinergic treatment is effective in FMS patient subgroups, and cholinergic signaling is a strong modulator of CNS and PNS immune processes. Therefore, we used whole blood small RNA-sequencing of female FMS patients and healthy controls to profile microRNA regulators of cholinergic transcripts (CholinomiRs). We compared microRNA profiles with those from Parkinson's disease (PD) patients with pain as disease controls. We validated the sequencing results with quantitative real-time PCR (qRT-PCR) and identified cholinergic targets. Further, we measured serum cholinesterase activity in FMS patients and healthy controls. Small RNA-sequencing revealed FMS-specific changes in 19 CholinomiRs compared to healthy controls and PD patients. qRT-PCR validated miR-182-5p upregulation, distinguishing FMS patients from healthy controls. mRNA targets of CholinomiRs bone morphogenic protein receptor 2 and interleukin 6 signal transducer were downregulated. Serum acetylcholinesterase levels and cholinesterase activity in FMS patients were unchanged. Our findings identified an FMS-specific CholinomiR signature in whole blood, modulating immune-related gene expression.

Keywords: fibromyalgia syndrome; cholinergic system; CholinomiRs; microRNA; miR-182-5p; Parkinson's disease

1. Introduction

Fibromyalgia syndrome (FMS) is a clinically heterogeneous chronic pain syndrome with a high global prevalence of approximately 2.7% [1,2]. FMS is frequently associated with somatic and mental co-morbidities accompanying predominantly musculoskeletal pain [3]. Adult women are primarily affected, but men may be underdiagnosed [4]. The pathophysiology of FMS remains incompletely understood, and no reliable biomarkers are

available, resulting in insufficient diagnostics and treatment [5]. Systemic pro-inflammatory profiles [6,7] and (sub-)clinical autoimmunity [8,9] are among the etiological factors discussed. FMS may aggregate in families and single nucleotide polymorphisms, e.g., in serotonin transporter genes (SLC64A4), the transient receptor potential vanilloid channel 2 gene (TRPV2), or mitochondrial genes, which have been associated with FMS symptoms; however, overall small sample sizes hamper conclusions on an individual patient basis [10,11]. Immune dysregulation based on genetic risk factors, e.g., in mitochondrial genes, may trigger peripheral neuro-inflammatory processes, which, in turn, can induce central and peripheral pain symptoms, and the process may be further enhanced by positive feedback loops between these components [12]. Of note, small nerve fiber degeneration is a common feature in FMS [13,14].

Regarding the autonomic nervous system, higher sympathetic and lower parasympathetic activity was proposed in FMS [15]. Accordingly, FMS patients often suffer from symptoms such as constipation or irritable bladder or bowel syndrome [3,16,17]. A major cholinergic regulator of parasympathetic function is the vagus nerve (VN), which innervates smooth muscles, the gastro-intestinal tract, the heart, and, importantly, immune cells within the spleen [18]. The VN interlinks local and systemic immune processes between the CNS and PNS [19–21], and immune cells also express all of the necessary components of the cholinergic machinery [22]. Together, cholinergic mechanisms play an important role in the regulation of cytokines and antibody production [23,24], thereby modulating inflammatory processes with potential implications for FMS pathophysiology and severity [25,26].

In line with the clinical heterogeneity of FMS, experimental assessment of immune correlates such as cytokine transcription or protein levels provide highly variable data, which often leads to conflicting results between different study cohorts [27,28]. Here, we investigated microRNAs (miRs) expression patterns in FMS, since these small RNAs act as posttranscriptional regulators in health and disease [29,30]. Importantly, miRs from blood can be easily obtained, serving as potential biomarkers, but also represent direct modulators in pain conditions [31]. We focused specifically on CholinomiRs, a class of miRs regulating the cholinergic system. Each CholinomiR may target five or more cholinergic mRNA transcripts, thereby modulating key processes that underlie inflammation, physiological stress, and anxiety [32–34].

We hypothesized that the dysregulation of the systemic cholinergic system is a potential causal element of FMS pathophysiology with an impact on inflammation processes in these patients. To test this hypothesis, we carried out small RNA-sequencing (RNA-seq) and quantitative real-time PCR (qRT-PCR) validation, followed by cholinergic mRNA target analysis and cholinesterase activity measurements in blood samples from FMS patients in comparison to healthy controls. Further, we compared the resultant FMS miR signature to those of patients suffering from Parkinson's disease (PD)-related pain as disease controls.

2. Materials and Methods

2.1. Study Participants and Biomaterial Collection

Figure 1 provides a synopsis of all study participants, the biomaterial used, and the experiments performed. Forty-nine female FMS patients and twenty-five age- and sex-matched healthy controls were part of a previously characterized cohort [35]. Briefly, FMS patients were recruited according to the 1990 and 2010 diagnostic criteria of the American College of Rheumatology (ACR), and all participants underwent complete neurological examination at the Department of Neurology, University of Würzburg. The study was approved by the Ethics Committee of the University of Würzburg Medical Faculty (#121/14), and all study participants gave written informed consent. For assessment of pain levels and pain-related impairment, the Graded Chronic Pain Scale (GCPS) was applied [36]. Mean pain intensity within the last six months was recorded on an 11-point numeric rating scale (NRS) with 0 = no pain and 10 = worst pain, defined as NRS_{Pain}. Furthermore, patients were stratified for their subjective degree of pain-associated impairment of daily life activities, which were also rated on the NRS with 0 = normal life activities and 10 = no daily life

activities possible, defined as $NRS_{Daily\ life}$. Hereby, we defined $NRS_{Daily\ life}$ 0–2 as "mildly impaired" and NRS 3–10 as "severely impaired".

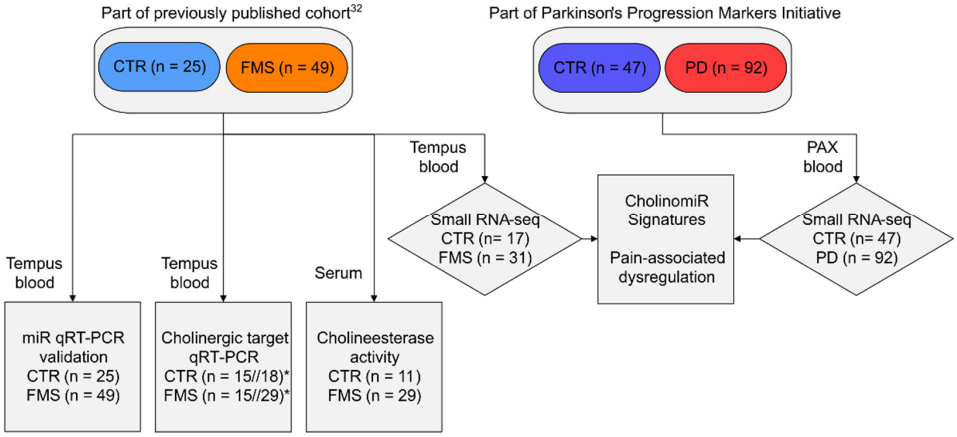

Figure 1. Study workflow. Abbreviations: CTR, healthy control; FMS, fibromyalgia syndrome; PD, Parkinson's disease; miR, microRNA; qRT-PCR, quantitative real-time PCR. Tempus blood, blood samples collected in Tempus™ Blood RNA Tubes; PAX blood, blood samples collected in PAXgene Vacutainer tubes. * For qRT-PCR either CTR (n = 15) versus FMS (n = 15) or CTR (n = 18) versus FMS (n = 29) samples were used.

Tempus™ Blood RNA Tubes (Thermo Fisher Scientific, Waltham, MA, USA) were used to collect 3 mL of whole blood from FMS patients and matched healthy controls. Blood was withdrawn in the morning with participants restrained from extensive physical activity and heavy meals the prior day, after overnight fasting. Cells were lysed and RNA was stabilized via 30 s of rigorous shaking of the tube. RNA was either extracted on the same day, or tubes were stored at −20 °C until extraction. The MagMAX™ for Stabilized Blood Tubes RNA Isolation Kit (Thermo Fisher Scientific, Waltham, MA, USA) was used for total RNA extraction according to the manufacturer's protocol. RNA quality and quantity were assessed with a NanoDrop™ One (Thermo Fisher Scientific, Waltham, MA, USA), and RNA was stored at −80 °C. Sequenced samples were analyzed via an Agilent 2100 Bioanalyzer system (Agilent Technologies, Santa Clara, CA, USA; see details for RNA quality in Supplementary File S1).

Regarding the miR signature control groups, we investigated sequencing data from the whole blood of women with PD and matched healthy controls, obtained from the Progression Markers Initiative (PPMI) database (https://www.ppmi-info.org/accessdata-specimens/download-data (accessed on 1 March 2021); updated information on the PPMI study is available at www.ppmi-info.org). In order to compare the PD cohort to our FMS and control cohort results, we only used blood samples drawn from female PD patients and controls who matched the following criteria: (1) Samples were taken at the baseline time point of the study, (2) patients were not taking any PD-related medication, (3) their age was ≤65 years, and (4) participants were from idiopathic (sporadic) PD and the control cohorts only. The Unified Parkinson Disease Rating Scale (UPDRS) was applied, and the item 1.9 pain and other sensations were utilized as $NRS_{Pain\ impairment}$, with NRS = 0–1 as no pain-related impairment and NRS = 2–4 as pain-related impairment.

PPMI provided small RNA-sequencing data from whole blood samples of PD patients and of matched healthy controls that were collected by venous draws in PAXgene Vacutainer tubes (Qiagen, Hilden, Germany). These were incubated at room temperature (18–25 °C) for 24 h before final storage at −80 °C. RNA was extracted using the PAXgene

blood miRNA Kit protocol (Qiagen, Hilden, Germany; see details for RNA quality in Supplementary File S1).

2.2. Small RNA-Sequencing and miR Analysis

We subjected a randomized subset of 31 FMS and 17 control blood samples to small RNA-sequencing. For this purpose, 300 ng RNA per sample served for library preparation using the NEB-Next® Multiplex Small RNA Library Prep Kit for Illumina® (Index Primers 1-48; NEB-E7560S; New England Biolabs, Ipswich, MA, USA) at the National Center for Genomic Technologies at the Hebrew University of Jerusalem. According to the information provided by the manufacturer, this kit contains a size selection step after PCR to ensure that only small RNAs up to 140 nt length are sequenced. Next generation short RNA-sequencing was conducted on an Illumina NextSeq 500, using two Illumina NextSeq 500/550 High Output Kit v2.5 (75 Cycles) flow cells (20024906), with 24 samples each (all Illumina, San Diego, CA, USA). Quality control was performed using FastQC, version 0.11.8 [37]. Short RNA was aligned to the miRBase version 21 using miRExpress 2.0 with default parameters with no mismatches allowed [38,39]. We defined a miR as "CholinomiR", if five or more cholinergic genes assessed by the previously published miR-targeting graph database ('miRNet') [40] were predicted targets of the respective miR. First, a minimum threshold of seven was applied for the prediction algorithm to define a targeting relationship towards a gene transcript and every DE miR. In the second step, miRs targeting more than four transcripts of a defined cholinergic gene list were termed CholinomiRs. To assess whether the found CholinomiRs were enriched in dysregulated FMS miRs, we compared their fraction against the fraction of detected, but not DE, miRs via Fisher's exact test. The Cytoscape software (v.3.9.0) was used for visualization of the miR-gene target connections [41].

Regarding the PD disease control cohort, sequencing data was provided by PPMI. In summary, small RNA was sequenced at Hudson Alpha's Genomic Services Lab on an Illumina NovaSeq6000 (San Diego, CA, USA). All samples were prepared using the Bioo smRNA library prep Kit (Bioo Scientific Corporation, Austin, TX, USA). Binary base calls were converted to FASTQ's using Illumina bcltofastq v1.8.4, and FASTQ's were merged and processed with miRMaster v1.0 [42]. To identify miRNAs, reads were mapped to miRBase v22 precursors with Bowtie 1.1.2 and were processed with miRMaster to allow up to 1 mismatch and 2 nt overlap at the 5′ end and 5 nt overlap at the 3′ end of the miRNA annotation [43,44]. The complete PPMI study information, including sample collection and other clinical protocols, is available at https://www.ppmi-info.org/ (accessed on 1 March 2021).

2.3. Validation of miR and mRNA Transcripts

For reverse transcription of miRs, we used the miRCURY LNA RT Kit (Qiagen, Hilden, Germany). A total of 10 ng RNA in 2 µL nuclease-free water was added to a mix containing 2 µL reaction buffer, 5 µL nuclease-free water, and 1 µL enzyme mix. Reactions were performed on a PRISM 7700 Cycler (Applied Biosystems, Waltham, MA, USA) under the following conditions: reverse transcription (42 °C, 60 min) and enzyme deactivation (95 °C, 5 min). For mRNA, TaqMan Reverse Transcription reagents (Thermo Fisher Scientific, Waltham, MA, USA) were used. For each sample, 250 ng mRNA was pre-incubated with 5 µL random hexamer at 85 °C for 3 min, followed by reverse transcription in a reaction mix, containing 10 µL 10× PCR buffer, 6.25 µL multiscribe reverse transcriptase, 2 µL RNase inhibitor, 22 µL $MgCl_2$, and 20 µL deoxyribonucleoside triphosphate. Reactions were performed on a PRISM 7700 Cycler (Applied Biosystems, Waltham, MA, USA) under the following conditions: annealing (25 °C, 10 min), reverse transcription (48 °C, 60 min), and enzyme inactivation (95 °C, 5 min). Transcribed cDNA was stored at −20 °C before further analysis.

A QPCR of miR and mRNA targets was carried out on a QuantStudio 3 (Thermo Fisher Scientific, Waltham, MA, USA) using the ΔΔCt method for relative quantification. The miRCURY LNA SYBR Green PCR Kit (Qiagen, Hilden, Germany) and pre-designed miRCURY

LNA miR PCR Assays (Qiagen, Hilden, Germany) were applied for each miR (see list of primers in Table 1). Following a dual selection approach, we included ten transcripts as potential endogenous controls for small RNAs. SNORD38B, SNORD44, SNORD48, 5S RNA, and hsa-miR-221-3p were selected from the literature. Furthermore, miRs with a mean base read level of >1000 reads within the small RNA-sequencing dataset were selected by their intra- and intergroup stability, assessed by NormFinder [45], identifying hsa-miR-942-5p, hsa-miR-194-5p, miR-93-5p, miR92a-3p, and miR423-5p as candidates. Twelve random CTR and FMS samples were used for validation via qRT-PCR. SNORD38B, SNORD44, SNORD48, and miR-423-5p were selected as suitable endogenous controls, based on Ct intergroup comparability and on standard deviation and range across all samples. To minimize the risk of a potentially skewed normalization by only one endogenous control, we normalized against the combined geometric mean of these four transcripts. Each well contained 5 µL 2× miRCURY SYBR Green Master Mix with 1 µL ROX per 50 µL, 1 µL primer, and 4 µL of 1:80 diluted cDNA. Functionality and specificity of SYBR green-based primers were checked via a melting curve step assessment. Gene expression analysis was performed with TaqMan qRT-PCR reagents (all Thermo Fisher Scientific, Waltham, MA, USA) with pre-designed Assays using RPL13A as an endogenous control. Each well contained 0.5 µL nuclease free water, 5 µL Fast Advanced Mastermix, 0.5 µL RPL13A primer, 0.5 µL target primer, and 3.5 µL cDNA.

Table 1. List of applied primer assays.

SYBR Green Primer	Assay Number	Company
hsa-miR-182-5p	YP00206070	Qiagen, Hilden, Germany
hsa-miR-194-5p	YP00204080	Qiagen, Hilden, Germany
hsa-miR-221-3p	YP00204532	Qiagen, Hilden, Germany
hsa-miR-423-5p	YP00205624	Qiagen, Hilden, Germany
hsa-miR-492-5p	YP00204053	Qiagen, Hilden, Germany
hsa-miR-92a-3p	YP00204258	Qiagen, Hilden, Germany
hsa-miR-93-5p	YP00204715	Qiagen, Hilden, Germany
5S	YP00203906	Qiagen, Hilden, Germany
SNORD38B	YP00203901	Qiagen, Hilden, Germany
SNORD44	YP00203902	Qiagen, Hilden, Germany
SNORD48	YP00203903	Qiagen, Hilden, Germany
Taqman Primer	**Assay Number**	**Company**
AChE	Hs00241307_m1	Thermo Fisher Scientific, Waltham, MA, USA
BDNF	Hs00380947_m1	Thermo Fisher Scientific, Waltham, MA, USA
BMP3	Hs00609638_m1	Thermo Fisher Scientific, Waltham, MA, USA
BMPR2	Hs00176148_m1	Thermo Fisher Scientific, Waltham, MA, USA
CHRNA4	Hs00181247_m1	Thermo Fisher Scientific, Waltham, MA, USA
CHRNB2	Hs01114010_g1	Thermo Fisher Scientific, Waltham, MA, USA
IL6ST	Hs00174360_m1	Thermo Fisher Scientific, Waltham, MA, USA
NGFR	Hs00609976_m1	Thermo Fisher Scientific, Waltham, MA, USA
NR1D2	Hs00233309_m1	Thermo Fisher Scientific, Waltham, MA, USA
RORA	Hs00536545_m1	Thermo Fisher Scientific, Waltham, MA, USA
SRSF6	Hs05331162_g1	Thermo Fisher Scientific, Waltham, MA, USA

Abbreviations: AChE, acetylcholinesterase; BDNF, brain derived neurotrophic factor; BMP3, bone morphogenetic protein 3; BMPR2, bone morphogenetic protein receptor 2; CHRNA4, cholinergic receptor nicotinic alpha 4 subunit; CHRNB2, cholinergic receptor nicotinic beta 2 subunit; IL6ST, interleukin 6 cytokine family signal transducer; NGFR, nerve growth factor receptor; NR1D2, nuclear receptor subfamily 1 group D member 2; RORA, RAR related orphan receptor A; SNORD, small nucleolar RNA; SRSF6, serine and arginine rich splicing factor 6.

2.4. Cholinesterase Activity Assay

From a randomly selected subset of study participants (FMS, n = 29; CTR, n = 11), the cholinergic status in serum samples was analyzed via Ellman's assay [46]. The thawed serum samples were diluted 1:6 in PBS and incubated with Ellman solution containing 0.1 M sodium phosphate buffer, with pH 7.4 and 0.5 mM 5,5′-dithiobis-(2-nitrobenzoic acid)

(DTNB). For acetylcholinesterase (AChE) activity, 10 mM of the specific inhibitor tetraisopropyl pyrophosphoramide (iso-OMPA; Sigma, St. Louis, MO, USA) was added at 1:200 dilution in Ellman's solution to block butyrylcholinesterase (BChE) activity. Samples were incubated for 90 min at room temperature. After adding the substrate acetylthiocholine (ATCh) in a final concentration of 1 mM, kinetic measurements were performed at 37 °C and 405 nm wavelength using a Tecan Spark microplate reader (Tecan Group, Männedorf, Switzerland). The activities of each sample were measured in triplicates and were repeated once. To diminish potential intra-test differences, each microtiter plate contained an in-house control triplicate of recombinant human AChE and BChE enzymes. Raw data were collected in units of "mean optical density (OD)/minute" and were processed as activity in nmol ATCh hydrolyzed/min/mL according to the Beer–Lambert law (A = εlc; molar absorptivity constant ε 2-nitro-5-thiobenzoate = 13,600), and they were multiplied by 6, accounting for the serum dilution factor.

2.5. Statistical Analysis and Visualization

Differential expression (DE) analysis of the transcriptomic profiles from the FMS cohort was performed using the "DESeq2" package via R platform [47,48]. Differences were assumed statistically significant at $p < 0.05$ after false discovery rate (FDR) correction, and data were filtered for a total count >300 across all samples. DE analysis of the PPMI PD cohort was conducted in the same manner in DESeq2. Counts per million (CPM) measurements for downstream analysis were calculated using the edgeR R package [49,50]. Principal component analysis (PCA) and linear discrimination analysis (LDA) were performed in R using the "stats" "MASS" packages accordingly, as well as the graphic packages "ggfortify", "ggplot2", and "ggConvexHull" [48,51–54]. Briefly, PCA components (PCs) were based on finding the biggest variability between samples, whereas LDA components (LDs) explored the biggest variability between the known groups (FMS_mild_imp, FMS_severe_imp, and control).

For data derived from qRT-PCR, correlations, and Ellman's assay, SPSS 27 (IBM, Armonk, NY, USA) was used for analysis and was plotted in GraphPad Prism 8 (GraphPad Software, Inc., La Jolla, CA, USA) for visualization. The Mann–Whitney U Test was used for comparison of two groups, and the Kruskal–Wallis test was used for correlations. When appropriate, Holm–Sidak post correction was applied. Furthermore, the open-source vector software Inkscape V 0.92 (https://inkscape.org (accessed on 12 March 2018)) was used, and graphical icons were integrated from Smart Servier Medical Art https://smart.servier.com/ (accessed on 21 December 2021)) under the CC BY 3.0 license for visualization.

3. Results

3.1. Clinical Characteristics

The main clinical characteristics of the study population are summarized in Table 2.

3.2. Identification and Characterization of Systemic CholinomiRs in FMS

Small RNA-seq of women with FMS (n = 31) versus female healthy controls (n = 17) (Figure 2A) revealed 26 down- and 43 up-regulated miRs. Assessment of miR-mRNA targeting relations connected to cholinergic genes [35] identified 19 altered CholinomiRs within the dataset (Figure 2B).

The FMS-modulated CholinomiRs included upregulation of hsa-miR-374a-5p, -9-5p, -182-5p, -548d-5p, -454-3p, -183-5p, -101-3p, -148a-3p, -7-5p, -128-3p, -186-5p, and -27b-3p. Hsa-miR-532-3p, -328-3p, -766-3p, -1275, -625-5p, -671-5p, and -3609 showed downregulation in FMS blood samples (Figure 2B). In general, upregulated CholinomiRs from Tempus-tube-derived RNA showed higher reads compared to downregulated ones (Figure 2C). Since these RNA samples contained mRNA and small RNA from the whole variety of blood cells, we used an open database to assign our CholinomiRs to subtypes of nucleated white blood cells (WBC) and to red blood cells (RBC). Low frequency transcripts referred predominantly to single or few cell types. For instance, hsa-miR-548d-5p was

restricted to monocytes, and hsa-miR-3609 was abundant only in CD4+ T cells. Hsa-miR-183-5p was restricted to RBC, but it exhibited one of the highest expression profiles across the sequenced samples (Figure 2B,C). Furthermore, CholinomiRs with stronger upregulation and more copies, reflected in higher counts such as hsa-miR-182-5p, hsa-miR-148a-3p, or hsa-miR-101-3p, were more broadly expressed according to the microRNA catalogue of human peripheral blood (http://134.245.63.235/ikmb-tools/bloodmiRs (accessed on 2 December 2021)). The larger fraction of CholinomiRs was upregulated and also connected to a higher number of cholinergic targets, potentially having more impact on the cholinergic system.

Table 2. Main clinical parameters of the study cohort that was restricted to women.

Parameter	FMS (n = 49)	FMS-CTR (n = 25)	PD (n = 92)	PD-CTR (n = 47)
Age, median (range)	53 (25–67)	53 (24–62)	56 (34–65)	56 (31–65)
BMI, median (range)	25 (17–40)	23 (17–42)	n.a	n.a
Individual patients on amitriptyline: (Regimen, mg, years)	6 0-0-1, 10, 10 0-0-1, 10, 1 0-0-1, 10, 2 on demand, 5, 2 1-0-0, 10, 1 0-0-1, 10, 1	none	none	none
Graded Chronic Pain Scale; mean pain intensity last 6 months (0–10) (range)	6 (2–9)	0 (0–8)	n.a	n.a
Unified Parkinson Disease Rating Scale;	n.a	n.a	0.83	0.46
Pain and other Sensations			(0–4)	(0–3)

Abbreviations: FMS, Fibromyalgia syndrome; FMS-CTR, healthy control cohort for FMS; PD, Parkinson's disease; healthy control cohort for PD; n.a., not applied.

3.3. CholinomiR Signature Is Pain-Related and FMS-Specific

A comparison of ratios between detected CholinomiRs within the set of DE (19 of 69; 27.5%) and not DE miRs (68 of 474; 14.3%) revealed enrichment of dysregulated CholinomiRs in FMS, indicating that the observed signature in whole blood RNA is not random ($p = 0.008$; Fishers's exact test). To evaluate the relevance of our CholinomiR subset for discriminating FMS patients from CTR, we compared the PCA pattern of all DE miRs to a PCA focusing on the 19 FMS-modulated CholinomiRs. The general PCA poorly differentiated both cohorts, and our CholinomiR-specific PCA yielded a slightly improved separation (Figure 3). When stratifying the group for the degree of daily life impairment due to pain in FMS and subjecting three groups to LDA, we achieved better discrimination from controls for all DE miRs as variables. This was further enhanced by applying only CholinomiRs as variables, distinguishing FMS with high daily life impairment without overlap versus the controls. Notably, only one FMS patient with low pain-related daily life impairment dispersed towards controls, and one dispersed towards the firmly impaired FMS subgroup (Figure 3).

Next, we asked if our CholinomiR signature is FMS-specific or if it reflects pain that may accompany other chronic diseases that involve immune-related alterations. For this purpose, we compared our findings with those of small RNA-seq of whole blood samples obtained from female PD patients (n = 92) versus female CTR (n = 47). Notably, 13 out of the 19 CholinomiRs determined in FMS patients were also detected in this analysis, affirming their expression in blood (Figure 4A). However, these CholinomiRs were not

dysregulated in PD, and only hsa-miR-128-3p showed a trend towards downregulation (Figure 4B) in contrast to upregulation in FMS.

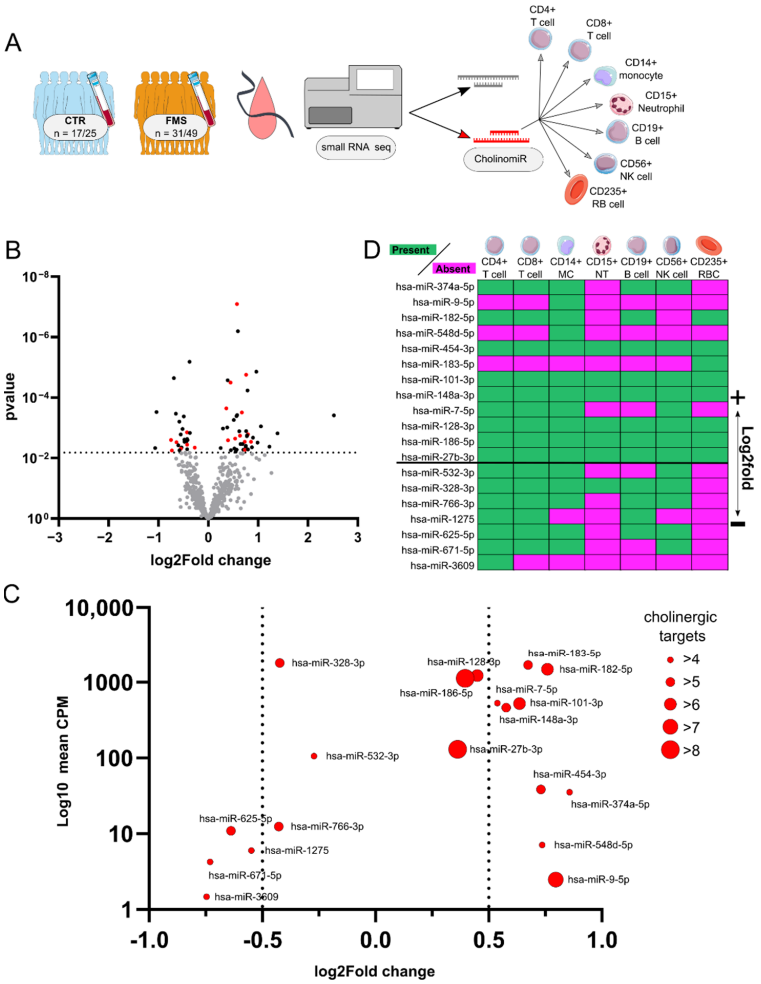

Figure 2. Small RNA-sequencing reveals 19 DE blood CholinomiRs in female FMS patients. (**A**) Blood collected in Tempus tubes from female FMS patients and matched controls was used for small RNA-sequencing and miR analysis. (**B**) Volcano plot of altered miR levels in FMS normalized to CTR, and the horizontal line indicates FDA-corrected threshold for DE miRs. Unchanged miRs are in grey, DE miRs are in black, and DE CholinomiRs are in red. (**C**) Counts per million of respective CholinomiRs and log2Fold change compared to CTR. Diameter of dots code for the number of predicted cholinergic targets. (**D**) Assignment of CholinomiRs to blood cell subtypes; magenta indicates absence, and green indicates presence in blood cell type according to [55]. Abbreviations: CholinomiR, cholinergic-targeting microRNA; CPM, counts per million; CTR, healthy controls; DE, differentially expressed; FDA, false discovery rate; FMS, fibromyalgia syndrome; MC, monocyte; miR, microRNA; NK, natural killer cell; NT, neutrophil; RBC, red blood cell.

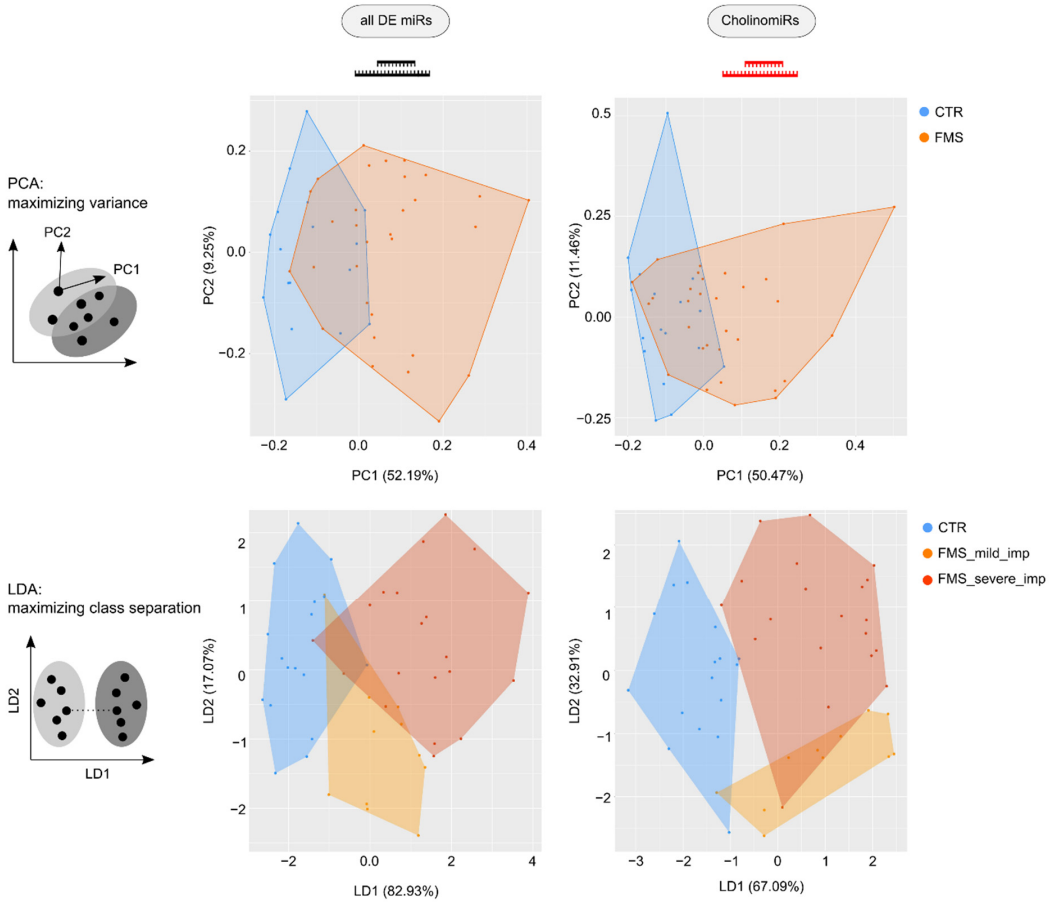

Figure 3. PCA and LDA (principles visualized in grey graphs) for all DE miRs and only CholinomiRs. Although PCA shows only minor improvements in group separation when focusing on CholinomiRs, using LDA with three groups and CholinomiRs leads to high discrimination capacity between healthy controls and FMS patients with mild pain-related daily life impairment (FMS_mild_imp) and severely pain-related daily life impairment (FMS_severe_imp). Abbreviations: CTR, healthy control; DE, differentially expressed; FMS, fibromyalgia syndrome; PCA, principal component analysis.

Pain is a relevant non-motor symptom in PD with significant impacts on patients' health-related quality of life [56]. Therefore, we applied our FMS CholinomiR signature in blood samples of PD patients as a predictor of pain-related everyday life impairment. Hsa-miR-625-5p showed a trend towards downregulation in PD patients who reported pain-related impairment (Figure 4C), in line with the downregulation observed in FMS. We also correlated CholinomiR expression with FMS patients' pain levels and found that hsa-miR-27b-3p (r = 0.373; p = 0.039) and hsa-miR-148a-3p (r = 0.362; p = 0.045) moderately correlated with NRS_{Pain} within the FMS cohort (Figure 4D,E). Taken together, these observations indicate biological relevance of CholinomiR alterations in FMS, distinct from PD patients, and hint towards an association with pain.

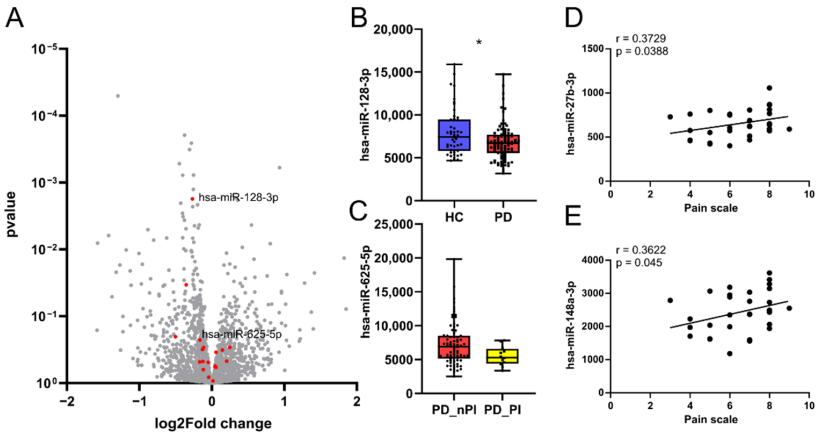

Figure 4. CholinomiRs are related to pain and form a specific FMS signature. Identified CholinomiRs may positively correlate with pain intensity. (**A**) FMS blood levels of hsa-miR-27b-3p (p = 0.039; padj = 0.530) and (**B**) hsa-miR.148a-3p (* p = 0.045; padj. = 0.563) increased with the mean pain level experienced in the past 6 months, but all 19 CholinomiRs failed to pass post-correction for multiple testing. Spearman correlation test with Holm–Sidak post correction. (**C**) Volcano plot of miRs in PD versus HC with no DE miRs. FMS CholinomiRs present in the PD dataset are marked in red. (**D**,**E**) Only comparing CPM expression levels of FMS CholinomiRs in PD revealed trends for lower hsa-miR-128-3p (p = 0.028; padj = 0.364) and within PD patients with pain related impairments an hsa-625-5p downregulation (p = 0.052; padj = 0.678). Mann–Whitney U tests with Holm–Sidak post correction. Abbreviations: CPM, counts per million; FMS, fibromyalgia syndrome; HC, healthy control; PD, Parkinson's disease; PD_nPI, Parkinson's disease without pain-related daily life impairment; PD_PI, Parkinson's disease with pain-related daily life impairment.

3.4. CholinomiR Hsa-miR-182-5p Is Upregulated in Women with FMS Compared to Healthy Controls

To experimentally validate our sequencing approach, we quantified hsa-miR-182-5p levels, using four selected small RNA transcripts as endogenous controls (Figure 5A). This broadly expressed CholinomiR showed a relatively strong upregulation (log2fold = 0.76) in small RNA-seq, revealing a twofold upregulation (median increase = 1.93) in FMS patients compared to CTR via qRT-PCR in our entire cohort (Figure 5B).

3.5. Female FMS Patients Inherit a Dense CholinomiR-Gene Transcript Network

The previously published miR-targeting graph database 'miRNet' allowed in-depth exploration of the CholinomiR-gene transcript network by integrating publicly available validated and predicted miR-gene interaction datasets [40]. Our analysis revealed 47 potential cholinergic targets and 118 miR-mRNA interactions (Figure 6) with upregulated cholinergic miRs, forming 80 connections compared to 38 connections of downregulated miRs (for details see Supplementary File S2).

Correspondingly, the miR-mRNA network showed a collective regulation of a subset of transcripts mostly targeted by upregulated miRs. Examples include bone morphogenetic protein receptor type 2 (BMPR2), linked to ten CholinomiRs (eight upregulated, two downregulated), RAR-related orphan receptor A (RORA) with seven connections (six upregulated, one downregulated), and interleukin 6 cytokine family signal transducer (IL6ST) with five upregulated CholinomiR connections, together indicating general downregulation of these transcripts. In contrast, the cholinergic receptor nicotinic beta 2 subunit (CHRNB2) was a predicted target of only downregulated CholinomiRs. Lastly, acetylcholinesterase (AChE), a key enzyme for cholinergic signaling via breakdown of

acetylcholine, was equally linked to three up- and three downregulated CholinomiRs (Figure 6). We compared our candidate gene list with an online mRNA sequencing dataset derived from healthy donor blood RNA, from the Human Protein Atlas (HPA) project [57] (RNA HPA blood cell gene data; https://www.proteinatlas.org/about/download (accessed on 27 February 2022)) to assess the expression profile of these miR targets across single immune cell subtypes (see Supplementary File S3). With 61.7% (29/47 genes), natural killer (NK) cells expressed the highest number of mRNA targets, followed by neutrophils with 57.5% (27/47), whereas myeloid dendritic cells showed the lowest numbers of detected mRNA targets at 44.7% (21/47). Among the top-targeted transcripts, BMPR2, IL6ST, RORA, and NR1D2 were expressed in almost all cell types, whereas ACHE and BDNF expression was not detected in this dataset. However, RBC was not included in the HPA dataset, which represents a large fraction of Tempus-tube-derived RNA, and no disease-associated immune cell data are included.

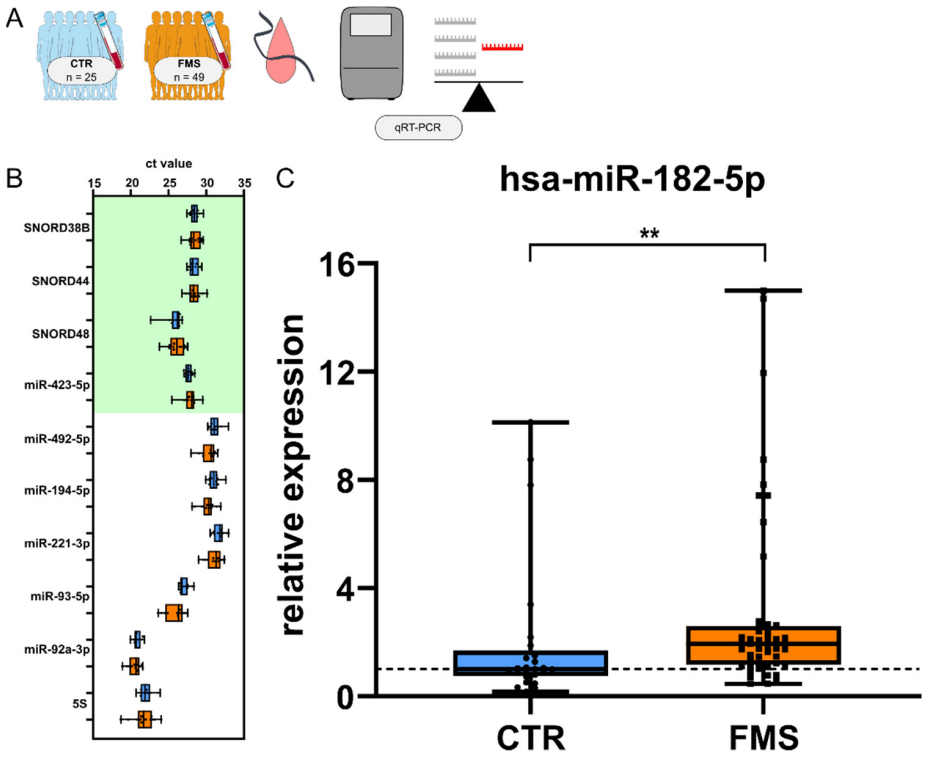

Figure 5. qRT-PCR validation of hsa-miR-182-5p. (**A**) Workflow illustrating cohorts and normalization of hsa-miR182-5p with four unaltered control transcripts. (**B**) Screening of SNORD38B, SNORD44, SNORD48, and hsa-miR-423-5p selected as controls for miR validation and indicated in green. (**C**) hsa-miR-182-5p median expression level is upregulated by twofold in FMS (n = 49), shown as normalized relative expression to CTR (n = 25). The dotted line represents median control expression. Mann–Whitney U Test, ** $p < 0.01$. Box and whiskers plots with min to max. Abbreviations: CTR, healthy controls; FMS, fibromyalgia syndrome; miR, microRNA; qRT-PCR, quantitative real-time PCR.

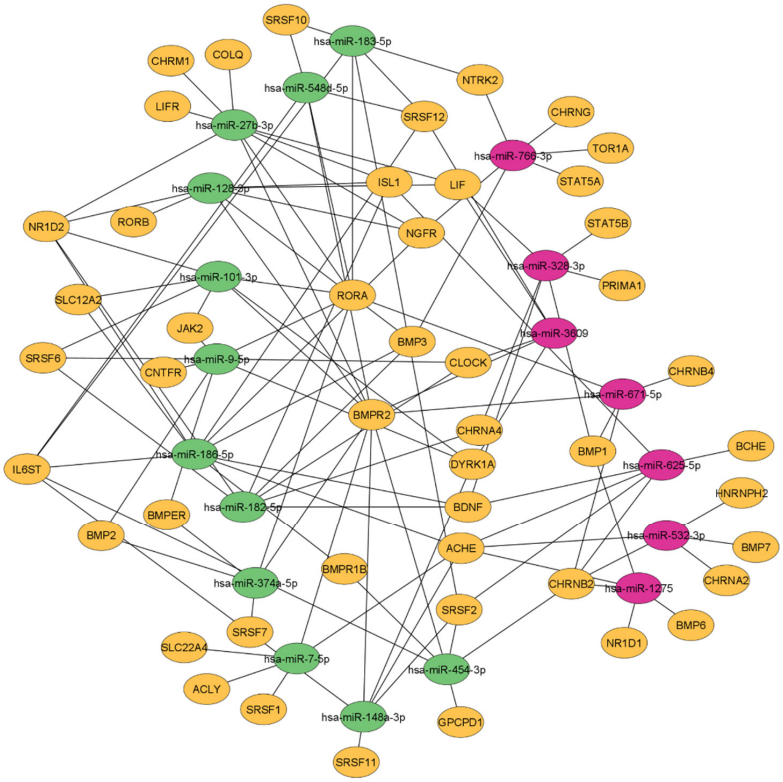

Figure 6. miR-gene interactions. Up-(green) and downregulated (magenta) FMS CholinomiRs are connected to their respective cholinergic target genes (orange) with a total of 47 targets. See comprehensive interaction summary with complete gene names in Supplementary File S2. Abbreviations: miR, microRNA.

3.6. Downregulation of Highly Targeted Cholinergic Gene Transcripts

To assess the direct influence of CholinomiRs on cholinergic transcript levels, we performed qRT-PCR with eleven associated target genes: BMPR2, IL6ST, RORA, nuclear receptor subfamily 1 group D member 2 (NR1D2), AChE, brain-derived neurotrophic factor (BDNF), nerve growth factor receptor (NGFR), bone morphogenetic protein 3 (BMP3), serine and arginine rich splicing factor 6 (SRSF6), cholinergic receptor nicotinic alpha 4 subunit (CHRNA4), and cholinergic receptor nicotinic beta 2 subunit (CHRNB2). Low numbers of CHRNA4 and CHRNB2 mRNA transcripts in whole blood RNA did not allow comparisons between FMS and CTR via qRT-PCR and were excluded from analysis. Within the group of cholinergic transcripts with five or more associated upregulated CholinomiRs, BMPR2 and IL6ST were downregulated (Figure 7B,C) in FMS, whereas RORA and NR1D2 expression levels were similar between FMS and CTR (Figure 7D,E). None of the other investigated transcripts were altered in FMS compared to CTR (Figure 7F–J).

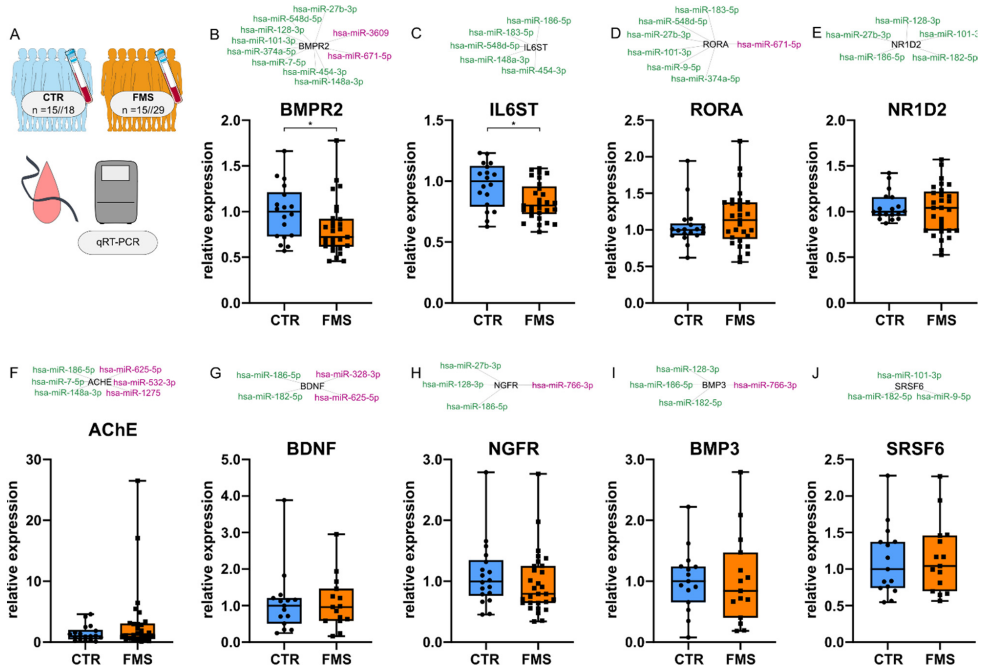

Figure 7. Transcript levels of related cholinergic mRNAs. (**A**) Workflow illustrates cohorts investigated. Global expression of two highly targeted transcripts BMPR2 (**B**) and IL6ST (**C**) was downregulated by 27.8% (* $p = 0.025$) and 19.9% (* $p = 0.022$), whereas RORA (**D**) and NR1D2 (**E**) were not altered in whole blood. ACHE (**F**) and BDNF (**G**), targeted equally by up- and down-regulated CholinomiRs, showed no altered expression, also seen in cholinergic transcripts NGFR (**H**), BMP3 (**I**), and SRSF6 (**J**), which were associated with fewer CholinomiRs. Randomly selected cohort subgroups with n = 29 FMS versus n = 18 CTR (**B**–**F**,**H**) or n = 15 FMS versus n = 15 CTR (**G**,**I**,**J**) were analyzed. Box and whisker plots with min to max. Mann–Whitney U test. Green color depicts upregulated miRs, whereas magenta labels depict downregulated miRs connected to the corresponding mRNA transcript in black.

3.7. Unchanged Cholinesterase Activity in FMS

Although not altered at the transcriptional level in FMS, we considered that AChE may be affected in FMS at the protein level, indicated by altered enzyme activity. The availability and concentration of acetylcholine (ACh) as the ligand of cholinergic signaling depends on its degradation by AChE and BChE. Hence, we measured the activity of total cholinesterases as well as AChE and BChE specific activity in serum samples of FMS patients. Notably, FMS and CTR serum exhibited similar levels of both total and AChE- or BChE-specific hydrolytic activity (Figure 8).

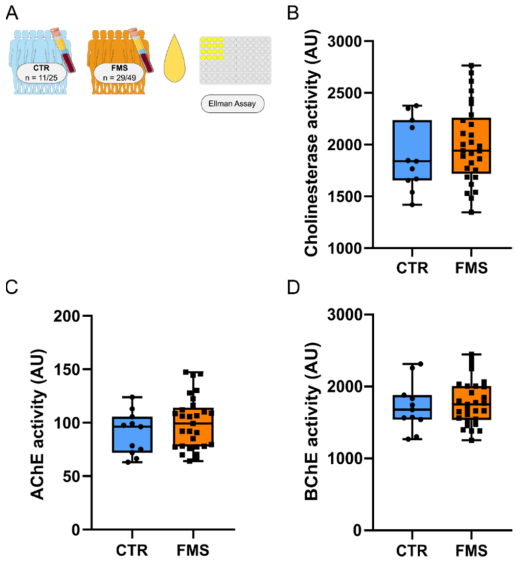

Figure 8. Cholinesterase activity in serum. (**A**) Cohorts and methods. (**B**) Total cholinesterase status in FMS and CTR sera (p = 0.401) and subdivision in (**C**) AChE-specific activity (p = 0.256) and (**D**) BChE-specific activity (p = 0.6224). Mann–Whitney U Test. Abbreviations: AChE, acetylcholinesterase; AU, arbitrary unit; CTR, healthy controls; FMS, fibromyalgia syndrome. Note that there is larger variability in FMS cholinesterase activity compared to that of CTR.

4. Discussion

We performed a detailed profiling of CholinomiRs in whole blood samples of patients with FMS and compared our data to healthy and disease controls. We found moderate DE of 69 miRs, including 19 cholinergic miRs that distinguished FMS from the investigated control groups and that may modulate downstream gene expression. CholinomiRs play an important role in orchestrating immune-related responses in neurodegenerative diseases, depression, and inflammatory disorders, including inflammatory bowel disease [58–61]. Only few studies have investigated miR levels in FMS blood so far. Two studies used serum, whereas one report focused on peripheral blood mononuclear cells (PBMC). Their approaches relied on miRNA microarrays with varying panels, a smaller sample size, and a single set of hybridization conditions, compromising the outcome of these tests [62–64]. Less than ten DE miRs were identified in each study, without overlap between studies, and none of the CholinomiRs we present here was reported. Hence, our small RNA-seq represents the first comprehensive and unbiased survey of miR expression in FMS.

Mapping our CholinomiRs to blood cell types revealed dysregulation of commonly expressed CholinomiRs, such as hsa-miR-27b-3p, hsa-miR-148a-3p, and hsa-miR-182-5p, but also that of cell-type-specific miRs, such as hsa-miR-3609 in CD4+ T cells or hsa-miR-548d-5p in CD14+ monocytes. CholinomiR dysregulation in FMS was nonrandom, and highly abundant members tended to be upregulated.

Focusing on DE CholinomiRs improved separation between FMS and healthy control groups, especially via LDA and subgrouping between low and high pain-related impairment in daily life. To evaluate whether our CholinomiR signature referred to a general pattern in chronic diseases with suspected immune-related component, we cross-examined expression of our CholinomiRs in female PD patients of comparable age. Intriguingly, FMS presented a strikingly higher and clearer overall DE of CholinomiRs than PD, in which only hsa-miR-128-3p showed a trend towards reduced expression compared to controls, inverse

to its upregulation in FMS. Hsa-miR-128-3p is involved in the neuronal oxidative stress response via interaction with the circular RNA circSLC8A1, which blocks its functioning and modulates the process of nonsense-mediated RNA decay [65–67]. PD patients with pain-related impairment showed a tendency towards hsa-miR-625-5p downregulation, inverse to its upregulation in FMS, hinting towards opposed pain-related function. In FMS, hsa-miR-148a-3p and 27b-3p positively correlated with pain intensities, indicating a putative association with pain severity. Interestingly, hsa-miR-27b-3p is implicated with inflammatory modulation of toll-like receptors [68]. Although we do not define a "unique" FMS CholinomiR signature, comparisons with healthy and disease controls may indicate distinct small-RNA-mediated mechanisms of pain in FMS and PD. Pain phenotypes, perceptions, and methodological assessments of pain substantially vary across individuals and between diseases. The exact roles of these candidate miRs in different pain conditions needs to be investigated in future studies with respective patient cohorts.

Validating our RNA-seq results, qRT-PCR confirmed the upregulation of hsa-miR-182-5p in FMS. This miR targets, e.g., BDNF, which predominantly derives from the central nervous system, but it is also secreted by activated immune cells and acts as a positive regulator of survival and differentiation of PNS and CNS neurons [69]. Reduced blood levels of BDNF have been reported in major depression (MD), and depressed mood is a frequent co-morbidity in FMS [3,70]. However, contrary to MD, some studies reported increased serum BDNF levels in FMS patients [71,72], whereas others did not find any deregulation [73], which obscures its role in FMS pathology. Our study exclusively focuses on blood RNA expression, leaving our findings hinting towards a potential lack of BDNF deregulation speculative. Hsa-miR-182-5p is also associated with NR1D2, which is a gene involved in circadian rhythmicity and which regulates lipid metabolism and inflammatory responses [74,75]. CholinomiRs also targeted RORA and Clock Circadian Regulators as further members of the circadian rhythm gene family. Intriguingly, circulation of leukocytes oscillates in a diurnal manner, and amplification of the circadian expression of pro-inflammatory mediators is known in chronic diseases [76]. As an example, the circadian regulator cortisol modulates T-cell activity and is assumed to play a role in FMS pathophysiology [77–79]. CholinomiR-gene transcript networks predicted further relevant candidates of immune regulation. BMPR2 and several BMPs are involved in NK activation and autoimmunity as part of the TGFβ superfamily [80–82]. IL6ST mediates immune responses by binding to other receptors, such as IL-6R, forming high-affinity receptor complexes [83].

We investigated these key mRNA transcripts targeted by CholinomiRs of interest via qRT-PCR in our whole blood samples. Indeed, BMPR2 and IL6ST levels were reduced in FMS patients in accordance with the miRs most prominent role of post-transcriptional repressors. The membrane receptors BMPR2 and IL6ST are pivotal components of the TGFβ-superfamily-mediated SMAD (BMPR2) and the IL-6-family-mediated JAK–STAT (IL6ST) pathways [84]. In general, the activation of IL-6-mediated pathways exerts pro-inflammatory cellular responses [83]. BMP signaling can be bidirectional, dependent on ligand–receptor combination and the respective cell [80,85], however, a link with autoimmunity is suspected, e.g., in multiple sclerosis, and BMPs can promote Th17 proliferation while suppressing T-reg cell generation [86,87]. Although further validation of our data is mandatory by investigating larger patient samples, CholinomiRs may act on BMPR2 and IL6ST in a compensatory manner to confine underlying pro-inflammatory processes in FMS. Investigated circadian transcripts RORA and NR1D2 and transcripts targeted by fewer miRs or connected to both up- and downregulated CholinomiRs, such as AChE and BDNF, were not altered in whole blood. Accordingly, serum AChE activity was sustained in FMS patients compared to controls. Together, this indicates that the observed CholinomiRs modifications may serve to maintain a balanced system.

Traditional screening approaches failed to identify robust pro-inflammatory "signatures" or precise immune-related pathways in FMS [27,28]. However, recent advances with in-depth analyses have revealed immune and neuro-immune mechanisms as potentially

involved in FMS pathophysiology. Passive transfer experiments and cell culture incubation along with immunoreaction in tissue sections indicated binding of FMS patient-derived IgG at the dorsal root ganglion level, representing a neuro-inflammatory component via the humoral system [8]. Moreover, a switch from circulating to resident hyper-responsive natural killer (NK) cells in FMS may participate in peripheral neurodegeneration [88]. Both NK activation and autoimmunity are linked to BMP signaling, e.g., via an autocrine activation pathway via BMP receptors and BMP ligands in NK cells [80–82], which fits our identified target genes BMP1, BMP2, BMP3, BMP7, BMP6, BMPER, BMPR1B, and, most importantly, BMPR2. Finally, changes in monocyte subtype distribution and amplified p38 MAPK/MK2 axis activity may be associated with FMS [89,90]. In this respect, monocyte-specific hsa-miR-9-5p and globally expressed hsa-miR-101-3p both target JAK2, which is pivotal for IL6/JAK2/STAT3 axis-mediated inflammation. Taken together, CholinomiRs may shift inflammatory processes via modulation of the systemic cholinergic system.

From the clinical point of view, our findings give further evidence for a distinct pathophysiology of FMS and draw attention to its links with the cholinergic system. Indeed, the anticholinergic drug amitriptyline is one of the first-line pharmacological treatment options for FMS patients [91,92]. Although we cannot rule out a potential effect of CholinomiRs on the individual response of FMS patients to anticholinergic medication, since only three (for small RNA-seq) and six (for qRT-PCR) FMS patients were on low dosages of amitriptyline (Table 1), we believe that this aspect deserves consideration in future studies. Given the individually diverse effects and side effects of amitriptyline in FMS, we speculate that a pathophysiological link to distinct CholinomiRs and related pathways may be possible.

5. Limitations

Analysis of circulating miRs from serum or plasma can be severely distorted by hemolysis during preparation [93], and little information can be drawn on source or effector cells. Blood sample processing and isolation of PBMC prior to analysis affects gene regulation within hours and may affect miR transcription even more rapidly [94–96]. In contrast, our approach allowed us to create a direct snap shot of the transcriptomic state, since all cells were immediately lysed and total RNA was stabilized [97]. However, several limitations must be addressed. Our assignment of miRs towards particular blood cell types relied on a database mapping approach and was not directly assessed. Only FMS patients with normal routine blood assessment results were included [35] to avoid conditions in which aberrant miR expression patterns may be affected by blood cell distributions, but we did not analyze single blood cell type percentages. Finally, expression changes of targets restricted to a single blood cell subtype or transcripts diametrically regulated across blood cells subtypes are likely masked within global blood RNA and can therefore not be identified via qRT-PCR. Experiments with sorted blood cells are necessary to disentangle immune-related mechanisms in the pathophysiology of FMS related to CholinomiRs, which may be particularly relevant for the identified genes involved in circadian rhythmicity.

FMS and control blood was obtained via Tempus tubes, and PD patient and respective control blood collection employed the PAX system. Both systems rely on direct cell lysis and RNA stabilization; nevertheless, a previous study called for caution in cross-evaluation of expression levels between both systems [98]. To avoid fallacious conclusions, we only compared whether global deregulation of CholinomiRs was seen against their respective control cohort.

Importantly, small non-coding RNA regulators also comprise a recently introduced class of tRNA fragments (tRF) with diverse cellular roles, including mRNA repression, that can take over miR functions in a 'changing of the guards' manner [60,99]. Hence, to gain insight into the detailed small RNA landscape, tRF analysis needs to be addressed in future studies for both FMS and PD.

6. Conclusions

We investigated systemic blood CholinomiR signatures in women with FMS and compared our data with those of healthy controls and patients with PD associated with somatic pain as disease controls. CholinomiRs play an important role in neurodegenerative and inflammatory diseases. In FMS subgroups, degeneration of peripheral small nerve fibers was observed, and inflammatory bowel disease and affective cognitive symptoms were common comorbidities. We found a distinct CholinomiR signature, which distinguishes FMS from healthy subjects and PD patients as disease controls and links these CholinomiRs with downstream immune-related mRNA transcripts. These findings provide evidence for miR regulation of immune cell processes in FMS with an emphasis on the systemic cholinergic system. Although the exact pathophysiological mechanisms remain unclear, CholinomiRs emerge as important post-transcriptional regulators, which may mediate pathological pro-inflammatory or compensatory effects in immune cells of FMS patients.

Supplementary Materials: The following supporting information can be downloaded at: https://www.mdpi.com/article/10.3390/cells11081276/s1, Supplementary File S1: RNA quality summary; Supplementary File S2: Scored CholinomiR-gene target list; Supplementary File S3: Expression profile of CholinomiR targets across blood immune cell subtypes.

Author Contributions: Conceptualization, N.Ü., D.S.G., C.S. and H.S.; methodology, C.E., S.V., G.M., D.S.G. and S.L.; software, S.L.; validation, N.Ü., D.S.G. and H.S.; formal analysis, C.E., S.V. and G.M.; investigation, C.E., S.V., G.M. and L.E.; resources, N.Ü. and H.S.; data curation, N.Ü., D.S.G., S.V., G.M. and H.S.; writing—original draft preparation, C.E., S.V., N.Ü. and H.S.; writing—review and editing, C.E., S.V., G.M., S.L., L.E., D.E., C.S., H.S. and N.Ü.; visualization, C.E. and S.V.; supervision, N.Ü. and H.S.; project administration, N.Ü.; funding acquisition, N.Ü. and H.S. All authors have read and agreed to the published version of the manuscript.

Funding: This research was funded by the German Research Foundation (Deutsche Forschungsgemeinschaft, DFG, UE171/4-1) and partly funded by Else Kröner-Fresenius-Stiftung (2014_A129). N.Ü. was funded by DFG (UE171/15-1). The authors further acknowledge support from the Israeli Ministry of Science, Technology and Space, Grant No. 53140 and the Israel Science Foundation (ISF), Grant no. 1016/18 to H.S., as well as support from the German Federal Ministry for Education and Research, Minerva fellowship to L.E. PPMI—a public-private partnership—is funded by the Michael J. Fox Foundation for Parkinson's Research and funding partners, including 4D Pharma, AbbVie Inc., AcureX Therapeutics, Allergan, Amathus Therapeutics, Aligning Science Across Parkinson's (ASAP), Avid Radiopharmaceuticals, Bial Biotech, Biogen, BioLegend, Bristol Myers Squibb, Calico Life Sciences LLC, Celgene Corporation, DaCapo Brainscience, Denali Therapeutics, The Edmond J. Safra Foundation, Eli Lilly and Company, GE Healthcare, GlaxoSmithKline, Golub Capital, Handl Therapeutics, Insitro, Janssen Pharmaceuticals, Lundbeck, Merck & Co. Inc., Meso Scale Diagnostics, LLC, Neurocrine Biosciences, Pfizer Inc., Piramal Imaging, Prevail Therapeutics, F. Hoffmann-La Roche Ltd. and its affiliated company Genentech Inc., Sanofi Genzyme, Servier, Takeda Pharmaceutical Company, Teva Neuroscience Inc., UCB, Vanqua Bio, Verily Life Sciences, Voyager Therapeutics Inc., and Yumanity Therapeutics Inc.

Institutional Review Board Statement: The study was approved by the Ethics Committee of the University of Würzburg Medical Faculty (#121/14) on 15 September 2014. The use of human-derived samples at the Hebrew University of Jerusalem was approved by the Hebrew University's Ethics committee.

Informed Consent Statement: All study participants gave written informed consent to publish this paper.

Data Availability Statement: Data used in the preparation of this article were obtained from the Parkinson's Progression Markers Initiative (PPMI) database (www.ppmi-info.org/access-data-specimens/download-data (accessed on 1 March 2021)). For up-to-date information on the study, visit ppmi-info.org.

Acknowledgments: We gratefully acknowledge excellent technical support from Franziska Karl-Schöller, Daniela Urlaub, and Danilo Prtvar during gene expression analysis at the Department of Neurology, University of Würzburg. The authors further acknowledge technical support for RNA

sequencing from the team at the National Center for Genomic Technologies at the Hebrew University of Jerusalem. All listed individuals consented to the acknowledgments.

Conflicts of Interest: The authors declare no conflict of interest.

References

1. Wolfe, F.; Clauw, D.J.; Fitzcharles, M.-A.; Goldenberg, D.L.; Häuser, W.; Katz, R.L.; Mease, P.J.; Russell, A.S.; Russell, I.J.; Walitt, B. 2016 Revisions to the 2010/2011 fibromyalgia diagnostic criteria. *Semin. Arthritis Rheum.* **2016**, *46*, 319–329. [CrossRef] [PubMed]
2. Queiroz, L.P. Worldwide epidemiology of fibromyalgia. *Curr. Pain Headache Rep.* **2013**, *17*, 356. [CrossRef] [PubMed]
3. Weir, P.T.; Harlan, G.A.; Nkoy, F.L.; Jones, S.S.; Hegmann, K.T.; Gren, L.H.; Lyon, J.L. The incidence of fibromyalgia and its associated comorbidities: A population-based retrospective cohort study based on International Classification of Diseases, 9th Revision codes. *J. Clin. Rheumatol.* **2006**, *12*, 124–128. [CrossRef] [PubMed]
4. Wolfe, F.; Walitt, B.; Perrot, S.; Rasker, J.J.; Häuser, W. Fibromyalgia diagnosis and biased assessment: Sex, prevalence and bias. *PLoS ONE* **2018**, *13*, e0203755. [CrossRef] [PubMed]
5. Häuser, W.; Sarzi-Puttini, P.; Fitzcharles, M.-A. Fibromyalgia syndrome: Under-, over-and misdiagnosis. *Clin. Exp. Rheumatol.* **2019**, *37*, 90–97. [PubMed]
6. Littlejohn, G.; Guymer, E. Neurogenic inflammation in fibromyalgia. *Semin. Immunopathol.* **2018**, *40*, 291–300. [CrossRef]
7. Rodriguez-Pintó, I.; Agmon-Levin, N.; Howard, A.; Shoenfeld, Y. Fibromyalgia and cytokines. *Immunol. Lett.* **2014**, *161*, 200–203. [CrossRef]
8. Goebel, A.; Krock, E.; Gentry, C.; Israel, M.R.; Jurczak, A.; Urbina, C.M.; Sandor, K.; Vastani, N.; Maurer, M.; Cuhadar, U. Passive transfer of fibromyalgia symptoms from patients to mice. *J. Clin. Investig.* **2021**, *131*, e144201. [CrossRef]
9. Dolcino, M.; Tinazzi, E.; Puccetti, A.; Lunardi, C. Gene expression profiling in fibromyalgia indicates an autoimmune origin of the disease and opens new avenues for targeted therapy. *J. Clin. Med.* **2020**, *9*, 1814. [CrossRef]
10. Park, D.-J.; Lee, S.-S. New insights into the genetics of fibromyalgia. *Korean J. Intern. Med.* **2017**, *32*, 984. [CrossRef]
11. van Tilburg, M.A.; Parisien, M.; Boles, R.G.; Drury, G.L.; Smith-Voudouris, J.; Verma, V.; Khoury, S.; Chabot-Doré, A.-J.; Nackley, A.G.; Smith, S.B. A genetic polymorphism that is associated with mitochondrial energy metabolism increases risk of fibromyalgia. *Pain* **2020**, *161*, 2860–2871. [CrossRef] [PubMed]
12. Benlidayi, I.C. Role of inflammation in the pathogenesis and treatment of fibromyalgia. *Rheumatol. Int.* **2019**, *39*, 781–791. [CrossRef] [PubMed]
13. Grayston, R.; Czanner, G.; Elhadd, K.; Goebel, A.; Frank, B.; Üçeyler, N.; Malik, R.A.; Alam, U. A systematic review and meta-analysis of the prevalence of small fiber pathology in fibromyalgia: Implications for a new paradigm in fibromyalgia etiopathogenesis. *Semin. Arthritis Rheum.* **2019**, *48*, 933–940. [CrossRef] [PubMed]
14. Üçeyler, N.; Zeller, D.; Kahn, A.-K.; Kewenig, S.; Kittel-Schneider, S.; Schmid, A.; Casanova-Molla, J.; Reiners, K.; Sommer, C. Small fibre pathology in patients with fibromyalgia syndrome. *Brain* **2013**, *136*, 1857–1867. [CrossRef] [PubMed]
15. Martínez-Martínez, L.-A.; Mora, T.; Vargas, A.; Fuentes-Iniestra, M.; Martínez-Lavín, M. Sympathetic nervous system dysfunction in fibromyalgia, chronic fatigue syndrome, irritable bowel syndrome, and interstitial cystitis: A review of case-control studies. *J. Clin. Rheumatol.* **2014**, *20*, 146–150. [CrossRef]
16. Solano, C.; Martinez, A.; Becerril, L.; Vargas, A.; Figueroa, J.; Navarro, C.; Ramos-Remus, C.; Martinez-Lavin, M. Autonomic dysfunction in fibromyalgia assessed by the Composite Autonomic Symptoms Scale (COMPASS). *J. Clin. Rheumatol.* **2009**, *15*, 172–176. [CrossRef]
17. Wolfe, F.; Clauw, D.J.; Fitzcharles, M.A.; Goldenberg, D.L.; Katz, R.S.; Mease, P.; Russell, A.S.; Russell, I.J.; Winfield, J.B.; Yunus, M.B. The American College of Rheumatology preliminary diagnostic criteria for fibromyalgia and measurement of symptom severity. *Arthritis Care Res.* **2010**, *62*, 600–610. [CrossRef]
18. Tracey, K.J. The inflammatory reflex. *Nature* **2002**, *420*, 853–859. [CrossRef]
19. Pavlov, V.A.; Tracey, K.J. The cholinergic anti-inflammatory pathway. *Brain Behav. Immun.* **2005**, *19*, 493–499. [CrossRef]
20. Ofek, K.; Soreq, H. Cholinergic involvement and manipulation approaches in multiple system disorders. *Chem. Biol. Interact.* **2013**, *203*, 113–119. [CrossRef]
21. Kawashima, K.; Fujii, T.; Moriwaki, Y.; Misawa, H. Critical roles of acetylcholine and the muscarinic and nicotinic acetylcholine receptors in the regulation of immune function. *Life Sci.* **2012**, *91*, 1027–1032. [CrossRef] [PubMed]
22. Fujii, T.; Mashimo, M.; Moriwaki, Y.; Misawa, H.; Ono, S.; Horiguchi, K.; Kawashima, K. Expression and function of the cholinergic system in immune cells. *Front. Immunol.* **2017**, *8*, 1085. [CrossRef] [PubMed]
23. Rosas-Ballina, M.; Tracey, K. Cholinergic control of inflammation. *J. Intern. Med.* **2009**, *265*, 663–679. [CrossRef] [PubMed]
24. Fujii, T.; Mashimo, M.; Moriwaki, Y.; Misawa, H.; Ono, S.; Horiguchi, K.; Kawashima, K. Physiological functions of the cholinergic system in immune cells. *J. Pharmacol. Sci.* **2017**, *134*, 1–21. [CrossRef]
25. Wåhlén, K.; Ernberg, M.; Kosek, E.; Mannerkorpi, K.; Gerdle, B.; Ghafouri, B. Significant correlation between plasma proteome profile and pain intensity, sensitivity, and psychological distress in women with fibromyalgia. *Sci. Rep.* **2020**, *10*, 12508. [CrossRef]
26. Martins, D.F.; Viseux, F.J.; Salm, D.C.; Ribeiro, A.C.A.; da Silva, H.K.L.; Seim, L.A.; Bittencourt, E.B.; Bianco, G.; Moré, A.O.O.; Reed, W.R. The role of the vagus nerve in fibromyalgia syndrome. *Neurosci. Biobehav. Rev.* **2021**, *131*, 1136–1149. [CrossRef]

27. Üçeyler, N.; Häuser, W.; Sommer, C. Systematic review with meta-analysis: Cytokines in fibromyalgia syndrome. *BMC Musculoskelet. Disord.* **2011**, *12*, 245. [CrossRef]
28. O'Mahony, L.F.; Srivastava, A.; Mehta, P.; Ciurtin, C. Is fibromyalgia associated with a unique cytokine profile? A systematic review and meta-analysis. *Rheumatology* **2021**, *60*, 2602–2614. [CrossRef]
29. Vishnoi, A.; Rani, S. MiRNA Biogenesis and Regulation of Diseases: An Overview. *Methods Mol. Biol.* **2017**, *1509*, 1–10. [CrossRef]
30. Fabian, M.R.; Sonenberg, N.; Filipowicz, W. Regulation of mRNA translation and stability by microRNAs. *Annu. Rev. Biochem.* **2010**, *79*, 351–379. [CrossRef]
31. Andersen, H.H.; Duroux, M.; Gazerani, P. MicroRNAs as modulators and biomarkers of inflammatory and neuropathic pain conditions. *Neurobiol. Dis.* **2014**, *71*, 159–168. [CrossRef] [PubMed]
32. Soreq, H. Checks and balances on cholinergic signaling in brain and body function. *Trends Neurosci.* **2015**, *38*, 448–458. [CrossRef] [PubMed]
33. Meydan, C.; Shenhar-Tsarfaty, S.; Soreq, H. MicroRNA regulators of anxiety and metabolic disorders. *Trends Mol. Med.* **2016**, *22*, 798–812. [CrossRef] [PubMed]
34. Nadorp, B.; Soreq, H. Predicted overlapping microRNA regulators of acetylcholine packaging and degradation in neuroinflammation-related disorders. *Front. Mol. Neurosci.* **2014**, *7*, 9. [CrossRef]
35. Evdokimov, D.; Frank, J.; Klitsch, A.; Unterecker, S.; Warrings, B.; Serra, J.; Papagianni, A.; Saffer, N.; Meyer zu Altenschildesche, C.; Kampik, D. Reduction of skin innervation is associated with a severe fibromyalgia phenotype. *Ann. Neurol.* **2019**, *86*, 504–516. [CrossRef]
36. Von Korff, M.; Ormel, J.; Keefe, F.J.; Dworkin, S.F. Grading the severity of chronic pain. *Pain* **1992**, *50*, 133–149. [CrossRef]
37. Andrews, S. FastQC: A Quality Control Tool for High Throughput Sequence Data. 2010. Available online: https://www.bioinformatics.babraham.ac.uk/projects/fastqc/ (accessed on 3 April 2022).
38. Griffiths-Jones, S.; Saini, H.K.; Van Dongen, S.; Enright, A.J. miRBase: Tools for microRNA genomics. *Nucleic Acids Res.* **2007**, *36*, D154–D158. [CrossRef]
39. Wang, W.-C.; Lin, F.-M.; Chang, W.-C.; Lin, K.-Y.; Huang, H.-D.; Lin, N.-S. miRExpress: Analyzing high-throughput sequencing data for profiling microRNA expression. *BMC Bioinform.* **2009**, *10*, 328. [CrossRef]
40. Lobentanzer, S.; Hanin, G.; Klein, J.; Soreq, H. Integrative transcriptomics reveals sexually dimorphic control of the cholinergic/neurokine interface in schizophrenia and bipolar disorder. *Cell Rep.* **2019**, *29*, 764–777.e765. [CrossRef]
41. Shannon, P.; Markiel, A.; Ozier, O.; Baliga, N.S.; Wang, J.T.; Ramage, D.; Amin, N.; Schwikowski, B.; Ideker, T. Cytoscape: A software environment for integrated models of biomolecular interaction networks. *Genome Res.* **2003**, *13*, 2498–2504. [CrossRef]
42. Fehlmann, T.; Backes, C.; Kahraman, M.; Haas, J.; Ludwig, N.; Posch, A.E.; Würstle, M.L.; Hübenthal, M.; Franke, A.; Meder, B. Web-based NGS data analysis using miRMaster: A large-scale meta-analysis of human miRNAs. *Nucleic Acids Res.* **2017**, *45*, 8731–8744. [CrossRef] [PubMed]
43. Kozomara, A.; Birgaoanu, M.; Griffiths-Jones, S. miRBase: From microRNA sequences to function. *Nucleic Acids Res.* **2019**, *47*, D155–D162. [CrossRef] [PubMed]
44. Langmead, B.; Trapnell, C.; Pop, M.; Salzberg, S.L. Ultrafast and memory-efficient alignment of short DNA sequences to the human genome. *Genome Biol.* **2009**, *10*, R25. [CrossRef]
45. Andersen, C.L.; Jensen, J.L.; Ørntoft, T.F. Normalization of real-time quantitative reverse transcription-PCR data: A model-based variance estimation approach to identify genes suited for normalization, applied to bladder and colon cancer data sets. *Cancer Res.* **2004**, *64*, 5245–5250. [CrossRef] [PubMed]
46. Ellman, G.L.; Courtney, K.D.; Andres Jr, V.; Featherstone, R.M. A new and rapid colorimetric determination of acetylcholinesterase activity. *Biochem. Pharmacol.* **1961**, *7*, 88–95. [CrossRef]
47. Love, M.I.; Huber, W.; Anders, S. Moderated estimation of fold change and dispersion for RNA-seq data with DESeq2. *Genome Biol.* **2014**, *15*, 550. [CrossRef]
48. R Core Team. *R: A Language and Environment for Statistical Computing*; R Foundation for Statistical Computing: Vienna, Austria, 2019. Available online: https://www.scirp.org/(S(lz5mqp453edsnp55rrgjct55))/reference/ReferencesPapers.aspx?ReferenceID=2631126 (accessed on 3 April 2022).
49. Robinson, M.D.; McCarthy, D.J.; Smyth, G.K. edgeR: A Bioconductor package for differential expression analysis of digital gene expression data. *Bioinformatics* **2010**, *26*, 139–140. [CrossRef]
50. McCarthy, D.J.; Chen, Y.; Smyth, G.K. Differential expression analysis of multifactor RNA-Seq experiments with respect to biological variation. *Nucleic Acids Res.* **2012**, *40*, 4288–4297. [CrossRef]
51. Venables, W.; Ripley, B. *Modern Applied Statistics*; Fourth, S., Ed.; Springer: New York, NY, USA, 2002.
52. Tang, Y.; Horikoshi, M.; Li, W. ggfortify: Unified interface to visualize statistical results of popular R packages. *R J.* **2016**, *8*, 474. [CrossRef]
53. Wickham, H. *ggplot2: Elegant Graphics for Data Analysis*; Springer: New York, NY, USA, 2016. Available online: https://cran.r-project.org/web/packages/ggplot2/citation.html (accessed on 27 February 2022).
54. Martin, C. ggConvexHull: Add a Convex Hull Geom to ggplot2. R Package Version 0.1. 0 2017. Available online: http://github.com/cmartin/ggConvexHull (accessed on 27 February 2022).

55. Juzenas, S.; Venkatesh, G.; Hübenthal, M.; Hoeppner, M.P.; Du, Z.G.; Paulsen, M.; Rosenstiel, P.; Senger, P.; Hofmann-Apitius, M.; Keller, A. A comprehensive, cell specific microRNA catalogue of human peripheral blood. *Nucleic Acids Res.* **2017**, *45*, 9290–9301. [CrossRef]
56. Buhmann, C.; Wrobel, N.; Grashorn, W.; Fruendt, O.; Wesemann, K.; Diedrich, S.; Bingel, U. Pain in Parkinson disease: A cross-sectional survey of its prevalence, specifics, and therapy. *J. Neurol.* **2017**, *264*, 758–769. [CrossRef] [PubMed]
57. Uhlen, M.; Karlsson, M.J.; Zhong, W.; Tebani, A.; Pou, C.; Mikes, J.; Lakshmikanth, T.; Forsström, B.; Edfors, F.; Odeberg, J. A genome-wide transcriptomic analysis of protein-coding genes in human blood cells. *Science* **2019**, *366*, eaax9198. [CrossRef] [PubMed]
58. Maharshak, N.; Shenhar-Tsarfaty, S.; Aroyo, N.; Orpaz, N.; Guberman, I.; Canaani, J.; Halpern, Z.; Dotan, I.; Berliner, S.; Soreq, H. MicroRNA-132 modulates cholinergic signaling and inflammation in human inflammatory bowel disease. *Inflamm. Bowel Dis.* **2013**, *19*, 1346–1353. [CrossRef] [PubMed]
59. Simchovitz, A.; Heneka, M.T.; Soreq, H. Personalized genetics of the cholinergic blockade of neuroinflammation. *J. Neurochem.* **2017**, *142*, 178–187. [CrossRef]
60. Winek, K.; Lobentanzer, S.; Nadorp, B.; Dubnov, S.; Dames, C.; Jagdmann, S.; Moshitzky, G.; Hotter, B.; Meisel, C.; Greenberg, D.S. Transfer RNA fragments replace microRNA regulators of the cholinergic poststroke immune blockade. *Proc. Natl. Acad. Sci. USA* **2020**, *117*, 32606–32616. [CrossRef]
61. Dagytė, G.; Den Boer, J.A.; Trentani, A. The cholinergic system and depression. *Behav. Brain Res.* **2011**, *221*, 574–582. [CrossRef]
62. Cerdá-Olmedo, G.; Mena-Durán, A.V.; Monsalve, V.; Oltra, E. Identification of a MicroRNA Signature for the Diagnosis of Fibromyalgia. *PLoS ONE* **2015**, *10*, e0121903. [CrossRef]
63. Masotti, A.; Baldassarre, A.; Guzzo, M.P.; Iannuccelli, C.; Barbato, C.; Di Franco, M. Circulating microRNA profiles as liquid biopsies for the characterization and diagnosis of fibromyalgia syndrome. *Mol. Neurobiol.* **2017**, *54*, 7129–7136. [CrossRef]
64. Bjersing, J.L.; Bokarewa, M.I.; Mannerkorpi, K. Profile of circulating microRNAs in fibromyalgia and their relation to symptom severity: An exploratory study. *Rheumatol. Int.* **2015**, *35*, 635–642. [CrossRef]
65. Bruno, I.G.; Karam, R.; Huang, L.; Bhardwaj, A.; Lou, C.H.; Shum, E.Y.; Song, H.-W.; Corbett, M.A.; Gifford, W.D.; Gecz, J. Identification of a microRNA that activates gene expression by repressing nonsense-mediated RNA decay. *Mol. Cell* **2011**, *42*, 500–510. [CrossRef]
66. Popp, M.W.; Maquat, L.E. Attenuation of nonsense-mediated mRNA decay facilitates the response to chemotherapeutics. *Nat. Commun.* **2015**, *6*, 6632. [CrossRef] [PubMed]
67. Hanan, M.; Simchovitz, A.; Yayon, N.; Vaknine, S.; Cohen-Fultheim, R.; Karmon, M.; Madrer, N.; Rohrlich, T.M.; Maman, M.; Bennett, E.R. A Parkinson's disease Circ RNA s Resource reveals a link between circ SLC 8A1 and oxidative stress. *EMBO Mol. Med.* **2020**, *12*, e11942. [CrossRef] [PubMed]
68. O'neill, L.A.; Sheedy, F.J.; McCoy, C.E. MicroRNAs: The fine-tuners of Toll-like receptor signalling. *Nat. Rev. Immunol.* **2011**, *11*, 163–175. [CrossRef] [PubMed]
69. Kerschensteiner, M.; Gallmeier, E.; Behrens, L.; Leal, V.V.; Misgeld, T.; Klinkert, W.E.; Kolbeck, R.; Hoppe, E.; Oropeza-Wekerle, R.-L.; Bartke, I. Activated human T cells, B cells, and monocytes produce brain-derived neurotrophic factor in vitro and in inflammatory brain lesions: A neuroprotective role of inflammation? *J. Exp. Med.* **1999**, *189*, 865–870. [CrossRef] [PubMed]
70. Lee, B.-H.; Kim, Y.-K. The roles of BDNF in the pathophysiology of major depression and in antidepressant treatment. *Psychiatry Investig.* **2010**, *7*, 231. [CrossRef]
71. Nugraha, B.; Korallus, C.; Gutenbrunner, C. Serum level of brain-derived neurotrophic factor in fibromyalgia syndrome correlates with depression but not anxiety. *Neurochem. Int.* **2013**, *62*, 281–286. [CrossRef]
72. Laske, C.; Stransky, E.; Eschweiler, G.W.; Klein, R.; Wittorf, A.; Leyhe, T.; Richartz, E.; Köhler, N.; Bartels, M.; Buchkremer, G. Increased BDNF serum concentration in fibromyalgia with or without depression or antidepressants. *J. Psychiatr. Res.* **2007**, *41*, 600–605. [CrossRef]
73. Baumeister, D.; Eich, W.; Saft, S.; Geisel, O.; Hellweg, R.; Finn, A.; Svensson, C.I.; Tesarz, J. No evidence for altered plasma NGF and BDNF levels in fibromyalgia patients. *Sci. Rep.* **2019**, *9*, 13667. [CrossRef]
74. Ramakrishnan, S.N.; Muscat, G.E. The orphan Rev-erb nuclear receptors: A link between metabolism, circadian rhythm and inflammation? *Nucl. Recept. Signal.* **2006**, *4*, e009. [CrossRef]
75. Gibbs, J.E.; Blaikley, J.; Beesley, S.; Matthews, L.; Simpson, K.D.; Boyce, S.H.; Farrow, S.N.; Else, K.J.; Singh, D.; Ray, D.W. The nuclear receptor REV-ERBα mediates circadian regulation of innate immunity through selective regulation of inflammatory cytokines. *Proc. Natl. Acad. Sci. USA* **2012**, *109*, 582–587. [CrossRef]
76. Scheiermann, C.; Kunisaki, Y.; Frenette, P.S. Circadian control of the immune system. *Nat. Rev. Immunol.* **2013**, *13*, 190–198. [CrossRef] [PubMed]
77. Dimitrov, S.; Benedict, C.; Heutling, D.; Westermann, J.; Born, J.; Lange, T. Cortisol and epinephrine control opposing circadian rhythms in T cell subsets. *Blood* **2009**, *113*, 5134–5143. [CrossRef] [PubMed]
78. Crofford, L.J.; Young, E.A.; Engleberg, N.C.; Korszun, A.; Brucksch, C.B.; McClure, L.A.; Brown, M.B.; Demitrack, M.A. Basal circadian and pulsatile ACTH and cortisol secretion in patients with fibromyalgia and/or chronic fatigue syndrome. *Brain Behav. Immun.* **2004**, *18*, 314–325. [CrossRef]
79. Weissbecker, I.; Floyd, A.; Dedert, E.; Salmon, P.; Sephton, S. Childhood trauma and diurnal cortisol disruption in fibromyalgia syndrome. *Psychoneuroendocrinology* **2006**, *31*, 312–324. [CrossRef] [PubMed]

80. Chen, W.; Ten Dijke, P. Immunoregulation by members of the TGFβ superfamily. *Nat. Rev. Immunol.* **2016**, *16*, 723–740. [CrossRef] [PubMed]
81. Robson, N.C.; Hidalgo, L.; McAlpine, T.; Wei, H.; Martínez, V.G.; Entrena, A.; Melen, G.J.; MacDonald, A.S.; Phythian-Adams, A.; Sacedón, R. Optimal effector functions in human natural killer cells rely upon autocrine bone morphogenetic protein signaling. *Cancer Res.* **2014**, *74*, 5019–5031. [CrossRef]
82. Eixarch, H.; Calvo-Barreiro, L.; Costa, C.; Reverter-Vives, G.; Castillo, M.; Gil, V.; Del Río, J.A.; Montalban, X.; Espejo, C. Inhibition of the BMP Signaling Pathway Ameliorated Established Clinical Symptoms of Experimental Autoimmune Encephalomyelitis. *Neurotherapeutics* **2020**, *17*, 1988–2003. [CrossRef]
83. Jones, S.A.; Jenkins, B.J. Recent insights into targeting the IL-6 cytokine family in inflammatory diseases and cancer. *Nat. Rev. Immunol.* **2018**, *18*, 773–789. [CrossRef]
84. Malemud, C.J.; Pearlman, E. Targeting JAK/STAT signaling pathway in inflammatory diseases. *Curr. Signal Transduct. Ther.* **2009**, *4*, 201–221. [CrossRef]
85. Antebi, Y.E.; Linton, J.M.; Klumpe, H.; Bintu, B.; Gong, M.; Su, C.; McCardell, R.; Elowitz, M.B. Combinatorial signal perception in the BMP pathway. *Cell* **2017**, *170*, 1184–1196.e1124. [CrossRef]
86. Eixarch, H.; Calvo-Barreiro, L.; Montalban, X.; Espejo, C. Bone morphogenetic proteins in multiple sclerosis: Role in neuroinflammation. *Brain Behav. Immun.* **2018**, *68*, 1–10. [CrossRef] [PubMed]
87. Yoshioka, Y.; Ono, M.; Osaki, M.; Konishi, I.; Sakaguchi, S. Differential effects of inhibition of bone morphogenic protein (BMP) signalling on T-cell activation and differentiation. *Eur. J. Immunol.* **2012**, *42*, 749–759. [CrossRef] [PubMed]
88. Verma, V.; Drury, G.L.; Parisien, M.; Özdağ Acarli, A.N.; Al-Aubodah, T.A.; Nijnik, A.; Wen, X.; Tugarinov, N.; Verner, M.; Klares, R., 3rd; et al. Unbiased immune profiling reveals a natural killer cell-peripheral nerve axis in fibromyalgia. *Pain* **2021**. [CrossRef] [PubMed]
89. Taylor, A.G.; Fischer-White, T.G.; Anderson, J.G.; Adelstein, K.E.; Murugesan, M.; Lewis, J.E.; Scott, M.M.; Gaykema, R.P.; Goehler, L.E. Stress, Inflammation and Pain: A Potential Role for Monocytes in Fibromyalgia-related Symptom Severity. *Stress Health* **2016**, *32*, 503–513. [CrossRef] [PubMed]
90. Nugraha, B.; Scheibe, R.; Korallus, C.; Gaestel, M.; Gutenbrunner, C. The p38/MK2 Axis in Monocytes of Fibromyalgia Syndrome Patients: An Explorative Study. *Medicina* **2021**, *57*, 396. [CrossRef]
91. Moore, R.A.; Derry, S.; Aldington, D.; Cole, P.; Wiffen, P.J. Amitriptyline for neuropathic pain and fibromyalgia in adults. *Cochrane Database Syst. Rev.* **2012**, *12*, Cd008242. [CrossRef]
92. Häuser, W.; Wolfe, F.; Tölle, T.; Üçeyler, N.; Sommer, C. The role of antidepressants in the management of fibromyalgia syndrome. *CNS Drugs* **2012**, *26*, 297–307. [CrossRef]
93. Kirschner, M.B.; Edelman, J.J.B.; Kao, S.C.-H.; Vallely, M.P.; Van Zandwijk, N.; Reid, G. The impact of hemolysis on cell-free microRNA biomarkers. *Front. Genet.* **2013**, *4*, 94. [CrossRef]
94. Baechler, E.; Batliwalla, F.; Karypis, G.; Gaffney, P.; Moser, K.; Ortmann, W.; Espe, K.; Balasubramanian, S.; Hughes, K.; Chan, J. Expression levels for many genes in human peripheral blood cells are highly sensitive to ex vivo incubation. *Genes Immun.* **2004**, *5*, 347–353. [CrossRef]
95. O'Connell, R.M.; Taganov, K.D.; Boldin, M.P.; Cheng, G.; Baltimore, D. MicroRNA-155 is induced during the macrophage inflammatory response. *Proc. Natl. Acad. Sci. USA* **2007**, *104*, 1604–1609. [CrossRef]
96. Simone, N.L.; Soule, B.P.; Ly, D.; Saleh, A.D.; Savage, J.E.; DeGraff, W.; Cook, J.; Harris, C.C.; Gius, D.; Mitchell, J.B. Ionizing radiation-induced oxidative stress alters miRNA expression. *PLoS ONE* **2009**, *4*, e6377. [CrossRef] [PubMed]
97. van der Sijde, F.; Li, Y.; Schraauwen, R.; de Koning, W.; van Eijck, C.H.; Mustafa, D.A. RNA from stabilized whole blood enables more comprehensive immune gene expression profiling compared to RNA from peripheral blood mononuclear cells. *PLoS ONE* **2020**, *15*, e0235413. [CrossRef] [PubMed]
98. Asare, A.L.; Kolchinsky, S.A.; Gao, Z.; Wang, R.; Raddassi, K.; Bourcier, K.; Seyfert-Margolis, V. Differential gene expression profiles are dependent upon method of peripheral blood collection and RNA isolation. *BMC Genom.* **2008**, *9*, 474. [CrossRef] [PubMed]
99. Shen, Y.; Yu, X.; Zhu, L.; Li, T.; Yan, Z.; Guo, J. Transfer RNA-derived fragments and tRNA halves: Biogenesis, biological functions and their roles in diseases. *J. Mol. Med.* **2018**, *96*, 1167–1176. [CrossRef] [PubMed]

7.2. Chapter II: Systemic up- and peripheral downregulation of microRNAs and transfer RNA fragments in fibromyalgia syndrome

Systemic up- and peripheral downregulation of microRNAs and transfer RNA fragments in fibromyalgia syndrome

Christoph Erbacher[1], Nimrod Madrer[2,3], Gilli Moshitzky [2,3], Sophia Weinbender[1], Danilo Prtvar[1], Dimitar Evdokimov[1], Stefan Unterecker[4], Claudia Sommer[1], David S. Greenberg[2,3], Hermona Soreq[2,3#], Nurcan Üçeyler [1#]

[1]Department of Neurology, University of Würzburg, 97080 Würzburg, Germany

[2] The Edmond & Lily Safra Center for Brain Sciences, The Hebrew University of Jerusalem, Jerusalem 9190401, Israel

[3]The Alexander Silberman Institute of Life Sciences, The Hebrew University of Jerusalem, Jerusalem 9190401, Israel

[4]Department of Psychiatry, Psychosomatics, and Psychotherapy, University of Würzburg, 97080 Würzburg Germany

[#]Joint senior authorship.

In preparation

June, 30 2022

Systemic up- and peripheral downregulation of microRNAs and transfer RNA fragments in fibromyalgia syndrome

Christoph Erbacher[1], Nimrod Madrer[2,3], Gilli Moshitzky [2,3], Sophia Weinbender[1], Danilo Prtvar[1], Dimitar Evdokimov[1], Stefan Unterecker[4] Claudia Sommer[1], David S. Greenberg[2,3], Hermona Soreq[2,3#], Nurcan Üçeyler[1*#]

[1]Department of Neurology, University of Würzburg, Josef-Schneider-Str. 11, 97080 Würzburg

[2]The Edmond & Lily Safra Center for Brain Sciences, The Hebrew University of Jerusalem, Jerusalem 9190401, Israel

[3]The Alexander Silberman Institute of Life Sciences, The Hebrew University of Jerusalem, Jerusalem 9190401, Israel

[4]Department of Psychiatry, Psychosomatics, and Psychotherapy, University of Würzburg, Germany

[#]Joint senior authorship.

***Corresponding author:**

Prof. Dr. Nurcan Üçeyler, MD

Department of Neurology, University of Würzburg,

Josef-Schneider-Str. 11, 97080 Würzburg, Germany

Phone: +49 931 201 23542

Fax: +49 931 201 623542

e-mail address: ueceyler_n@ukw.de

Abstract

Fibromyalgia syndrome (FMS) is a frequent chronic widespread pain condition. FMS causes high social and psychological burden and health-economic costs due to the lack of objective diagnostic criteria and identification of the underlying pathomechanisms. Small RNAs are post-transcriptional key modulators of cellular pathways which might be instrumental as biomarkers. Systemic alterations in blood and the peripheral nervous system in terms of small nerve fiber pathology are established in FMS. Here, we investigated complete small RNA transcriptomes at systemic and local level.

53 female FMS patients were recruited according to current diagnostic criteria along with matched healthy controls (hCO) and patients with major depression and chronic physical widespread pain serving as disease controls (dCO). Patients underwent detailed medical interview, questionnaire assessment, and neurological examination. Via small RNA sequencing, transcriptomes of FMS versus hCO from stabilized whole blood RNA (31 vs 17) and primary patient-derived keratinocyte cultures (32 vs 14) were compared. Small RNA representatives and pathway analysis-derived mRNA targets were validated by qRT-PCR compared to hCO and dCO. Finally, the capability of small RNAs as correlates for clinical parameter was assessed.

Small RNAs in FMS were predominantly upregulated in whole blood, while downregulated in keratinocytes. Deregulated blood tRNA fragments (tRFs) showed comparable length to microRNAs (miRs), however, altered keratinocyte tRFs consisted mostly of longer fragments. In blood, hsa-miR-575-5p, hsa-miR-182-5p, and tRF-20-40KK5Y39 distinguished FMS from hCO and dCO. FoxO pathway and RNA processing/splicing/translation were identified as relevant pathways in blood. In keratinocytes, hsa-miR503-5p expression was reduced. Small RNA gene targets indicated modulation of epithelial function, e.g., via adherens and adhesion pathways and TGFB1 expression was diminished in FMS keratinocytes.

For both sites, small RNAs correlated predominantly with clinical widespread pain.

We present distinct changes of global small RNA transcriptomes in female FMS patients on systemic and local level. Altered tRFs may exert miR-like functions in blood but diverging functions in keratinocytes. Mirs and tRFs are associated with disease relevant pathways and may pave the road for objective diagnostic tools in FMS.

Introduction

Despite decades of research, the mechanisms underlying development and persistence of chronic and widespread pain as the cardinal symptom of fibromyalgia syndrome (FMS) are poorly understood.[1,2] Options for standardized diagnosis are limited, since no objective diagnostic criteria exists and socioeconomic costs are high, due to a lack of effective treatment that mostly falls short of meeting patients` needs.[3,4] Morphological and functional changes at central and peripheral nervous system (CNS, PNS) level correlating with FMS have been observed.[5] Higher neuronal activity in sensory regions of the brain, cerebral hypoperfusion, impairment of the dopaminergic system, and regional decrease of grey matter volume were reported in FMS patients compared to healthy controls.[6] However, these findings lack specificity and may generally be found in chronic pain disorders.[7,8] Systemically, no definite cytokine, autoantibody target, or immune cell signature was identified so far despite reports on a pro-inflammatory profile in FMS patients.[9-11] In the PNS, one consistent finding in up to two thirds of women with FMS is small fiber pathology (SFP) manifesting as altered sensory perception, burning pain, and reduced intraepidermal nerve fiber density (IENFD), the latter also correlating with FMS severity.[12,13] Importantly, keratinocytes, encompassing and ensheathing IENF in the epidermis, were identified as active players in somatosensory and nociceptive signal transduction.[14-17] Still, SFP is also not specific for FMS and the underlying mechanisms are diverse and incompletely understood.[18] The currently most discussed pathophysiological model of FMS proposes peripherally triggered or maintained contributing factors that lead to a sustained centralized pain state.[19] Therefore, identification of such peripheral processes may provide an opportunity for the development of objective biomarkers and accessible therapeutic sites for FMS treatment. MicroRNAs (miRs) represent a class of non-coding RNAs and are discussed as promising clinical biomarkers and disease modifiers.[20,21]

Previously, we and others found changes in transcription levels of miRs, both in blood and skin samples of FMS patients.[22-25] However, these studies were limited either by the application of microarrays with low dynamic range, sensitivity, specificity, and number of detectable miRs compared to RNA sequencing, or by assessment of single pre-selected miRs via qRT-PCR. Mechanistically, miRs act as posttranscriptional gene regulators, via complementary binding against subsequent mRNA and subsequent degradation or translational repression by interaction with RNA-induced silencing complex (RISC) and argonaute 2 (Ago2).[26] Importantly, a new class of small RNA derived from transfer RNAs (tRNA) and named tRNA fragments (tRFs) increasingly attracts attention.[27] TRFs can drive mRNA suppression in a miR manner, but may exert a range of additional effects independent of miR.[28,29] The functional variability of tRF is tied to their heterogeneous origin (nuclear tRNAs or mitochondrial tRNAs and the particular tRNA part) and nucleotide (nt) length ranging from 18-50 nt.[30]

In this study, we aimed to uncover complete miR and tRF expression profiles in whole blood and epidermal keratinocytes obtained from FMS patients compared to healthy and disease controls via small RNA sequencing and determine modulated gene pathways.

Materials and methods

Study participants

Study participants were part of a previously characterized cohort.[12] In short, female FMS patients, recruited according to the 1990 and 2010 diagnostic criteria of the American College of Rheumatology (ACR), matching healthy controls (hCO), and patients with major depression as disease control (dCO) were recruited at the Department of Neurology and the Department of Psychiatry, University of Würzburg. The diagnosis of major depression was made based on the Diagnostic and Statistical Manual of Mental Disorders-IV (S.U.). The second inclusion criterion

for disease controls was chronic widespread pain, comprising pain for ≥3 months in multiple body regions. The study was approved by the Ethics Committee of the University of Würzburg Medical Faculty (#121/14) and all study participants gave written informed consent.

FMS and dCO patients underwent complete neurological examination. The study cohort was assessed with several standardized questionnaires, including the Graded Chronic Pain Scale (GCPS; 6 months recall),[31] the Fibromyalgia Impact Questionnaire (FIQ),[32] and the German version of the Neuropathic Pain Symptom Inventory (NPSI; 24 hours recall).[33,34] The "Allgemeine Depressionsskala"(ADS) was used for assessing depressive symptoms.[35] The widespread pain index (WPI) was only applied for FMS patients[36]. Pain intensity was reported on an 11-point numeric rating scale with 0 = no pain and 10 = worst pain.[12] To exclude confounding factors and other etiologies of pain in FMS laboratory tests were performed as previously reported.[12]

Biomaterial collection

Peripheral blood-derived stabilized RNA collected via Tempus Tubes was acquired, as previously described.[37] Skin samples were obtained from the upper thigh and lower leg of study participants via punch biopsies (hCO, FMS 6-mm and dCO 3-mm punch) following a standardized procedure to assess IENFD. [38] In case of FMS and hCO, primary keratinocytes were additionally obtained from upper thigh biopsies via an established protocol[38]. In brief, the epidermis was manually dissected from the dermis and small pieces were placed in 25-cm^2 cell culture flasks, bedewed with DMEM medium (DMEM/F12, 120 U/ml penicillin, 100 µg/ml streptomycin [all Thermo Fisher Scientific, Waltham, MA, USA], and 10% FCS [Merck, Darmstadt, Germany]). Upon outgrowth of basal keratinocytes, medium was changed to keratinocyte medium (EpiLife Medium supplemented with 1% EpiLife defined growth

supplement, 120 U/ml penicillin, 100 µg/ml streptomycin, [all Thermo Fischer Scientific, Waltham, MA, USA]). Medium was changed every 3-4 days. Keratinocytes were split into the next passage before reaching confluence via TrypLE Express (Thermo Fisher Scientific, Waltham, MA, USA). Total RNA was extracted after one passage by lysis of cells with Qiazol and the miRNeasy Mini Kit (Qiagen, Hilden, Germany). A NanoDrop™ One (Thermo Fisher Scientific, Waltham, MA, USA) was used to check RNA quantity and quality and samples were stored at -80°C until further processing.

Small RNA sequencing

Small RNA-seq was conducted as previously described.[37] Briefly, 300 ng RNA per sample were used for library preparation via NEB-Next® Multiplex Small RNA Library Prep Kit for Illumina® (Index Primers 1-48; NEB-E7560S; New England Biolabs, Ipswich, MA, USA) at the National Center for Genomic Technologies at the Hebrew University of Jerusalem, Israel. For next generation short RNA-sequencing, the Illumina NextSeq 500 was used with two Illumina NextSeq 500/550 High Output Kit v2.5 (75 Cycles) flow cells (20024906) (all Illumina, San Diego, CA, USA). Short RNA FASTQ files were checked for quality using FastQC[39] and then adaptors were removed using FLEXBAR[40] according to pipelines' manuals. Output (adaptor-less) fastq files were aligned to miRNAs using miRExpress[42] or to tRFs using MINT-map.[41] Differential expression (DE) analysis was done using DESeq2[43] and all visualizations were done using ggplot2[44] in R.[45] In case of keratinocyte tRF analysis via DESeq2, the raw counts of six hCO and three FMS samples and controls were excluded from analysis.

Pathway analysis and gene target selection

For prediction of gene pathways modified by altered miRs, we applied mirPath v.3 (DIANA tools; https://dianalab.e-ce.uth.gr/html/mirpathv3/index.php?r=mirpath; assessed at 04.05.2022).

166 [46] Three miR-mRNA interaction prediction tools, Tarbase v7.0, TargetScan (with mirPath v.3
167 default settings), and microT-CDS v5.0 (with mirPath v.3 default threshold) were used and the
168 underlying KEGG and Gene ontology for biological processes (GO:BP) pathways determined via
169 genes union. Only miRs with a log2 fold change of ≤ ±0.5 were applied, both for whole blood
170 and keratinocyte pathway analysis. Pathways with FDR corrected $p<0.05$ were further analyzed.
171 Currently, few databases are available for tRF-mRNA interaction. Therefore, we only used
172 tRFTar (http://trftars.cmuzhenninglab.org:3838/tar/; assessed at 04.05.2022)[47] for potential tRF
173 targeted gene transcripts and pathways. All tRF and target element types were included, advanced
174 options "only when tRF highly expressed" and "only co-expressing TGI" deactivated. Only genes
175 targeted by at least three tRFs were considered to condense the number of associated pathways
176 for blood tRFs, while all gene targets were included for keratinocyte tRFs. All DE tRFs were
177 applied, since all transcripts had a log2 fold change of ≤ ±0.5. As for miRs, we analyzed KEGG
178 and GO:BP pathways for tRF from whole blood and keratinocyte derived RNA.

179 **Small RNA size selection**

180 Since total RNA extracted samples contain not only tRF but also full length tRNA transcripts, a
181 size selection step was carried out prior to qRT-PCR for tRF quantification.[48] One µg of RNA
182 adjusted to 12.5 µl with ddH^2O was mixed 1:1 with loading buffer II (Thermo Fisher Scientific,
183 Waltham, MA, USA) and incubated at 85°C for 5 min in a Primus 96 Thermo cycler (Peqlab,
184 Erlangen, Germany).
185

186 Low range ssRNA ladder (50-1000 nt long, New England BioLabs, Ipswich, MA, USA) was
187 incubated at 90°C for 5 min and a microRNA ladder (17-25 nt long, New England BioLabs,
188 Ipswich, MA, USA) incubated at 95°C for 5 min and kept on ice afterwards. Precast 15% Mini-

PROTEAN® TBE-Urea Gels (10 well, 30 µl; Biorad, Hercules, California, USA) were inserted in a Protean electrophoresis cell (Biorad, Hercules, CA, USA), filled with 0.5x tris-borated buffer (TBE, Thermo Fisher Scientific, Waltham, MA, USA) and respective wells loaded with both ladders and 25 µL of total RNA samples. Gels were run at 150 V for 50 min and subsequently incubated in in X0.5 TBE (Biorad, Hercules, CA, USA) buffer containing 1:6000 Syber (Thermo Fisher Scientific, Waltham, MA, USA) at RT on a shaker for 12 min. A gel docu system (Intas Science Imaging, Göttingen, Germany) was used to cut out gel pieces with sterile scalpels between 17-50 nt for isolation of small RNAs including tRFs and miRs. Gels were incubated in 810 µl of 3M NaCl over-night at 4°C under mild shaking. Subsequently, the supernatant was mixed 1:1 with isopropanol and incubated at -20°C over night and three µL of glycogen (Roche, Basel, Switzerland) were used to precipitate the size-selected RNA. After centrifugation with 16,000x g at 4°C for 1h, the pellet was washed with 70% ethanol in ddH^2O, centrifuged again for 15 min and air-dried. RNA was resuspended in ddH^2O and incubated for 5 min at 55°C prior to storage at -80°C. RNA concentrations were determined via 2100 bioanalyzer pico kit (Agilent, Santa Clara, CA, USA) at the Core Unit Systems Medicine, University of Würzburg, Germany.

qRT-PCR validation of small RNAs and gene targets

To validate representative small RNA transcripts and potentially regulated gene transcripts within pathways, we applied qRT-PCR using the ΔΔCt method.

For cDNA synthesis of small RNAs, miRCURY LNA RT Kit (Qiagen, Hilden, Germany) was used with 10 ng RNA in 2 µL nuclease-free water added to a master mix with 2 µL reaction buffer, 5 µL nuclease-free water, and 1 µL enzyme mix.

Reverse transcription was conducted on a PRISM 7700 Cycler (Applied Biosystems, Waltham,

212 MA, USA) at 42°C for 60 min and subsequent enzyme deactivation at 95°C for 5 min. cDNA
213 was stored at -20°C. Prior to use cDNA was diluted 1:80 (1:20 for hsa-miR-576-5p) in nuclease
214 free water according to the manufacturer`s recommendation. Total RNA was used for miRs,
215 while only size-selected RNA samples were applied for tRF quantification. Since no universal
216 endogenous controls exist for small RNAs, we tested several transcripts for each set of RNA
217 samples (see Figure S1). The selected endogenous controls for each set of RNA samples are
218 listed in Table 1.

219 Table 1: Combined endogenous controls applied for miR and tRF expression level normalization.

Small RNA type	Whole blood RNA	Keratinocyte RNA
miR	SNORD38B	SNORD38B
	SNORD44	SNORD44
	SNORD48	5S
	hsa-miR-423-5p	hsa-miR-20a-5p
tRF	hsa-miR-92b-3p	not applicable
	hsa-miR-505-3p	
	hsa-miR-942-5p	

220

221 Small RNA qRT-PCRs were run on a QuantStudio 3 (Thermo Fisher Scientific, Waltham, MA,
222 USA) with miRCURY LNA SYBR Green PCR reagents and pre-designed miRCURY LNA miR
223 PCR Assays, except for tRF-20KK-5Y93 primers, which were custom ordered (all Qiagen,
224 Hilden, Germany).

225

226 Small RNA qRT-PCR cycler conditions were 2 min at 50°C, 10 min at 95°C, followed by 40
227 cycles of 10s at 95°C and 1 min at 60°C. Each primer set was run in triplicate, with each well
228 containing 5 µl SYBR green master mix with 1:50 ROX, 1 µl primers (all Qiagen, Hilden,

229 Germany) and 4 µl cDNA. A list of all small RNA primers is given in Table 2.

230

231 Table 2: Small RNA primers applied in our study.

Assay target	Assay Number	Application
SNORD38B	YP00203901	1, 3, 4, 6
SNORD44	YP00203902	1, 3, 4, 6
SNORD48	YP00203903	1, 3, 4
hsa-miR-423-5p	YP00205624	1, 4
hsa-miR-194-5p	YP00204080	1
hsa-miR-221-3p	YP00204532	1
hsa-miR-942-5p	YP00204440	1, 2, 5
hsa-miR-92a-3p	YP00204258	1
hsa-miR-93-5p	YP00204715	1
5S	YP00203906	1, 3, 6
hsa-miR-182-5p	YP00206070	7
hsa-miR-576-5p	YP00206064	7
hsa-miR-1976	YP02112898	7
hsa-miR-361-3p	YP00204008	1, 2
hsa-miR-501-3p	YP00204178	1, 2, 5
hsa-miR-505-3p	YP00204214	1, 2, 5
hsa-miR-505-5p	YP00205657	1, 2
hsa-miR-222-5p	YP00204314	2
TRF-20-40KK5Y93	YCP0058890	8
U6	YP02119464	3
hsa-miR-20a-5p	YP00204292	3, 6
hsa-miR-503-5p	YP00204334	9

232

233 Assays were used as follows: 1) tested as endogenous control for blood miR; 2) tested as
234 endogenous control for blood tRF; 3) tested as endogenous control for keratinocyte miR; 4)
235 applied as endogenous control for blood miR; 5) applied as endogenous control for blood tRF; 6)
236 applied as endogenous control for keratinocyte miR; 7) blood miR target of interest; 8) blood tRF
237 target of interest; 9) keratinocyte miR target of interest. All primers were acquired from Qiagen,
238 Hilden, Germany.

For cDNA synthesis of mRNA transcripts from total RNA, TaqMan Reverse Transcription reagents (Thermo Fisher Scientific, Waltham, MA, USA) were applied. 250 ng mRNA was pre-incubated with 5 µl random hexamer at 85°C for 3 min, and reverse transcription carried out after addition of a master mix with 10 µl 10× PCR buffer, 6.25 µl MultiScribe reverse transcriptase, 2 µl RNase inhibitor, 22 µl $MgCl_2$, and 20 µl deoxyribonucleoside triphosphate. Reverse transcription was conducted on a PRISM 7700 Cycler (Applied Biosystems, Waltham, MA, USA) with annealing at 25°C for 10 min, followed by 48°C for 1h. mRNA qRT-PCRs were run on a QuantStudio 3 (Thermo Fisher Scientific, Waltham, MA, USA) with following cycler conditions: 2 min at 50°C, 2 min at 95°C, and 40 cycles of 3s 95°C and 30s 60°C. Samples were run in triplicates, with each well as duplex (containing primers for target and endogenous control). Each well contained 5 µl TaqMan Fast Advanced Mastermix (Thermo Fisher Scientific, Waltham, MA, USA), 3.5 µl cDNA, 0.5 µl RNase free H2O 0.5 µl target primer, and 0.5 µl endogenous control primer (all Thermo Fisher Scientific, Waltham, MA, USA). RPL13A served as endogenous control, both for whole blood and keratinocyte samples.[37,49] A list of all used mRNA primers is given in Table 3.

Table 3: List of qRT-PCR primer assay for mRNA quantification.

Target	Assay Number
ADAM15	Hs00187052_m1
CDKN1A	Hs00355782_m1
EIF5A	Hs00744729_s1
EP300	Hs00914212_m1
FOXO1	Hs01054576_m1
HNRNPL	Hs00704853_s1
IGF1R	Hs00609566_m1
INSR	Hs00961554_m1
MAP2K7	Hs01588450_m1
MAPK1	Hs01046830_m1
RPL13A	Hs04194366_g1
TGF1B	Hs99999918_m1

Abbreviations: ADAM15, ADAM metallopeptidase domain 15; CDKN1A, cyclin dependent kinase inhibitor 1A; EIF5A, eukaryotic translation initiation factor 5A; EP300, E1A binding protein P300; FOXO1, forkhead box O1; HNRNPL, heterogeneous nuclear ribonucleoprotein L; IGF1R, insulin like growth factor 1 receptor; INSR, insulin receptor; MAP2K7, mitogen-activated protein kinase 7; MAPK1, mitogen-activated protein kinase 1; RPL13A, ribosomal protein L13a; TGFB1, transforming growth factor beta 1. All primers were acquired from Thermo Fisher Scientific, Waltham, MA, USA.

Results

Clinical characteristics of study cohorts

Table 4 summarizes the main epidemiological data of the study cohorts. For 18 FMS patients, both blood and keratinocyte RNA was sequenced, while from additional 13 FMS patients only blood and from 14 FMS patients only keratinocyte RNA was used. Further, 8 FMS patient samples were only used for qRT-PCR.

Table 4: Epidemiological data of study cohorts.

Parameter median (range)	FMS (total)	FMS (blood seq)	FMS (kera seq)	hCO	dCO
N	53	31	32	34	15
Age	52.9 (25.0-67.2)	52.2 (25.0-67.2)	50.9 (25.0-65.5)	52.1 (23.9-61.7)	50.6 (21.7-58.4)
BMI	25.4 (16.6-39.5)	24.0 (16.6-36.8)	25.4 (16.6-39.5)	24.4 (16.7-41.5) (n = 33/34)	26.7 (20.3-43.3) (n = 13/15)
GCPS (6 month mean)	6.0 (2.0-9.0)	7.0 (3.0-9.0)	6.0 (2.0-9.0)	0.0 (0.0-8.0) (n = 28/34)	7.0 (3.0-10.0)
FIQ sum score	43.9 (8.7-63.3)	43.4 (31.5-63.3)	43.8 (8.7-59.7)	3.0 (0.0-50.9) (n = 24/34)	46.0 (1.0-71.0)
WPI sum score	15.0 (7.0-19.0)	15.0 (8.0-19.0)	16.0 (8.0-19.0)	n.a.	n.a.
NPSI sum score	0.4 (0.1-0.8)	0.4 (0.1-0.8)	0.4 (0.1-0.8)	0.0 (0.0-0.3) (n = 28/34)	0.3 (0.0-0.6)

ADS sum score	23.0 (7.0-51.0)	21.0 (7.0-51.0)	22.0 (7.0-45.0)	5.5 (0.0-44.0) (n = 28/34)	38.0 (22.0-55.0)
IENF group* (0-3) [%]	0 (35.8%) 1 (17.0%) 2 (18.9%) 3 (28.3%)	0 (22.6%) 1 (19.4%) 2 (25.8%) 3 (32.3%)	0 (40.6%) 1 (6.3%) 2 (21.9%) 3 (31.3%)	0 (47.1%) 1 (35.3%) 2 (11.8% 3 (5.9%) (n = 17/34)	0 (75%) 1 (0%) 2 (0%) 3 (25%) (n (8/15)

*0 = no IENF reduction, 1 = distal IENF reduction, 2 = proximal IENF reduction, 3 = generalized IENF reduction. Established in-house thresholds for pathological IENF reduction were applied (distal < 6 IENF/mm; proximal < 8 IENF/mm). Abbreviations: ADS, Allgemeine Depressionsskala; BMI, body mass index; FIQ, Fibromyalgia Impact Questionnaire; GCPS, Graded Chronic Pain Scale; IENF, intraepidermal nerve fiber; n.a., not applied; NPSI, Neuropathic Pain Symptom Inventory; WPI, Widespread Pain Index.

Systemic small RNA alterations in FMS manifest as bi-symmetric miR regulation but mere tRF upregulation in whole blood samples

Via small RNA-seq of stabilized whole blood RNA samples (Fig. 1A), we identified 69 deregulated (DE) miRs (Fig. 1B) and 22 tRFs (Fig. 1C-F). While for miRs, both up- (62.3%) and downregulated (37.7%) transcripts were found, intriguingly all tRFs were upregulated. Of note, all DE tRFs derived from nuclear tRNAs (Fig. 1C) and most were 3`-tRFs and i-tRFs (Fig. 1D). Even more compelling, all DE tRFs showed a sequence length comparable to miRs (16-22 nt, median 22 nt; Fig 1E). There was no preference as for a specific amino acid-coding tRNA in whole blood tRFs (Fig. 1F).

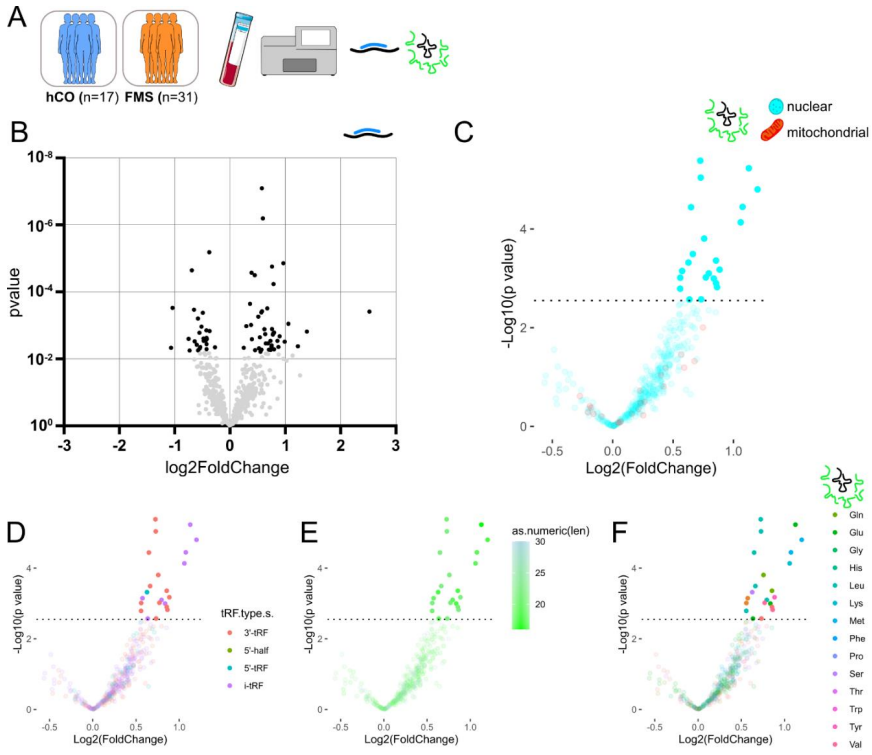

Figure 1. Bi-directional miR regulation and upregulated short tRFs in whole blood of female FMS patients. (A) Sequencing design. (B) Volcano plot of detected miRs with 69 DE miRs (black) and unaltered miRs (grey, semitransparent). (C) Volcano plot of tRFs with 22 altered transcripts and unaltered tRFs (semitransparent) labeled by nuclear (blue) or mitochondrial (red) origin. TRFs are further characterized by their type (D), nt length (E), and parent tRNA amino acid coding (F). See complete list of DE miRs and tRFs in Table S1 & S2. Abbreviations: as.numeric(len), fragment length; hCO, healthy control; FMS, fibromyalgia syndrome. Amino acids: Gln, glutamine; Glu, glutamic acid; Gly, glycine; His, histidine; Leu, leucine; Lys, lysine; Met, methionine; Phe, phenylalanine; Pro, proline; Ser, serine; Thr, threonine; Trp, tryptophan, Tyr, tyrosine; Val, valine.

miRs target gene transcripts of FoxO signaling pathway, while tRF are associated with RNA processes in whole blood

We extracted relevant gene pathways (KEGG) and biological processes (GO:BP) potentially modified by FMS derived small RNA profiles (Fig. 2A). For miRs, the conjunction of three databases revealed six KEGG pathways, while 65 GO:BP terms overlapped (Fig. 2B). For tRFs five KEGG pathways and 139 GO:BP terms passed the threshold of $q < 0.05$. Most top GO:BP terms were linked with mRNA metabolism, splicing, and translation. We chose the FoxO signaling pathway (Tarbase $p = 2.94E-05$; TargetScan $p = 0.013$; microT-CDS $p = 3.39E-06$) for detailed characterization of miR regulation, due to its relevance in immune cell regulation, e.g. in proliferation, apoptosis, inflammation, and oxidative stress.[50,51] Annotated gene targets from Tarbase were highlighted in the KEGG pathway (Fig. 2D) and all gene targets with minimum of five miR regulators ranked (Fig. 2E). Within the 'input arm', mostly insulin signaling and PI3Akt signaling genes were targeted. Both, positive and negative regulators of FOXO1and FOXO3, like MDM2 proto-oncogene (MDM2), protein kinase AMP-activated catalytic subunit alpha 1 (PRKAA1), and E1A binding protein P300 (EP300) were predicted to be modified. The number of miR-gene interactions on FOXO regulated 'output genes' was highest for cell cycle associated genes like cyclin D1 (CCND1), cyclin D2 (CCND2), and cyclin dependent kinase inhibitor 1B (CDKN1B). Also, superoxide dismutase 2 (SOD2) and ATM serine/threonine Kinase (ATM) referring to oxidative stress resistance and DNA repair represent relevant targets. For tRFs, all gene targets were ranked by number of implicated tRFs (Fig. 2F), and by appearance in GO:BP terms (Fig. 2G), depicting mitogen-activated protein kinase kinase 7 (MAP2K7), eukaryotic translation initiation factor 5A (EIF5A), and heterogeneous nuclear ribonucleoprotein L (HNRNPL) as promising starting points to investigate the impact of these small RNAs on RNA transcripts. Notably, 18 out of 22 of DE blood tRFs were associated with gene transcripts.

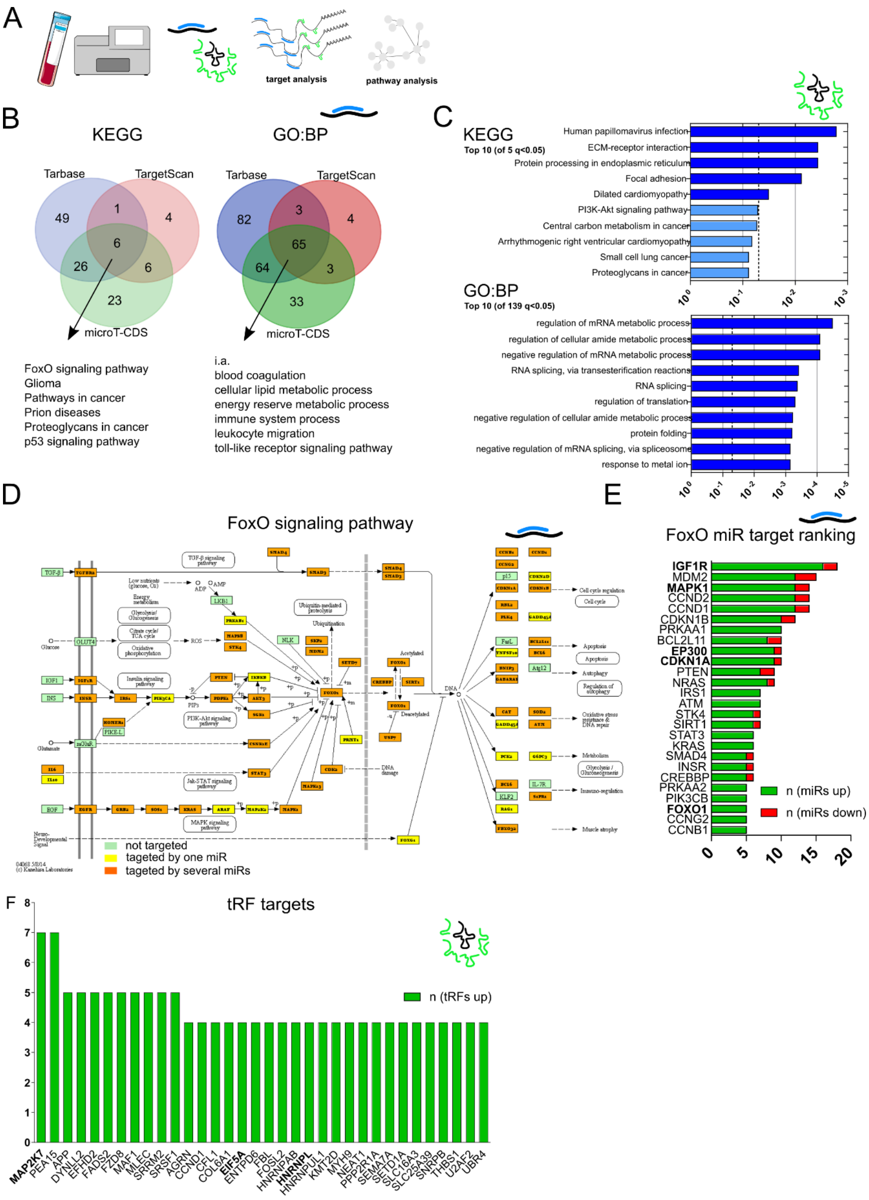
A
target analysis
pathway analysis
B
KEGG
GO:BP
Tarbase
TargetScan
microT-CDS
49
1
4
6
26
6
23
82
3
4
65
64
3
33
FoxO signaling pathway
Glioma
Pathways in cancer
Prion diseases
Proteoglycans in cancer
p53 signaling pathway
i.a.
blood coagulation
cellular lipid metabolic process
energy reserve metabolic process
immune system process
leukocyte migration
toll-like receptor signaling pathway
C
KEGG
Top 10 (of 5 q<0.05)
Human papillomavirus infection
ECM-receptor interaction
Protein processing in endoplasmic reticulum
Focal adhesion
Dilated cardiomyopathy
PI3K-Akt signaling pathway
Central carbon metabolism in cancer
Arrhythmogenic right ventricular cardiomyopathy
Small cell lung cancer
Proteoglycans in cancer
GO:BP
Top 10 (of 139 q<0.05)
regulation of mRNA metabolic process
regulation of cellular amide metabolic process
negative regulation of mRNA metabolic process
RNA splicing, via transesterification reactions
RNA splicing
regulation of translation
negative regulation of cellular amide metabolic process
protein folding
negative regulation of mRNA splicing, via spliceosome
response to metal ion
D
FoxO signaling pathway
not targeted
tageted by one miR
tageted by several miRs
E
FoxO miR target ranking
IGF1R
MDM2
MAPK1
CCND2
CCND1
CDKN1B
PRKAA1
BCL2L11
EP300
CDKN1A
PTEN
NRAS
IRS1
ATM
STK4
SIRT1
STAT3
KRAS
SMAD4
INSR
CREBBP
PRKAA2
PIK3CB
FOXO1
CCNG2
CCNB1
n (miRs up)
n (miRs down)
0
5
10
15
20
F
tRF targets
n (tRFs up)
MAP2K7
PEA15
APP
DYNLL2
EFHD2
FADS2
FZD8
MAF1
MLEC
SRRM2
SRSF1
AGRN
CCND1
CFL1
COL6A1
EIF5A
ENTPD6
FBL
FOSL2
HNRNPAB
HNRNPL
HNRNPUL1
KMT2D
MYH9
NEAT1
PPP2R1A
SEMA7A
SETD1A
SLC16A3
SLC25A39
SNRPB
THBS1
U2AF2
UBR4

Figure 2. Gene transcript targeting and pathway analysis of miRs and tRFs from whole blood small RNA-seq in FMS compared to healthy controls. (A) Analysis outline. (B) Few miR regulated KEGG pathways are identified by all three target-prediction algorithms (n = 5) and include 'FoxO signaling pathway', while 65 GO:BP pathways converged covering a wide range of processes, like 'immune system process' and 'leukocyte migration'. (C) For tRFs, five KEGG pathways, including 'Protein processing in endoplasmatic reticulum', 'ECM-receptor interaction', and 'Focal adhesion' reached the threshold of $q< 0.05$, whereas 139 GO:BP terms emerged. The top 10 of GO:BP aggregated terms of mRNA metabolic, splicing, and translation processes. (D) Targeted gene transcripts involved in FoxO signaling pathways by one (yellow) or several (orange) miRs and (E) targets ranked by number of interacting miRs. Green represents upregulated interacting miRs and red downregulated interacting miRs. (F) Ranked gene transcripts interacting with tRFs and gene transcripts ranked by occurrence in top 10 GO:BP terms (G). FMS, fibromyalgia syndrome; GO:BP, Gene ontology biological process; KEGG, Kyoto Encyclopedia of Genes and Genomes; miR, microRNA; RNA-seq, RNA sequencing tRF, tRNA derived fragment.

Small RNAs and subsequent gene pathway representative changes in blood are specific for FMS compared to patients with major depression

We validated hsa-miR-576-5p and hsa-miR-182-5p as upregulated miRs targeting gene transcripts in the FoxO signaling pathway (e.g., CDKN1A for 576-5p and FOXO1, EP300, and IGF1R by 182-5p and one downregulated miR (hsa-miR-1976) not involved in this pathway via qRT-PCR. To further test the suitability of these miRs as a blood biomarker for FMS, we included a disease control group of women with major depression with additional physical pain (Fig. 3A). While upregulation of hsa-miR-576-5p and hsa-miR-182 in FMS whole blood were confirmed, hsa-miR-1976 expression was not altered in qRT-PCR.

Furthermore, comparing the expression levels of these miRs versus the dCO group revealed even higher levels in the disease controls (Fig. 3B-D). When validating a first tRF after size selection, only the FMS group showed an increase of TRF-20-40KK5Y93 versus hCO and also versus dCO (Fig. 3E). We then analyzed predicted targets of the FoxO signaling pathway supposed to be affected by miR deregulation, but only found an upregulation of CDKN1A in FMS versus hCO (Fig. 3F), while FOXO1, MAPK1, and IGF1R were not changed. For tRF targets, we focused on the highest ranged target MAP2K7, showing only a trend of downregulation and EIF5A and HNRNPL as being involved in RNA processes, surprisingly showing upregulation in dCO, but no change in FMS compared to hCO (Fig. 3G).

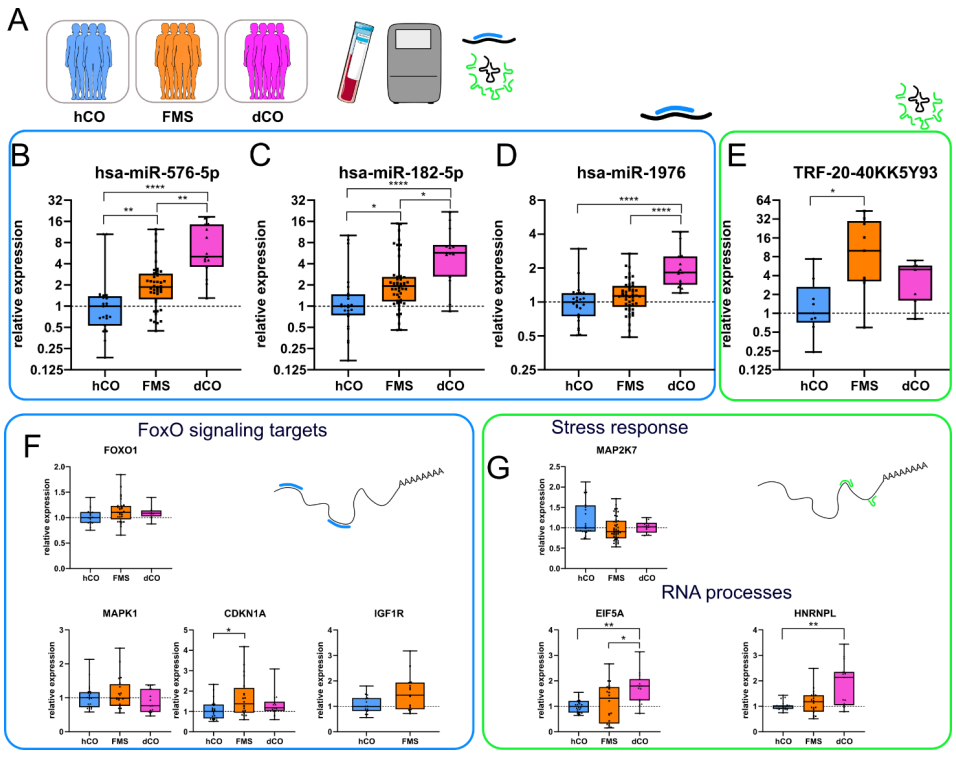

Figure 3. Altered whole blood small RNA candidates distinguish FMS from hCO and dCO and may regulate representative gene transcripts of predicted pathways. (A) Experiment setup. (B) Upregulation of hsa-miR-576-5p (hCO-FMS $p < 0.01$; hCO-dCO $p < 0.0001$; FMS-dCO $p < 0.05$) and (C) hsa-miR-182-5p (hCO-FMS $p < 0.05$; hCO-dCO $p < 0.0001$; FMS-dCO $p < 0.05$) in FMS compared to hCO was validated via qRT-PCR, with further elevation of these transcripts in the dCO cohort. (D) Minor downregulation of hsa-miR-1976 in FMS was not apparent in qRT-PCR but was however upregulated in dCO compared to FMS and hCO. (E) TRF-20-40KK5Y93 was selectively upregulated in FMS versus hCO and dCO. (F) Within predicted gene transcript targets of miRs in the FoxO signaling pathway, only CDKN1A was upregulated in FMS compared to healthy controls ($p < 0.05$), with no changes in FOXO1, MAPK1, and IGF1R expression. No alterations were seen in the dCO group investigated for FOXO1, MAPK1, and CDKN1A. (G) TRF target MAP2K7 involved cellular stress response showed comparable expression between hCO, FMS, and dCO. In case of RNA processing transcripts, EIF5A was increased in the dCO cohort versus hCO and FMS ($p < 0.01$; $p < 0.05$) and HNRNPL upregulated versus hCO ($p < 0.01$). Kruskal-Wallis-Test with Dunn`s correction was applied, except for IGF1R, where Mann-Whitney-U test was carried out. N = 23 hCO vs 43 FMS vs 15 dCO (B), n = 24 hCO vs 49 FMS vs 15 dCO (C-D), n = 9 hCO vs 9 FMS vs 7 dCO (E), n = 18 hCO vs 29 FMS vs 8 dCO (FOXO1), n = 15 hCO vs 15 FMS (IGF1R), n = 24 hCO vs 20 FMS vs 15 dCO (MAPK1, CDKN1A, MAP2K7, HNRNPL, EIF5A). Abbreviations: CDKN1A, cyclin dependent kinase inhibitor 1A; dCO, disease control; EIF5A, eukaryotic translation initiation factor 5A; FMS, fibromyalgia syndrome; FOXO1, forkhead box O1; hCO, healthy control; HNRNPL, heterogeneous nuclear ribonucleoprotein L; IGF1R, insulin like growth factor 1 receptor; MAP2K7, mitogen-activated protein kinase kinase 7; MAPK1, mitogen-activated protein kinase 1.

Peripheral small RNA alterations in FMS patient-derived keratinocytes are present with predominant miR and nuclear-derived tRF downregulation

Small RNA-seq from keratinocyte-derived RNA (Fig. 3A) identified 41 DE miRs (Fig. 3B), which were mostly downregulated (90.2% downregulated versus 9.8% upregulated) and 22 tRFs with a similar trend (77.3% downregulated versus 22.7% upregulated; Fig. 4C-F). Within these tRFs, only two mitochondrial tRFs were found among the four upregulated transcripts (Fig. 4C). Strikingly, the majority of downregulated tRFs were 5`-tRFs and 5`-half tRFs with longer nt length (19-43, median: 43). Furthermore, downregulated tRFs primarily derived from the two tRNAs coding for glutamic acid.

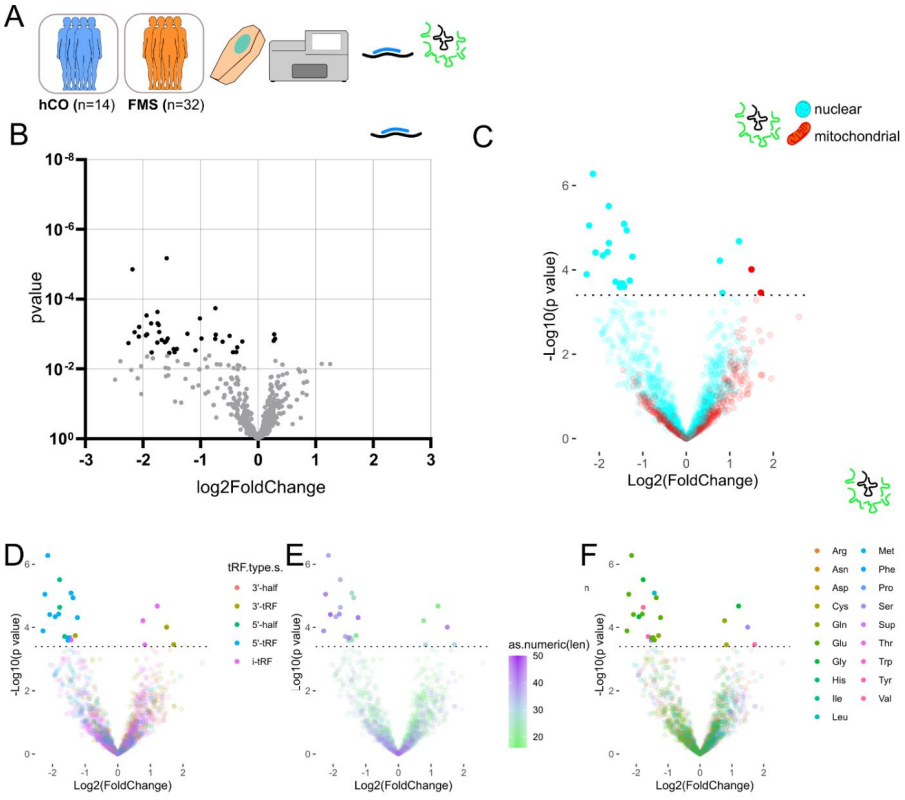

389 **Figure 4.** Overall downregulation of small RNAs in primary keratinocytes of female FMS
390 patients. (A) Sequencing design. (B) Volcano plot of detected miRs with 41 DE miRs (black) and
391 non-altered miRs (grey, semitransparent). (C) Volcano plot of tRFs with 22 altered transcripts
392 and non-altered tRFs (semitransparent) labeled of nuclear (blue) or mitochondrial (red) origin.
393 TRF type (D), nt length (E), and parent tRNA amino acid coding (F) are displayed for detailed
394 characterization. See complete list of DE small RNAs in Table S3 & S4. Abbreviations:
395 as.numeric(len), fragment length; hCO, healthy control; FMS, fibromyalgia syndrome. Amino
396 acids: Arg, Arginine; Asn, Asparagine; Asp, Aspartic acid; Cys, Cysteine; Gln, Glutamine; Glu,
397 Glutamic acid; Gly, Glycine; His, Histidine; Ile, Isoleucine; Leu, Leucine; Met, Methionine; Phe,
398 Phenylalanine; Pro, Proline; Ser, Serine; Sup, nonsense suppressor; Thr, Threonine; Trp,
399 Tryptophan; Tyr, Tyrosine; Val, Valine.

400

401 **Adherens/adhesion and AMPK pathways are targeted by miRs, while epithelial processes are**
402 **linked to tRFs in primary keratinocytes from FMS patients**

403 Target and pathway analysis for primary keratinocyte small RNAs were carried out in analogy to
404 whole blood (Fig 5A). The overlap between miR databases for KEGG implicated 'AMPK
405 (adenosine monophosphate-activated protein kinase) signaling pathway' (Tarbase p =2.03E-05;
406 TargetScan p = 0.018; microT-CDS p =0.002) and 'Proteoglycans in cancer' (Tarbase p = 9.27E-
407 16; TargetScan p = 0.003; microT-CDS p = 3.37E-06) as affected pathways (Fig. 5B). Yet,
408 'Adherens junction' (Tarbase p = 1.69E-05; microT-CDS p = 1.44E-05) and 'Focal adhesion'
409 (Tarbase p = 8.60E-05; microT-CDS p = 0.008) were also considered, because both were
410 identified in Tarbase and microT-CDS, while Targetscan included the related pathway 'Cell
411 adhesion molecules (CAMs)' (p = 2.70E-4).

412 Overlapping for all three databases, 19 GO:BP terms were found, including ‘membrane
413 organization’, ‘neurotrophin TRK receptor signaling pathway’, and ‘response to stress’. In case
414 of tRF, only 6 of 22 DE candidates were associated with regulation of gene transcripts, with no
415 targets shared by at least three tRFs. Therefore, all targeted gene transcripts were included in the
416 pathway analysis, leading to three KEGG pathways and 28 GO:BP terms passing the threshold
417 and the majority of top GO:BP terms referred to cell growth, proliferation, and migration of
418 epithelial cells (Fig. 5C). We further investigated miR targets IGF1R and INSR expression
419 involved in adherens junctions and AMPK pathway (Fig. 5D) and TGFB1 as a tRF associated
420 target, involved in most GO:BP processes (Fig. 5E).

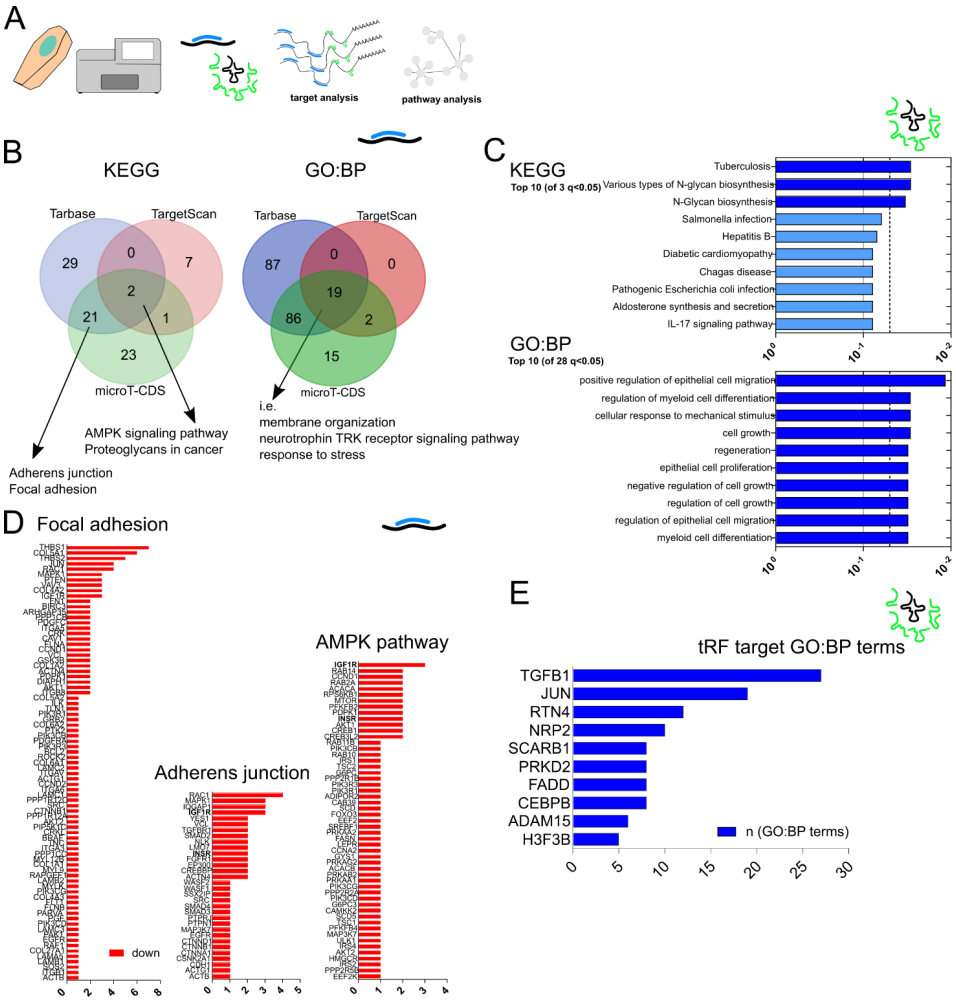

Figure 5. Gene transcript targeting and pathway analysis of miRs and tRFs from keratinocyte small RNA-seq in FMS compared to healthy controls (A) Analysis outline. (B) Only 'AMPK signaling pathway' and 'Proteoglycans in caner' intersected as KEGG pathways of all three target-prediction algorithms, while adherens junctions and focal adhesion overlapped between Tarbase and microT-CDS, with the similar pathway of cell adhesion molecules in Targetscan. 19

pathways overlapped in GO:BP terms, including ‘membrane organization’, ‘neurotrophin TRK receptor signaling pathway’, and ‘response to stress’. (C) No tRF gene transcripts were targeted by 3 ≥ tRFs, therefore all single gene targets were used to predict affected pathways and led to three KEGG pathways passing the corrected threshold and 28 GO:BP terms. (D) Ranked gene transcripts within focal adhesion, adherens junction, and AMPK pathway were only associated with downregulated miRs (red). (E) Predicted tRF targets, ranked by occurrence in GO:BP terms. Abbreviations: AMPK, adenosine monophosphate-activated protein kinase; FMS, fibromyalgia syndrome; GO:BP, gene ontology biological process; KEGG, Kyoto Encyclopedia of Genes and Genomes; miR, microRNA; RNA-seq, RNA sequencing; tRF, tRNA fragment.

Hsa-miR-503-5p changes do not correspond to changes in selected associated pathway genes, but tRF associated target TGFB1 expression is markedly extenuated in FMS keratinocytes

We validated one representative miR from keratinocyte sequencing (Fig. 6A) which was downregulated in FMS versus hCO (Fig. 6B), while potential downstream targets IGF1R and INSR associated with adherens junctions and AMPK pathway were not altered (Fig. 6C). Within target transcripts of tRFs, TGFB1 was downregulated in FMS keratinocytes versus hCO, while ADAM15 levels were similar between both groups (Fig 6D).

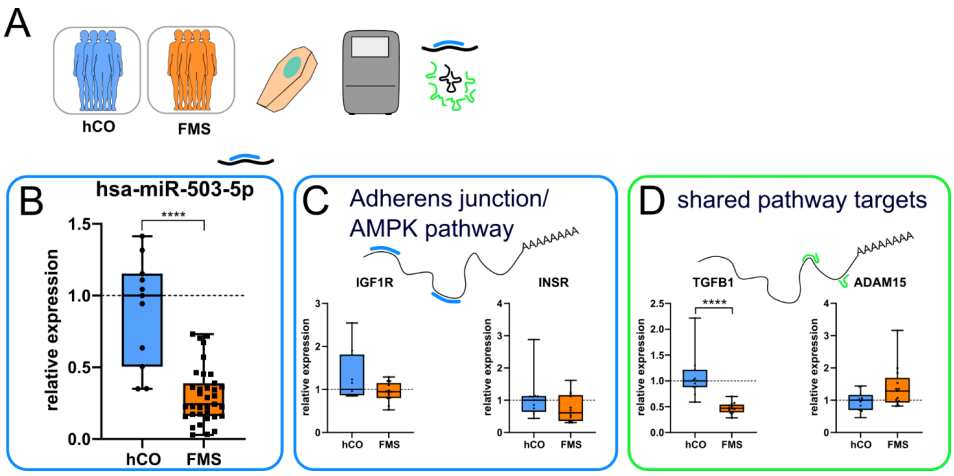

Figure 6. Validation of reduced hsa-miR-503-5p and expression levels of selected small RNA targets in FMS keratinocytes. (A) Outline. (B) Expression of hsa-miR-503-5p was validated via qRT-OPCR, showing markedly reduced expression levels in FMS compared to hCO ($p < 0.0001$). (C) Gene expression of adherens junction/AMPK pathway related targets were not changed in FMS. (D) Expression of TGFB1, involved in 27 of 28 GO:BP terms and targeted by tRF-25-S3M8309NDJ was decreased in FMS keratinocytes versus hCO ($p < 0.0001$), while ADAM15, involved in 6 GO:BP terms and targeted by tRF-20-BMW36D46 was not modified. Mann-Whitney-U test, n = 11 hCO vs 35 FMS (B) and 11 hCO vs 13 (C-D). Abbreviations: ADAM15, ADAM Metallopeptidase Domain 15; AMPK, adenosine monophosphate-activated protein kinase; FMS, fibromyalgia syndrome; hCO, healthy control; IGF1R, insulin like growth factor 1 receptor; INSR, insulin receptor; TGFB1, transforming growth factor beta 1.

Small RNAs inherit potential as marker for FMS severity

Finally, we linked the sequencing-derived expression data of DE small RNAs with the most prominent and frequently assessed clinical FMS characteristics to investigate, if these transcripts are indicative for disease and symptom severity (Fig. 7A). To avoid over-stringent correction for multiple testing in this exploratory approach, we applied a correlation strength cutoff of ±0.4, instead of a p-correction, to retain moderate-strong associations. Interestingly, the WPI score showed the most prominent correlations with miRs in blood and keratinocytes (Fig. 7B, C). While no tRF passed our threshold in whole blood (Fig. 7D), the severity of small fiber reduction was positively associated with tRF-40-86J8WPMN1E8Y7Z2R and tRF-30-JZOYJE22RRN3 (Fig. 7E).

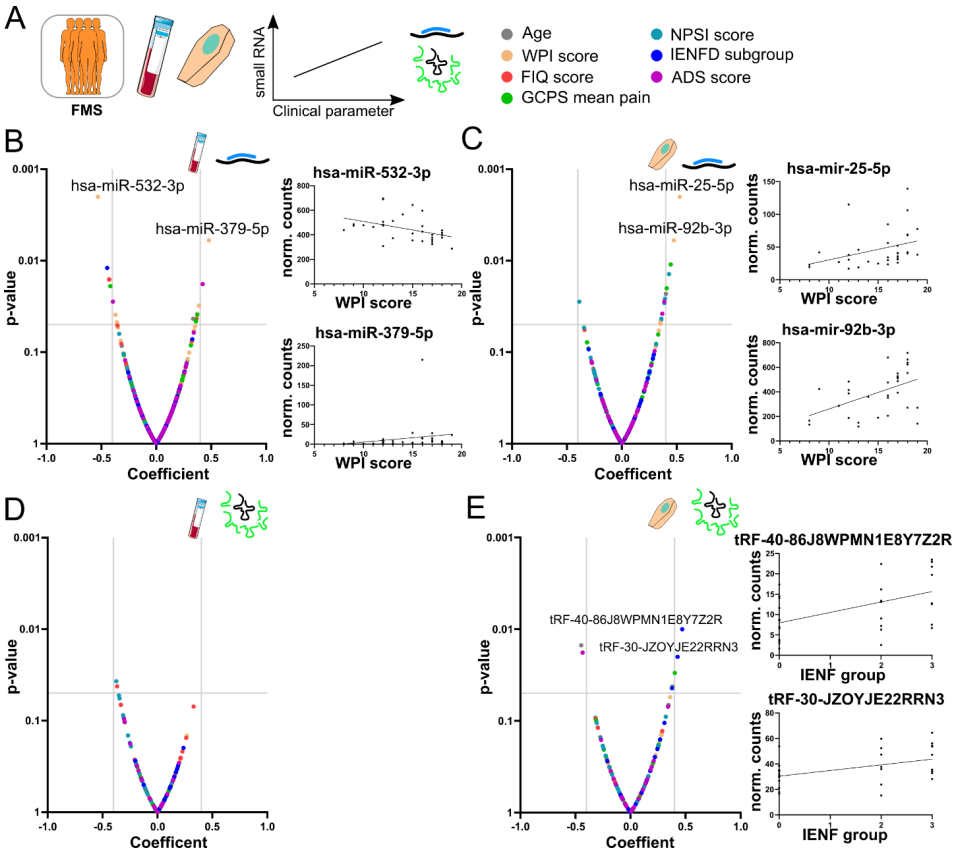

Figure 7. Relevance of small RNAs as correlates for clinical parameter in FMS (A) Outline indicating the applied parameter age (grey), WPI score (orange), FIQ score (red), GCPS mean pain recall last six months (green), NPSI score (cyan), IENF subgroup (blue), and ADS score (magenta) in FMS patients. (B) Volcano plot summarizing p-value and spearman coefficient strength for blood miRs and clinical parameter. WPI/hsa-miR-532-3p (r = -0.531, p = 0.002), WPI/hsa-miR-379-5p r =0.48, p = 0.006), IENF/hsa-miR-6855-3p r = -0.447, p = 0.0117), FIQ/hsa-miR-4433a-5p (r =-0.431, P = 0.0155), FIQ/hsa-miR-1976 (r = -0.428, p= 0.0164), ADS/hsa-miR-323b-3p (r = 0.422, p = 0.018),

476 and GCPS/hsa-miR-6726-3p (r = -0.418, p =0.019) were identified. (C) Corresponding volcano
477 plot for keratinocyte miRs with WPI/hsa-mir-25-5p (r = 0.527, p = 0.002), WPI/hsa-mir-92b-3p
478 (r = 0.474, p = 0.006), GCPS/hsa-mir-125b-1-3p (r = 0.446, p = 0.011), WPI/hsa-mir-485-3p (r =
479 0.444, p = 0.011), NPSI/hsa-mir-576-3p (r = 0.430, p = 0.014), GCPS/hsa-let-7a-2-3p (r = 0.409,
480 p = 0.020), and Age/hsa-mir-122-5p (r = 0.401, p = 0.023) as correlations passing the threshold.
481 (D) No tRF was strongly associated with clinical parameter in blood, while IENF/tRF-40-
482 86J8WPMN1E8Y7Z2R (r = 0.470, p = 0.010), Age/tRF-20-BMW36D46 (r = -0.448, p = 0.015),
483 ADS/tRF-40-B9I1KQSX0DIJZ726 (r = -0.435, p = 0.018), IENF/tRF-30-JZOYJE22RRN3 (r =
484 0.428, p = 0.020), and GCPS/tRF-26-Q3V2Y7RZ81D (r = 0.402, p = 0.030) were linked in
485 keratinocytes. Abbreviations: ADS, Allgemeine Depressionsskala; FIQ, Fibromyalgia Impact
486 Questionnaire; FMS, fibromyalgia syndrome; GCPS, Graded Chronic Pain Scale; IENF,
487 intraepidermal nerve fiber; miR, microRNA; norm. counts, normalized counts; NPSI,
488 Neuropathic Pain Symptom Inventory; tRF, tRNA fragment; WPI, Widespread Pain Index.

489 **Discussion**

490 We describe and characterize altered systemic and local small RNA profiles in female FMS
491 patients. While miR alterations in various blood components (whole blood, WBCs, serum) were
492 already discussed in FMS, [23-25,52] we now expand this view towards tRFs, representing a new
493 class of small non-coding RNAs, with yet to understand implications in posttranscriptional
494 regulations. Intriguingly, not only blood samples, but also locally derived keratinocytes from the
495 upper thigh of patients showed profound changes of miR and tRF expression patterns, with an
496 overall decrease in these small RNAs.

497

While upregulation of miR candidates hsa-miR-182-5p and hsa-miR-575-5p in FMS was confirmed via qRT-PCR, their expression was even further increased in our disease control group of major depression patients with chronic physical pain. Therefore, depressive mood or pain in general might be closer associated with these miRs than specific FMS pain. The slight downregulation of hsa-miR-1976 in FMS could not be confirmed via qRT-PCR, illustrating the caution needed for selecting representative targets and may be attributed to lower accuracy and robustness of qRT-PCR. However, hsa-miR-1976 was elevated in the dCO group, distinguishing healthy subjects from FMS. In turn, tRF-20-40KK5Y93 was higher expressed only in FMS compared to hCO and dCO, promoting tRFs as new candidates for specific FMS biomarkers. First prospects for the diagnostic value of tRFs are arising within the field of cancer,[53] but also other etiologies like nonalcoholic fatty liver disease, where blood tRFs might emerge as a minimally invasive alternative to liver biopsy in determining the fibrosis.[54] However, more 'quick and easy' detection methods relying on standardized protocols need to be established to facilitate discovery of robust tRF biomarkers that can be applied in clinical context.

To determine and address the influence of altered small RNAs on gene transcripts and whole pathways, we first applied available target prediction tools based on computational and validated interactions. For blood miRs, the implicated FoxO signaling pathway represents a highly relevant regulator of immune cell activity, e.g. in T helper cells.[50] Notably, miR-182 was reported as a key modulator of this pathway and directly targets FOXO1.[55] Surprisingly, our quantified gene expression levels of predicted targets were mostly unchanged, except for a moderate upregulation of CDKN1A in FMS. MiR-mRNA target expression are not necessarily inversely correlated as positive regulation on mRNA transcripts were described.[56,57] Further, miR levels can reflect pathological[58] or compensatory mechanisms,[59] therefore general assumptions of changes e.g. in

521 the FoxO pathway are precluded. A screening of all associated genes within a given pathway
522 needs to be considered in future.

523 In keratinocytes derived from FMS patients, we found a general decrease of miR and tRF
524 expression levels, which was validated for hsa-miR-503-5p. The predicted pathways for miR and
525 tRF targets were interconnected, with a focus on epithelial growth, differentiation, migration and
526 involving adherens and adhesion pathways. This result is of high relevance for potential
527 molecular mechanisms in small fiber pathology. The cellular interplay between keratinocytes and
528 intraepidermal nerve fibers for innervation/denervation,[60,61] but also nerve fiber ensheathment[16]
529 and even nociception and cutaneous pain are increasingly recognized.[62] The involvement of short
530 miR-like sized tRFs in blood, but longer tRFs with presumably different functions in
531 keratinocytes represents a fascinating finding. Future studies are needed to elucidate, whether
532 keratinocytes rely on longer tRFs for regulation of cellular processes in general.

533 We found reduced expression of the TGFB1 gene in FMS keratinocytes. TGF-β1 is known for its
534 role in wound healing, regulating keratinocyte migration and proliferation.[63] Changes in
535 keratinocyte TGF-β1 release modifies the epidermal environment and does affect other skin cells,
536 like resident dendritic cells and T-Cells.[64,65]

537 Few small RNAs showed explicit correlation with clinical parameter. MiRs in blood and
538 keratinocytes were mostly associated with WPI and GCPS, indicating expression changes
539 connected to the pain state. Previous studies tried to link miR expression with cardinal FMS
540 symptoms; no correlations with peripheral blood mononuclear cells derived miRs were found, [23]
541 miR-103a-3p, miR-320a, and miR-374b-5p from the circulating miR fraction correlated with pain
542 in FMS patients, [66] and let-7d from white blood cells correlated positively with IENFD and
543 GCPS.[22] Differences in recruitment parameter, blood components and miR quantification

methods could account for discrepancies between these findings and our results.
No blood tRFs passed our threshold, while five tRFs in keratinocytes were linked to with our assessed parameter, with two tRFs higher expressed with more severe IENF loss.

Conclusion

We present first comprehensive small RNA signatures in whole blood (systemic) and keratinocytes (peripheral) of FMS patients compared to healthy and disease controls. Systemic upregulation of miRs and tRFs were contrasted by peripheral downregulation of miRs and tRFs. We identify novel associated pathways and showcase the potential of small RNAs as diagnostic biomarkers and indicators for disease severity.

Acknowledgments

We thank Prof. Deckert and his team for their help recruiting patients with major depressive disorder with chronic widespread pain. We thank Margarete Göbel and Elena Katzowitsch from the Core Unit Systems Medicine, University of Würzburg for technical help with size selected RNA measurements, and Daniela Urlaub and Danilo Prtvar from the Department of Neurology, University of Würzburg for their support with qRT-PCRs.

Author contributions

Conceptualization: N.Ü., H.S., D.S.G. C.S.; methodology: C.E., N.M., G.M., S.W., D.S.G.; validation: N.Ü., D.S.G., H.S.; formal analysis: C.E., N.M, G.M.; investigation: C.E., G.M., D.P., S.W, D.E.; resources: N.Ü., H.S, S.U.; data curation: N.Ü., D.S.G., G.M., H.S.; writing: C.E., N.Ü., N.M.; visualization: C.E., N.M; supervision: N.Ü., H.S.; project administration: N.Ü.; funding acquisition: N.Ü., H.S.. All authors agreed to publication of this manuscript within this dissertation.

Competing Interests

The authors declare no conflict of interests.

References

1 Häuser, W., Sarzi-Puttini, P. & Fitzcharles, M.-A. Fibromyalgia syndrome: under-, over-and misdiagnosis. *Clin. Exp. Rheumatol.* **37**, 90-97 (2019).

2 Sluka, K. A. & Clauw, D. J. Neurobiology of fibromyalgia and chronic widespread pain. *Neuroscience* **338**, 114-129, doi:10.1016/j.neuroscience.2016.06.006 (2016).

3 Arnold, L. M. & Clauw, D. J. Challenges of implementing fibromyalgia treatment guidelines in current clinical practice. *Postgrad. Med.* **129**, 709-714 (2017).

4 Bidari, A., Parsa, B. G. & Ghalehbaghi, B. Challenges in fibromyalgia diagnosis: from meaning of symptoms to fibromyalgia labeling. *Korean J. Pain* **31**, 147-154 (2018).

5 Sarzi-Puttini, P., Giorgi, V., Marotto, D. & Atzeni, F. Fibromyalgia: an update on clinical characteristics, aetiopathogenesis and treatment. *Nat. Rev. Rheumatol.* **16**, 645-660, doi:10.1038/s41584-020-00506-w (2020).

6 Schweinhardt, P., Sauro, K. M. & Bushnell, M. C. Fibromyalgia: a disorder of the brain? *Neuroscientist* **14**, 415-421, doi:10.1177/1073858407312521 (2008).

7 May, A. Structural brain imaging: a window into chronic pain. *Neuroscientist* **17**, 209-220, doi:10.1177/1073858410396220 (2011).

8 Sundermann, B. *et al.* Subtle changes of gray matter volume in fibromyalgia reflect chronic musculoskeletal pain rather than disease-specific effects. *Eur. J. Neurosci.* **50**, 3958-3967, doi:10.1111/ejn.14558 (2019).

9 O'Mahony, L. F., Srivastava, A., Mehta, P. & Ciurtin, C. Is fibromyalgia associated with a unique cytokine profile? A systematic review and meta-analysis. *Rheumatology* **60**, 2602-2614 (2021).

10 Paiva, E. S., da Costa, E. D. & Scheinberg, M. Fibromyalgia: an update and immunological aspects. *Curr. Pain Headache Rep.* **12**, 321-326, doi:10.1007/s11916-008-0054-x (2008).

11 Coskun Benlidayi, I. Role of inflammation in the pathogenesis and treatment of fibromyalgia. *Rheumatol. Int.* **39**, 781-791, doi:10.1007/s00296-019-04251-6 (2019).

12 Evdokimov, D. *et al.* Reduction of skin innervation is associated with a severe fibromyalgia phenotype. *Ann. Neurol.*, doi:10.1002/ana.25565 (2019).

13 Grayston, R. *et al.* in *Semin. Arthritis Rheum.* 933-940 (Elsevier).

14 Baumbauer, K. M. *et al.* Keratinocytes can modulate and directly initiate nociceptive responses. *eLife* **4**, doi:10.7554/eLife.09674 (2015).

15 Moehring, F. *et al.* Keratinocytes mediate innocuous and noxious touch via ATP-P2X4 signaling. *eLife* **7**, doi:10.7554/eLife.31684 (2018).

16 Jiang, N. *et al.* A conserved morphogenetic mechanism for epidermal ensheathment of nociceptive sensory neurites. *eLife* **8**, e42455 (2019).

17 Talagas, M. *et al.* Keratinocytes Communicate with Sensory Neurons via Synaptic-like Contacts. *Ann. Neurol.* **88**, 1205-1219, doi:10.1002/ana.25912 (2020).

18 Üçeyler, N. Small fiber pathology—a culprit for many painful disorders? *Pain* **157**, S60-S66 (2016).

19 Cohen, H. Controversies and challenges in fibromyalgia: a review and a proposal. *Ther. Adv. Musculoskelet. Dis.* **9**, 115-127 (2017).
20 Wang, J., Chen, J. & Sen, S. MicroRNA as Biomarkers and Diagnostics. *J. Cell. Physiol.* **231**, 25-30, doi:10.1002/jcp.25056 (2016).
21 Andersen, H. H., Duroux, M. & Gazerani, P. MicroRNAs as modulators and biomarkers of inflammatory and neuropathic pain conditions. *Neurobiol. Dis.* **71**, 159-168 (2014).
22 Leinders, M. *et al.* Increased cutaneous miR-let-7d expression correlates with small nerve fiber pathology in patients with fibromyalgia syndrome. *Pain* **157**, 2493-2503, doi:10.1097/j.pain.0000000000000668 (2016).
23 Cerdá-Olmedo, G., Mena-Durán, A. V., Monsalve, V. & Oltra, E. Identification of a microRNA signature for the diagnosis of fibromyalgia. *PLoS One* **10**, e0121903, doi:10.1371/journal.pone.0121903 (2015).
24 Masotti, A. *et al.* Circulating microRNA profiles as liquid biopsies for the characterization and diagnosis of fibromyalgia syndrome. *Mol. Neurobiol.* **54**, 7129-7136 (2017).
25 Braun, A., Evdokimov, D., Frank, J., Sommer, C. & Üçeyler, N. MiR103a-3p and miR107 are related to adaptive coping in a cluster of fibromyalgia patients. *PLoS One* **15**, e0239286, doi:10.1371/journal.pone.0239286 (2020).
26 Winter, J., Jung, S., Keller, S., Gregory, R. I. & Diederichs, S. Many roads to maturity: microRNA biogenesis pathways and their regulation. *Nat. Cell Biol.* **11**, 228-234 (2009).
27 Pederson, T. Regulatory RNAs derived from transfer RNA? *Rna* **16**, 1865-1869 (2010).
28 Su, Z., Wilson, B., Kumar, P. & Dutta, A. Noncanonical roles of tRNAs: tRNA fragments and beyond. *Annu. Rev. Genet.* **54**, 47-69 (2020).
29 Krishna, S., Raghavan, S., DasGupta, R. & Palakodeti, D. tRNA-derived fragments (tRFs): establishing their turf in post-transcriptional gene regulation. *Cell. Mol. Life Sci.* **78**, 2607-2619 (2021).
30 Yu, M. *et al.* tRNA-derived RNA fragments in cancer: current status and future perspectives. *J. Hematol. Oncol.* **13**, 121, doi:10.1186/s13045-020-00955-6 (2020).
31 Von Korff, M., Ormel, J., Keefe, F. J. & Dworkin, S. F. Grading the severity of chronic pain. *Pain* **50**, 133-149 (1992).
32 Offenbaecher, M., Waltz, M. & Schoeps, P. Validation of a German version of the Fibromyalgia Impact Questionnaire (FIQ-G). *J. Rheumatol.* **27**, 1984-1988 (2000).
33 Bouhassira, D. *et al.* Development and validation of the Neuropathic Pain Symptom Inventory. *Pain* **108**, 248-257, doi:10.1016/j.pain.2003.12.024 (2004).
34 Sommer, C. *et al.* A modified score to identify and discriminate neuropathic pain: a study on the German version of the Neuropathic Pain Symptom Inventory (NPSI). *BMC Neurol.* **11**, 104, doi:10.1186/1471-2377-11-104 (2011).
35 Radloff, L. The CES-D: a self-report symptom scale to detect depression in the general population. *Appl .Psychol. Meas.* **3**, 385-401 (1977).
36 Wolfe, F. *et al.* Fibromyalgia criteria and severity scales for clinical and epidemiological studies: a modification of the ACR Preliminary Diagnostic Criteria for Fibromyalgia. *J. Rheumatol.* **38**, 1113-1122 (2011).
37 Erbacher, C. *et al.* Distinct CholinomiR Blood Cell Signature as a Potential Modulator of the Cholinergic System in Women with Fibromyalgia Syndrome. *Cells* **11**, 1276 (2022).
38 Karl, F. *et al.* Patient-derived in vitro skin models for investigation of small fiber pathology. *Ann. Clin. Transl. Neurol.* **6**, 1797-1806, doi:10.1002/acn3.50871 (2019).
39 Andrews, S. (http://www.bioinformatics.babraham.ac.uk/projects/fastqc/, 2010).
40 Dodt, M., Roehr, J. T., Ahmed, R. & Dieterich, C. FLEXBAR-Flexible Barcode and Adapter Processing for Next-Generation Sequencing Platforms. *Biology (Basel)* **1**, 895-905, doi:10.3390/biology1030895 (2012).

41 Loher, P., Telonis, A. G. & Rigoutsos, I. MINTmap: fast and exhaustive profiling of nuclear and mitochondrial tRNA fragments from short RNA-seq data. *Sci. Rep.* **7**, 41184, doi:10.1038/srep41184 (2017).

42 Wang, W.-C. *et al.* miRExpress: analyzing high-throughput sequencing data for profiling microRNA expression. *BMC Bioinform.* **10**, 1-13 (2009).

43 Love, M. I., Huber, W. & Anders, S. Moderated estimation of fold change and dispersion for RNA-seq data with DESeq2. *Genome Biol.* **15**, 1-21 (2014).

44 Wickham, H. *ggplot2: elegant graphics for data analysis*. (Springer: New York, NY, USA, 2016).

45 Team, R. C. The R project for statistical computing Available at: https://www.r-project.org. *Accessed January* **26** (2018).

46 Vlachos, I. S. *et al.* DIANA-miRPath v3.0: deciphering microRNA function with experimental support. *Nucleic Acids Res.* **43**, W460-466, doi:10.1093/nar/gkv403 (2015).

47 Xiao, Q. *et al.* tRFTars: predicting the targets of tRNA-derived fragments. *J. Transl. Med.* **19**, 88, doi:10.1186/s12967-021-02731-7 (2021).

48 Winek, K. *et al.* Transfer RNA fragments replace microRNA regulators of the cholinergic poststroke immune blockade. *PNAS* **117**, 32606-32616 (2020).

49 Karl, F. *et al.* Fibromyalgia versus small fiber neuropathy: diverse keratinocyte transcriptome signature. *Pain* (2021).

50 Peng, S. L. Foxo in the immune system. *Oncogene* **27**, 2337-2344, doi:10.1038/onc.2008.26 (2008).

51 Wang, Y., Zhou, Y. & Graves, D. T. FOXO transcription factors: their clinical significance and regulation. *Biomed Res. Int.* **2014**, 925350, doi:10.1155/2014/925350 (2014).

52 Bjersing, J. L., Bokarewa, M. I. & Mannerkorpi, K. Profile of circulating microRNAs in fibromyalgia and their relation to symptom severity: an exploratory study. *Rheumatol. Int.* **35**, 635-642, doi:10.1007/s00296-014-3139-3 (2015).

53 Zhu, P., Yu, J. & Zhou, P. Role of tRNA-derived fragments in cancer: novel diagnostic and therapeutic targets tRFs in cancer. *Am. J. Cancer Res.* **10**, 393-402 (2020).

54 Huang, P. *et al.* Elevation of plasma tRNA fragments as a promising biomarker for liver fibrosis in nonalcoholic fatty liver disease. *Sci. Rep.* **11**, 5886, doi:10.1038/s41598-021-85421-0 (2021).

55 Haftmann, C. *et al.* Lymphocyte signaling: regulation of FoxO transcription factors by microRNAs. *Ann. N. Y. Acad. Sci.* **1247**, 46-55, doi:10.1111/j.1749-6632.2011.06264.x (2012).

56 Song, R., Liu, Q., Liu, T. & Li, J. Connecting rules from paired miRNA and mRNA expression data sets of HCV patients to detect both inverse and positive regulatory relationships. *BMC Genom.* **16 Suppl 2**, S11, doi:10.1186/1471-2164-16-s2-s11 (2015).

57 Vasudevan, S. Posttranscriptional upregulation by microRNAs. *Wiley Interdiscip. Rev. RNA* **3**, 311-330, doi:10.1002/wrna.121 (2012).

58 Gulyaeva, L. F. & Kushlinskiy, N. E. Regulatory mechanisms of microRNA expression. *J. Transl. Med.* **14**, 143, doi:10.1186/s12967-016-0893-x (2016).

59 Ebert, M. S. & Sharp, P. A. Roles for microRNAs in conferring robustness to biological processes. *Cell* **149**, 515-524, doi:10.1016/j.cell.2012.04.005 (2012).

60 Roggenkamp, D. *et al.* Atopic keratinocytes induce increased neurite outgrowth in a coculture model of porcine dorsal root ganglia neurons and human skin cells. *J. Invest. Dermatol.* **132**, 1892-1900, doi:10.1038/jid.2012.44 (2012).

61 Ulmann, L. *et al.* Trophic effects of keratinocytes on the axonal development of sensory neurons in a coculture model. *Eur. J. Neurosci.* **26**, 113-125, doi:10.1111/j.1460-9568.2007.05649.x (2007).

62 Stucky, C. L. & Mikesell, A. R. Cutaneous pain in disorders affecting peripheral nerves. *Neurosci. Lett.* **765**, 136233, doi:10.1016/j.neulet.2021.136233 (2021).

63 Raja, R., Sivamani, K., Garcia, M. S. & Isseroff, R. R. Wound re-epithelialization: modulating keratinocyte migration in wound healing. *Front. Biosci. - Landmark* **12**, 2849-2868 (2007).
64 Mohammed, J. *et al.* TGFβ1 overexpression by keratinocytes alters skin dendritic cell homeostasis and enhances contact hypersensitivity. *J. Invest. Dermatol.* **133**, 135-143 (2013).
65 Mestrallet, G. *et al.* Human Keratinocytes Inhibit CD4+ T-Cell Proliferation through TGFB1 Secretion and Surface Expression of HLA-G1 and PD-L1 Immune Checkpoints. *Cells* **10**, 1438 (2021).
66 Bjersing, J. L., Bokarewa, M. I. & Mannerkorpi, K. Profile of circulating microRNAs in fibromyalgia and their relation to symptom severity: an exploratory study. *Rheumatol. Int.* **35**, 635-642 (2015).

Supplementary data

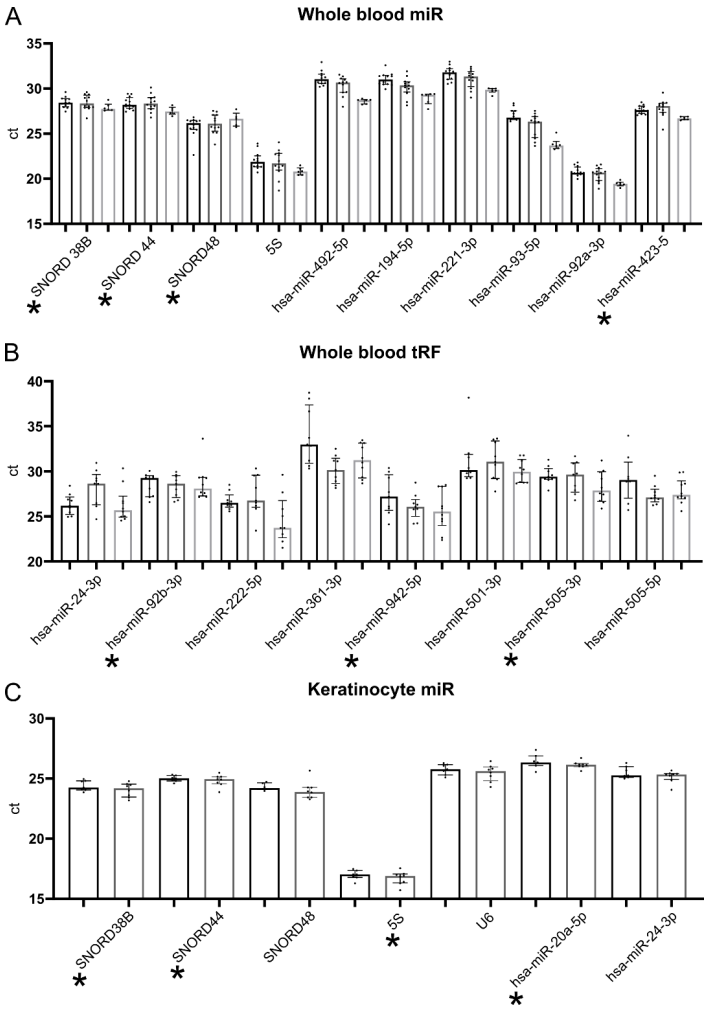

Figure S1. Evaluation of endogenous controls. (A) For normalization of whole blood miRs from Tempus Tubes in qRT-PCR ten transcripts were tested with samples from hCO (n = 12, black bars), FMS (n = 12, dark grey bars), and dCO (n = 6, light grey bars). (B) Eight transcripts were assessed for size selected Tempus Tube derived RNA from hCO (n = 9, black bars), FMS (n = 9,

721 dark grey bars), and dCO (n = 10, light grey bars). (C) In case of keratinocyte miR qRT-PCR
722 seven potential endogenous control transcripts were screened with hCO (n = 7, black bars) versus
723 FMS (n = 8, light grey bars). Selected endogenous controls are marked by asterisks and were
724 used in combination via geometric mean. Abbreviations: dCO, disease control; FMS,
725 fibromyalgia syndrome; hCO, healthy control; miR, microRNA; qRT-PCR, quantitative real-time
726 PCR; tRF, tRNA derived fragment.

727

728 Table S1: List of all DE miRs in Tempus Tube blood of FMS patients versus hCO.

Rank	miRs	baseMean	log2FoldChange	lfcSE	stat	pvalue	padj
1	hsa-miR-148a-3p	2139.84	0.58	0.11	5.37	8.02E-08	4.35E-05
2	hsa-miR-192-5p	669.28	0.59	0.12	4.98	6.39E-07	1.74E-04
3	hsa-miR-326	130.98	-0.38	0.08	-4.51	6.53E-06	1.18E-03
4	hsa-miR-576-5p	151.80	0.97	0.22	4.34	1.40E-05	1.89E-03
5	hsa-miR-182-5p	6921.24	0.76	0.18	4.30	1.75E-05	1.90E-03
6	hsa-miR-3653-5p	26.99	-0.69	0.16	-4.24	2.27E-05	2.05E-03
7	hsa-let-7i-5p	312800.86	0.39	0.09	4.20	2.66E-05	2.06E-03
8	hsa-miR-128-3p	5697.83	0.45	0.11	4.16	3.19E-05	2.17E-03
9	hsa-miR-664a-3p	33.89	0.79	0.20	4.02	5.82E-05	3.51E-03
10	hsa-miR-27b-3p	599.67	0.36	0.10	3.69	2.26E-04	1.23E-02
11	hsa-miR-183-5p	7989.70	0.67	0.19	3.61	3.12E-04	1.35E-02
12	hsa-miR-218-5p	9.93	2.52	0.71	3.55	3.89E-04	1.35E-02
13	hsa-miR-25-5p	304.73	-0.49	0.14	-3.53	4.22E-04	1.35E-02
14	hsa-miR-340-5p	44.43	0.57	0.16	3.53	4.13E-04	1.35E-02
15	hsa-miR-660-5p	24.14	0.58	0.16	3.56	3.77E-04	1.35E-02
16	hsa-miR-6726-3p	164.92	-0.65	0.18	-3.58	3.40E-04	1.35E-02
17	hsa-miR-935	8.43	-1.04	0.29	-3.61	3.00E-04	1.35E-02
18	hsa-miR-148b-5p	61.83	0.51	0.15	3.46	5.49E-04	1.65E-02
19	hsa-let-7d-3p	14276.37	-0.58	0.17	-3.42	6.28E-04	1.79E-02
20	hsa-miR-126-5p	91.73	1.06	0.32	3.32	8.99E-04	2.44E-02
21	hsa-miR-25-3p	125185.95	0.38	0.12	3.30	9.66E-04	2.50E-02
22	hsa-miR-1229-3p	132.34	-0.52	0.16	-3.26	1.10E-03	2.59E-02
23	hsa-miR-425-3p	287.60	0.29	0.09	3.27	1.06E-03	2.59E-02

24	hsa-let-7f-5p	76281.11	0.76	0.24	3.22	1.29E-03	2.83E-02
25	hsa-miR-576-3p	24.38	0.62	0.19	3.22	1.30E-03	2.83E-02
26	hsa-miR-766-3p	54.99	-0.43	0.13	-3.19	1.41E-03	2.94E-02
27	hsa-miR-1976	417.92	-0.37	0.12	-3.18	1.47E-03	2.96E-02
28	hsa-miR-379-5p	11.38	1.39	0.44	3.17	1.53E-03	2.96E-02
29	hsa-miR-877-3p	19.26	-0.55	0.18	-3.15	1.65E-03	2.99E-02
30	hsa-miR-9-5p	11.97	0.80	0.25	3.15	1.64E-03	2.99E-02
31	hsa-miR-101-3p	2527.49	0.64	0.20	3.12	1.81E-03	3.07E-02
32	hsa-miR-98-5p	2092.98	0.78	0.25	3.13	1.77E-03	3.07E-02
33	hsa-miR-99a-5p	274.07	0.77	0.25	3.11	1.89E-03	3.11E-02
34	hsa-miR-335-3p	15.83	0.90	0.29	3.07	2.11E-03	3.38E-02
35	hsa-miR-1343-3p	124.82	-0.48	0.16	-3.03	2.47E-03	3.50E-02
36	hsa-miR-186-5p	5198.64	0.40	0.13	3.01	2.58E-03	3.50E-02
37	hsa-miR-3609	6.51	-0.75	0.25	-3.02	2.53E-03	3.50E-02
38	hsa-miR-6885-3p	26.14	-0.42	0.14	-3.02	2.54E-03	3.50E-02
39	hsa-miR-6894-3p	47.61	-0.42	0.14	-3.04	2.36E-03	3.50E-02
40	hsa-miR-7-5p	2509.29	0.54	0.18	3.05	2.28E-03	3.50E-02
41	hsa-miR-374a-5p	171.72	0.86	0.29	2.98	2.90E-03	3.58E-02
42	hsa-miR-454-3p	184.84	0.73	0.25	2.98	2.89E-03	3.58E-02
43	hsa-miR-6812-3p	19.55	-0.48	0.16	-2.98	2.90E-03	3.58E-02
44	hsa-miR-769-3p	21.27	-0.44	0.15	-2.99	2.75E-03	3.58E-02
45	hsa-miR-3613-5p	24.56	0.99	0.33	2.96	3.07E-03	3.62E-02
46	hsa-miR-625-5p	49.75	-0.64	0.22	-2.97	3.01E-03	3.62E-02
47	hsa-miR-10a-5p	85.70	0.65	0.22	2.93	3.44E-03	3.92E-02
48	hsa-miR-454-5p	14.77	0.69	0.23	2.92	3.46E-03	3.92E-02
49	hsa-miR-328-3p	8051.13	-0.42	0.15	-2.91	3.60E-03	3.99E-02
50	hsa-miR-4723-3p	12.45	-0.60	0.21	-2.90	3.79E-03	4.11E-02
51	hsa-miR-548ad-5p	30.90	0.75	0.26	2.88	3.98E-03	4.23E-02
52	hsa-miR-3143	7.46	1.23	0.43	2.86	4.21E-03	4.38E-02
53	hsa-miR-323b-3p	27.35	0.88	0.31	2.85	4.42E-03	4.38E-02
54	hsa-miR-532-3p	482.96	-0.27	0.10	-2.84	4.52E-03	4.38E-02
55	hsa-miR-548ae-5p	30.02	0.75	0.26	2.86	4.30E-03	4.38E-02
56	hsa-miR-6855-3p	10.83	-0.54	0.19	-2.84	4.48E-03	4.38E-02
57	hsa-miR-140-3p	7958.31	0.25	0.09	2.83	4.65E-03	4.39E-02
58	hsa-miR-4433a-5p	23.32	-1.07	0.38	-2.83	4.69E-03	4.39E-02
59	hsa-miR-144-5p	933.92	0.52	0.19	2.82	4.81E-03	4.43E-02
60	hsa-miR-1275	26.46	-0.55	0.19	-2.81	4.90E-03	4.43E-02
61	hsa-miR-143-3p	131.01	0.57	0.20	2.79	5.32E-03	4.48E-02
62	hsa-miR-221-5p	41.95	0.45	0.16	2.77	5.52E-03	4.48E-02

63	hsa-miR-339-5p	467.82	-0.42	0.15	-2.80	5.12E-03	4.48E-02
64	hsa-miR-548ay-5p	39.22	0.70	0.25	2.79	5.32E-03	4.48E-02
65	hsa-miR-548d-5p	33.78	0.74	0.26	2.78	5.37E-03	4.48E-02
66	hsa-miR-671-5p	20.06	-0.73	0.26	-2.77	5.61E-03	4.48E-02
67	hsa-miR-6789-3p	14.12	-0.58	0.21	-2.77	5.55E-03	4.48E-02
68	hsa-miR-7704	51.83	0.80	0.28	2.79	5.21E-03	4.48E-02
69	hsa-miR-450a-5p	27.57	0.55	0.20	2.74	6.10E-03	4.80E-02

729 Abbreviations: FMS, fibromyalgia syndrome; hCO, healthy control; lfcSE, standard error of the

730 log2FoldChange estimate; padj, Benjamini-Hochberg adjusted p-value.

731

732 Table S2: List of all DE tRFs in Tempus Tube blood of FMS patients versus hCO.

Rank	TRFs	baseMean	log2FoldChange	lfcSE	stat	pvalue	padj
1	tRF-16-9N1EWJ0	13.73	1.13	0.25	4.53	5.9E-06	1.2E-03
2	tRF-21-WB8647O5D	100.75	0.73	0.16	4.60	4.1E-06	1.2E-03
3	tRF-22-WB8647O52	259.93	0.73	0.16	4.44	9.1E-06	1.2E-03
4	tRF-18-WB0Q37DW	53.97	1.20	0.28	4.32	1.6E-05	1.6E-03
5	tRF-19-WB0Q37IO	40.48	1.08	0.26	4.13	3.6E-05	2.4E-03
6	tRF-22-WB86N7O52	100.12	0.65	0.16	4.13	3.6E-05	2.4E-03
7	tRF-19-JMRPFQIX	10.10	1.06	0.27	3.97	7.3E-05	4.2E-03
8	tRF-22-8BWS72092	14.80	0.76	0.20	3.78	1.6E-04	7.9E-03
9	tRF-22-WB863IP52	101.57	0.66	0.18	3.60	3.2E-04	1.4E-02
10	tRF-18-H9R8B7D2	20.35	0.86	0.24	3.52	4.4E-04	1.8E-02
11	tRF-18-S3M83004	53.64	0.63	0.18	3.49	4.8E-04	1.8E-02
12	tRF-20-40KK5Y93	275.72	0.57	0.17	3.39	7.1E-04	2.2E-02
13	tRF-22-WE884U1D2	11.63	0.89	0.26	3.40	6.7E-04	2.2E-02
14	tRF-19-WB8647HU	31.39	0.80	0.24	3.36	7.9E-04	2.3E-02
15	tRF-18-18YKISD8	8.40	0.84	0.25	3.29	1.0E-03	2.4E-02
16	tRF-21-WB08Q2B5D	8.73	0.77	0.23	3.30	9.6E-04	2.4E-02
17	tRF-22-WD8YQ84V2	51.55	0.56	0.17	3.30	9.7E-04	2.4E-02
18	tRF-21-8EKSPM85D	7.57	0.86	0.27	3.23	1.3E-03	2.8E-02
19	tRF-22-WEK8Q2B52	12.33	0.86	0.27	3.17	1.5E-03	3.2E-02
20	tRF-21-WB863IP5D	32.09	0.56	0.18	3.15	1.6E-03	3.3E-02
21	tRF-19-18YKISIM	22.35	0.64	0.21	3.00	2.7E-03	4.9E-02
22	tRF-22-WEPSJR852	31.82	0.73	0.24	3.00	2.7E-03	4.9E-02

733 Abbreviations: FMS, fibromyalgia syndrome; hCO, healthy control; lfcSE, standard error of the

734 log2FoldChange estimate; padj, Benjamini-Hochberg adjusted p-value.

735

736 Table S3: List of all DE miRs in keratinocytes of FMS patients versus hCO.

Rank	miR	baseMean	log2FoldChange	lfcSE	stat	pvalue	padj
1	hsa-mir-122-5p	25.29	-1.59	0.35	-4.50	6.74E-06	3.47E-03
2	hsa-mir-485-5p	8.54	-2.18	0.50	-4.35	1.39E-05	3.58E-03
3	hsa-let-7a-2-3p	11.00	-0.98	0.31	-3.21	1.34E-03	2.91E-02
4	hsa-mir-10b-3p	7.82	-2.25	0.72	-3.12	1.81E-03	2.91E-02
5	hsa-mir-10b-5p	855.86	-2.15	0.65	-3.32	8.85E-04	2.91E-02
6	hsa-mir-125b-1-3p	427.65	-1.23	0.37	-3.30	9.80E-04	2.91E-02
7	hsa-mir-127-3p	202.07	-1.74	0.50	-3.48	4.93E-04	2.91E-02
8	hsa-mir-134	26.70	-1.62	0.52	-3.14	1.71E-03	2.91E-02
9	hsa-mir-136-5p	15.88	-2.07	0.60	-3.42	6.23E-04	2.91E-02
10	hsa-mir-148b-3p	2902.39	0.30	0.09	3.20	1.36E-03	2.91E-02
11	hsa-mir-151a-3p	29138.08	-0.27	0.09	-3.15	1.63E-03	2.91E-02
12	hsa-mir-25-5p	61.48	-1.01	0.28	-3.57	3.57E-04	2.91E-02
13	hsa-mir-26a-1-5p	90826.30	0.28	0.09	3.29	1.02E-03	2.91E-02
14	hsa-mir-26a-2-5p	90828.80	0.28	0.09	3.29	1.02E-03	2.91E-02
15	hsa-mir-30e-3p	1903.09	0.27	0.09	3.16	1.56E-03	2.91E-02
16	hsa-mir-3182	11.59	-1.57	0.49	-3.21	1.34E-03	2.91E-02
17	hsa-mir-365a-5p	191.82	-0.74	0.20	-3.74	1.83E-04	2.91E-02
18	hsa-mir-369-3p	23.35	-1.93	0.59	-3.29	1.01E-03	2.91E-02
19	hsa-mir-369-5p	17.69	-1.95	0.60	-3.27	1.08E-03	2.91E-02
20	hsa-mir-379-5p	140.41	-1.73	0.50	-3.46	5.46E-04	2.91E-02
21	hsa-mir-381-3p	570.96	-1.94	0.53	-3.62	2.92E-04	2.91E-02
22	hsa-mir-382-5p	38.42	-1.59	0.50	-3.16	1.60E-03	2.91E-02
23	hsa-mir-411-3p	17.16	-1.75	0.56	-3.13	1.76E-03	2.91E-02
24	hsa-mir-411-5p	157.42	-1.72	0.52	-3.33	8.72E-04	2.91E-02
25	hsa-mir-487b	5.75	-2.07	0.64	-3.24	1.18E-03	2.91E-02
26	hsa-mir-493-3p	100.25	-1.75	0.47	-3.68	2.31E-04	2.91E-02
27	hsa-mir-494	23.02	-1.86	0.53	-3.48	4.96E-04	2.91E-02
28	hsa-mir-503-5p	1202.80	-0.62	0.20	-3.15	1.65E-03	2.91E-02
29	hsa-mir-576-3p	280.61	-0.49	0.15	-3.26	1.13E-03	2.91E-02
30	hsa-mir-654-3p	97.39	-1.67	0.53	-3.18	1.48E-03	2.91E-02

31	hsa-mir-92b-3p	481.18	-0.74	0.23	-3.20	1.37E-03	2.91E-02
32	hsa-mir-92b-5p	30.35	-0.74	0.22	-3.28	1.04E-03	2.91E-02
33	hsa-mir-200a-5p	1834.04	-0.36	0.12	-3.04	2.40E-03	3.74E-02
34	hsa-mir-409-3p	159.31	-1.41	0.47	-3.00	2.67E-03	3.97E-02
35	hsa-mir-493-5p	133.86	-1.47	0.49	-3.00	2.70E-03	3.97E-02
36	hsa-mir-3662	15.09	-1.09	0.37	-2.97	2.93E-03	4.19E-02
37	hsa-mir-1296	59.16	-0.44	0.15	-2.94	3.33E-03	4.30E-02
38	hsa-mir-136-3p	18.09	-1.85	0.63	-2.93	3.34E-03	4.30E-02
39	hsa-mir-4473	38.12	-0.38	0.13	-2.94	3.26E-03	4.30E-02
40	hsa-mir-485-3p	9.95	-1.45	0.49	-2.94	3.32E-03	4.30E-02
41	hsa-mir-370	147.80	-1.54	0.53	-2.92	3.49E-03	4.39E-02

737 Abbreviations: FMS, fibromyalgia syndrome; hCO, healthy control; lfcSE, standard error of the

738 log2FoldChange estimate; padj, Benjamini-Hochberg adjusted p-value.

739

740 Table S4: List of all DE tRFs in keratinocytes of FMS patients versus hCO.

Rank	trf	baseMean	log2FoldChange	lfcSE	stat	pvalue	padj
1	tRF-36-86V8WPMN1E8Y7ZD	18.88	-2.15	0.43	-5.02	5.29E-07	1.48E-03
2	tRF-34-P4R8YP9LON4VHM	21.63	-1.78	0.38	-4.67	3.08E-06	4.31E-03
3	tRF-25-PS5P4PW3FJ	44.17	-1.43	0.32	-4.46	8.18E-06	4.98E-03
4	tRF-40-86V8WPMN1E8Y7Z2R	10.08	-2.23	0.50	-4.44	8.91E-06	4.98E-03
5	tRF-26-86V8WPMN1EE	90.84	-1.37	0.31	-4.39	1.15E-05	5.35E-03
6	tRF-19-VBY9PY1I	30.21	1.21	0.28	4.25	2.10E-05	8.09E-03
7	tRF-34-79MP9PMNH5IS15	30.30	-1.78	0.42	-4.23	2.31E-05	8.09E-03
8	tRF-39-86J8WPMN1E8Y7ZFV	37.30	-1.81	0.44	-4.12	3.78E-05	9.89E-03
9	tRF-43-86V8WPMN1E8Y7Z2RY	5.79	-2.08	0.51	-4.11	3.89E-05	9.89E-03
10	tRF-35-P4R8YP9LON4VN1	22.59	-1.92	0.47	-4.08	4.58E-05	1.05E-02
11	tRF-42-87R8WP9I1EWJQZ2SJ	14.20	-1.24	0.30	-4.06	4.87E-05	1.05E-02
12	tRF-22-NYDRFO8UN	23.91	0.77	0.19	4.01	6.09E-05	1.22E-02
13	tRF-40-B9I1KQSX0DIJZ726	17.31	1.50	0.38	3.90	9.76E-05	1.82E-02
14	tRF-39-86V8WPMN1E8Y7ZFV	20.02	-2.29	0.60	-3.83	1.28E-04	2.24E-02
15	tRF-20-BMW36D46	14.68	-1.30	0.35	-3.74	1.81E-04	2.97E-02
16	tRF-29-I3VF4YO9XE1H	8.41	-1.47	0.40	-3.71	2.10E-04	2.98E-02
17	tRF-35-11W4QFE3FVSYER	12.83	-1.63	0.44	-3.73	1.92E-04	2.98E-02
18	tRF-40-86J8WPMN1E8Y7Z2R	16.52	-1.52	0.41	-3.70	2.13E-04	2.98E-02

19	tRF-25-S3M8309NDJ	14.03	-1.53	0.42	-3.66	2.55E-04	3.23E-02
20	tRF-26-Q3V2Y7RZ81D	6.56	-1.43	0.39	-3.66	2.49E-04	3.23E-02
21	tRF-30-5Z2IUIX1Q7O6	20.07	1.71	0.48	3.58	3.46E-04	4.11E-02
22	tRF-30-JZOYJE22RRN3	33.50	0.83	0.23	3.57	3.53E-04	4.11E-02

741 Abbreviations: FMS, fibromyalgia syndrome; hCO, healthy control; lfcSE, standard error of the

742 log2FoldChange estimate; padj, Benjamini-Hochberg adjusted p-value.

743

7.3. Chapter III: Interaction of human keratinocytes and nerve fiber terminals at the neuro-cutaneous unit

Interaction of human keratinocytes and nerve fiber terminals at the neuro-cutaneous unit

Christoph Erbacher[1], Sebastian Britz[2], Philine Dinkel[1, #], Thomas Klein[1], Markus Sauer[3], Christian Stigloher[2], Nurcan Üçeyler[1*]

[1]Department of Neurology, University of Würzburg, 97080 Würzburg, Germany

[2]Imaging Core Facility, Biocenter, University of Würzburg, 97074 Würzburg, Germany

[3]Department of Biotechnology and Biophysics, University of Würzburg, 97074 Würzburg, Germany

Current affiliation: [#]Institute of Clinical Genetics, Technical University Dresden, 01307 Dresden, Germany

eLife, in revision

preprint on bioRxiv

https://doi.org/10.1101/2022.02.23.481592

February 26, 2022

Interaction of human keratinocytes and nerve fiber terminals at the neuro-cutaneous unit

Christoph Erbacher[1], Sebastian Britz[2], Philine Dinkel[1,#], Thomas Klein[1], Markus Sauer[3], Christian Stigloher[2], Nurcan Üçeyler[1*]

[1]Department of Neurology, University of Würzburg, 97080 Würzburg, Germany

[2] Imaging Core Facility, Biocenter, University of Würzburg, 97074 Würzburg, Germany

[3]Department of Biotechnology and Biophysics, University of Würzburg, 97074 Würzburg, Germany

Current affiliation:

[#]Institute of Clinical Genetics, Technical University Dresden, 01307 Dresden, Germany

Corresponding author:

Prof. Dr. Nurcan Üçeyler, MD

Department of Neurology, University of Würzburg,

Josef-Schneider-Str. 11, 97080 Würzburg, Germany

Phone: +49 931 201 23542

Fax: +49 931 201 623542

e-mail address: ueceyler_n@ukw.de

Abstract:

Traditionally, peripheral sensory neurons hold the monopole of transducing external stimuli. Current research moves epidermal keratinocytes into focus as sensors and transmitters of nociceptive and non-nociceptive sensations, tightly interacting with intraepidermal nerve fibers at the neuro-cutaneous unit. In animal models, epidermal cells establish close contacts and ensheath sensory neurites. However, ultrastructural morphological and mechanistic data examining the human keratinocyte-nociceptor interface are sparse. We investigated this exact interface in human skin applying super-resolution array tomography, expansion microscopy, and structured illumination microscopy. We show keratinocyte ensheathment of nociceptors and connexin 43 plaques at keratinocyte-nociceptor contact sites in healthy native skin. We further derived a fully human co-culture system, modeling ensheathment and connexin 43 plaques *in vitro*. Unraveling human intraepidermal nerve fiber ensheathment and interaction sites marks a milestone in research at the neuro-cutaneous unit. These findings are mind-changers on the way to decipher the mechanisms of cutaneous nociception.

1. Introduction

Impairment of the thinly-myelinated A-delta and unmyelinated C-nerve fibers may underlie small nerve fiber pathology observed in patients with peripheral (Birklein, 2005; Lacomis, 2002; Üçeyler *et al.*, 2013) and central nervous system diseases (Nolano *et al.*, 2008; Weis *et al.*, 2011). Cutaneous nerve fiber degeneration and sensitization are hallmarks of small fiber pathology, however, the underlying pathomechanisms are unclear (Üçeyler, 2016). The impact of skin cells on nociceptive and non-nociceptive stimulus detection is increasingly recognized (Lumpkin and Caterina, 2007; Stucky and Mikesell, 2021).

Physiologically, keratinocytes are the predominant cell type in the epidermis and actively participate in sensory signal transduction and nociception at the neuro-cutaneous unit (NCU). In animal *in vitro* cell culture models, selective thermal, chemical, or mechanical keratinocyte stimulation led to activation of co-cultured peripheral neurons (Klusch *et al.*, 2013; Mandadi *et al.*, 2009; Sondersorg *et al.*, 2014). Using animal models, nociceptive behavior was induced in mice selectively expressing transient receptor potential vanilloid 1 (TRPV1) in keratinocytes after capsaicin treatment (Pang *et al.*, 2015). Mice expressing channelrhodopsin-2 in keratinocytes also displayed pain behavior and intraepidermal nerve fiber (IENF) derived evoked nerve fiber action potentials during laser stimulation (Baumbauer *et al.*, 2015).

For underlying functional stimulus transduction of keratinocytes and IENF, signaling molecules such as adenosine triphosphate (ATP) are increasingly recognized (Mandadi *et al.*, 2009; Moehring *et al.*, 2018). Hemichannels or gap junctions formed by connexins and pannexins, or vesicular transport may conduct ATP signaling towards afferent nerve fibers (Barr *et al.*, 2013; Maruyama *et al.*, 2018; Sondersorg *et al.*, 2014). Signaling might happen via specialized synapse-like connections to IENF (Talagas *et al.*, 2020b). In *Danio rerio* and *Drosophila* models, nerve endings are frequently ensheathed by epidermal cells (Jiang *et al.*,

2019; O'Brien *et al.*, 2012) and tunneling of fibers through keratinocytes in human skin has recently been shown via confocal microscopy (Talagas *et al.*, 2020a). However, the exact mechanisms and mode of signal transduction at the NCU remain elusive.

In an embryonal stem cell-derived 2D human cell culture model, physical contacts between sensory neurons and keratinocytes were observed hinting towards close coupling (Krishnan-Kutty *et al.*, 2017). Still, direct and systematic information on ensheathment of human IENF is scarce and ultrastructural architecture or molecular processes remain obscure. Deciphering these contact zones in the human system may profoundly change the understanding of somatosensory processing in health and disease. Ultimately, altered keratinocyte signal molecule release or dysfunctional signaling sites may contribute to cutaneous pain perception (Talagas *et al.*, 2017), which could open novel avenues for treatment of small fiber pathology and neuropathic pain (Keppel Hesselink *et al.*, 2017).

We aimed at studying exactly these contact zones between keratinocytes and IENF at the NCU in the human system to gain insights on ultrastructure and potential crosstalk in the epidermis. A correlative light and electron microscopy approach via super-resolution array tomography (srAT) in high-pressure frozen, freeze substituted samples (Markert *et al.*, 2017) and expansion microscopy (ExM) (Tillberg *et al.*, 2016) in diagnostically relevant paraformaldehyde-fixed tissue sections revealed ensheathment and pore protein connexin 43 (Cx43) plaques in native human skin. We further succeeded to establish a fully human keratinocyte and sensory neuron co-culture, which inherited both features of the NCU. We propose a crucial role of nerve fiber ensheathment and Cx43-based keratinocyte-fiber contacts in neuropathic pain and small fiber pathology widening the scope of somatosensorics to non-neuronal cells.

Materials and methods

Participants

Healthy volunteers were recruited at the Department of Neurology, University of Würzburg, Germany. For srAT, a 2-mm skin punch biopsy was taken from the back at th10 level (device by Stiefel GmbH, Offenbach, Germany) under local anesthesia following a standard procedure (Üçeyler *et al.*, 2010). Tissue sections for ExM and cell cultures were acquired from 6-mm skin biopsy samples taken from the upper thigh according to a previously published protocol (Karl *et al.*, 2019). Our study was approved by the Würzburg Medical School Ethics committee (#135/15).

srAT sample preparation

Biopsies were immediately wetted in freezing solution composed of 20 % (w/v) polyvinylpyrrolidon in phosphate buffered saline (PBS) (0.1 M, pH = 7.4) to prevent dehydration. The epidermal layer was manually dissected from dermal and subdermal compartments of the skin sample and transferred into a type A aluminium specimen carrier (Leica Microsystems, Wetzlar, Germany) with recesses of 200 µm containing polyvinylpyrrolidon and capped with a second carrier without recess (Leica Microsystems, Wetzlar, Germany). Subsequent high pressure freezing and freeze substitution was applied as described previously (Markert *et al.*, 2016). 100-nm serial sections were cut via a histo Jumbo Diamond Knife (DiATOME, Biel, Switzerland) with an ultra-microtome EM UC7 (Leica Microsystems, Wetzlar, Germany). Sections were held together as array by adhesive glue (pattex gel compact, Henkel, Düsseldorf-Holthausen, Germany), mixed with xylene (AppliChem, Darmstadt, Germany) and Spinel Black 47400 pigment (Kremer pigmente, Aichstetten,

Germany), which was added to the lower side of the LR-White block prior to cutting. Ribbons were collected on poly-L-lysine coated slides (Thermo Fisher Scientific, Waltham, MA, USA).

srAT immunolabeling, fluorescence imaging, and image processing

Primary and secondary antibodies used for srAT experiments are listed in Table 1. Ultrathin serial tissue sections were encircled via a pap pen (Science Services, München, Germany). A blocking solution containing 0.05 % (v/v) tween20 and 0.1% (w/v) bovine serum albumin in PBS was added for 5 min. Primary antibodies diluted 1:400 in blocking solution were then dropped onto the slides while the initial solution was withdrawn by applying filter paper on the adjacent side of the encircled area. Primary antibodies were incubated for 1 hour in closed humid chambers at room temperature (RT). Samples were washed four times with PBS in 5 min intervals. Afterwards, secondary antibodies were applied for 30 min at RT at 1:400 dilution in blocking solution containing 1:10,000 4',6-diamidino-2-phenylindole (DAPI; Sigma Aldrich, St. Louise, MO, USA) in the closed humid chamber. Samples were washed again four times with PBS and a last washing step with double distilled H_2O (ddH_2O) for 5 min was added. Slides were dried with filter paper, mounted in mowiol 4-88 (Roth, Karlsruhe, Germany), and covered with high precision cover glass No. 1.5H (Roth, Karlsruhe, Germany).

129 **Table 1:** Antibodies and directly conjugated markers. Used reagents in each experiment are
130 indicated under the column 'Application'.

Primary antibodies	Company	Catalog number	Application
Actin ExM 546 (phalloidin derivate)	Chrometra, Kortenaken, Belgium	na	ExM
Cholera Toxin Subunit B (Recombinant), Alexa Fluor 488 Conjugate	Thermo Fisher Scientific, Waltham, ME, USA	C34775	ICC
Monoclonal mouse anti- protein gene product 9.5	AbD serotec, Puchheim, Germany	7863-1004	srAT
Monoclonal rabbit anti-S100β	Abcam, Cambridge, UK	ab52642	srAT
Mouse anti-Neurofilament marker (pan-neuronal, cocktail)	BioLegend, San Diego, CA, USA	837801	ICC
Polyclonal guinea pig anti-Desmoplakin	Progen, Heidelberg, Germany	DP-1	srAT
Polyclonal rabbit anti- protein gene product 9.5	Zytomed, Berlin, Germany	516- 3344	ExM
Polyclonal rabbit anti-Connexin 43	Sigma Aldrich, St. Louise, MO, USA	C6219	srAT, ExM, ICC
Rabbit polyclonal anti-Synaptophysin	Merck, Darmstadt, Germany	AB9272	ICC
Wheat germ agglutinin, Alexa Fluor 647 conjugate	Thermo Fisher Scientific, Waltham, ME, USA	W32466	ICC
Secondary antibodies			
Alexa Fluor 488 donkey anti-mouse	Dianova, Hamburg, Germany	715-545-150	srAT, ExM
CF568 donkey anti-rabbit	Biotium, Fremont, CA, USA	20098-1	ICC
CF633 goat anti-rabbit	Biotium, Fremont, CA, USA	20122-1	ExM, ICC
Cy3 goat anti-guinea pig	Dianova, Hamburg, Germany	106-165-003	srAT
SeTau-647 anti-Rabbit	Conjugated antibody kindly provided by Prof. Markus Sauer, Department of Biotechnology and Biophysics, University of Würzburg, Germany.		srAT

131 Abbreviations: ExM, expansion microscopy; ICC, immunohistochemistry; srAT, super-resolution
132 array tomography

Image acquisition was performed with the Zeiss ELYRA S.1 SR-SIM with 63x oil-immersion objective plan-apochromat 63x, NA 1.4 Oil Dic M27 and ZEN (black edition) software (all Zeiss, Oberkochen, Germany) with PCO Edge 5.5 sCMOS camera (PCO, Kelheim, Germany), using three rotations. 700 nm z-stacks in 100 nm increments around the observed focal point of DAPI staining per section were imaged. Fluorescence images were processed via image J (version 1.51n, National Institute of Health, Bethesda, MD, USA). Channels were assigned to a defined color code and minimum and maximum of the image histogram adjusted for each channel separately.

The image slice with the brightest signal and best focus within the z-stack was determined for each channel separately to adjust for different light emission wavelength of fluorophores. Each channel was exported as a portable network graphic (png) format file.

Electron microscopy sample preparation and imaging

For contrasting and carbon coating of the samples, cover glasses were removed and mowiol was washed out with ddH_2O and blow dried. The object glass area containing the ribbon was cut out with a diamond pen (Roth, Karlsruhe, Germany). A 2.5% (w/v) uranyl acetate (Merck, Darmstadt, Germany) in ethanol solution was dropped onto the sections and incubated for 15 min at RT. Sections were briefly washed in 100% ethanol, 50% (v/v) ethanol in ddH_2O, and 100% ddH_20, followed by 10 min incubation at RT with 50% (v/v) lead citrate solution in decocted H_2O containing 80 mM lead citrate (Merck, Darmstadt, Germany) and 0.12 M trisodium citrate (AppliChem, Darmstadt, Germany) (Reynolds, 1963). After washing in ddH_2O, sections were dried and attached to specimen pin mounts via carbon conductive tape (Plano, Wetzlar, Germany). Conductive silver (Plano, Wetzlar, Germany) was applied, connecting the glass with the edges of the holder. A 5-nm carbon coat was applied, using a CCU-010 carbon

coating machine (Safematic, Bad Ragaz, Switzerland). Serial sections were imaged in a JSM-7500F field emission scanning electron microscope (SEM; JEOL, Tokyo, Japan) with an acceleration voltage of 5 kV, a probe current of 0.3 nA, and a working distance of 6.0 mm. At each area of interest, several images with increasing magnification were acquired.

srAT image processing, correlation, and modelling

Montage and alignment of scanning electron microscopy (SEM) images were achieved via the ImageJ plugin TrakEM2 (version 1.0a, 04.07.2012) (Cardona *et al.*, 2012; Schindelin *et al.*, 2012). Images corresponding to the same section at different magnifications were merged within one layer with least squares montage in similarity mode and an alignment error of 10-20 pixel. After each z-layer was positioned, serial 100-nm sections were orientated via align layers, using similarity as transformation mode and 20-100 pixel alignment error. The area of interest in each layer was exported in a tagged image file (tif) format. To correlate immunofluorescence (IF) and SEM information, associated IF channel images and montaged SEM images were loaded into the vector graphics editor program Inkscape (version 0.92.3, 11.03.2018) and processed according to a standardized protocol (Markert *et al.*, 2017). IF channel images were overlaid and linked, leaving only the DAPI channel visible as first image layer. Opacity of IF images was reduced and DAPI labeled heterochromatin was used as an independent and unbiased landmark for correlation. Linked IF images were linearly transformed (rotation and resizing, but no distortions) to fit the cell nuclei orientation of the EM image. When adequate overlay was achieved, a rectangular area containing the region of interest (ROI) was extracted and each layer exported as a png file. Corresponding IF and EM images were then imported into the image editor GIMP2 (Version 2.10.0, 02.05.2018) for appropriate overlay and exported as png files. For tracing IENF in 3D, the open source software package IMOD was used (Kremer *et al.*, 1996).

Alternating 100-nm sections were imaged via IF and correlated with their corresponding EM images. Within the 100-nm stepwise srAT stack, the trajectory of an IENF was volumetric reconstructed as extrapolated tubular structure. Its position was determined based on PGP9.5 localization available for every second section. Furthermore, distinguishable electron density compared to keratinocyte cytoplasm and absence of desmosomes between adjacent keratinocytes were considered to identify the IENF in the EM context.

Skin cryosections

PFA fixed 10-µm skin cryosections were blocked in 10% BSA(w/v) in PBS for 30 min and incubated with primary antibodies against 1:100 PGP9.5 and Cx43 in 0.1% (w/v) saponin and 1% (w/v) BSA in PBS over night at 4°C.Applied antibodies are listed in Table 1. After washing with PBS, secondary antibodies were applied for 2 h at RT with 1% BSA(w/v) in PBS. After washing, sections were covered with droplets of PBS and stored at 4°C until further processing.

Expansion microscopy

ExM was adapted from former published protocols (Tillberg *et al.*, 2016; Zhao *et al.*, 2017). Skin sections were incubated with PBS containing 0.1 mg/ml Acryloyl-X (Thermo Fisher Scientific, Waltham, MA, USA) in dimethyl-sulfoxide (Sigma Aldrich, St. Louis, MO, USA) over night at RT. Afterwards, 33 nM expandable phalloidin derivate Actin ExM 546 (Chrometra, Kortenaken, Belgium), labeling actin cytoskeleton, was applied in PBS with 1% (w/v) BSA and 0.1 mg/ml Acryloyl-X for 1 h at RT. Subsequently, a monomer solution containing 8.625% (w/w) sodium acrylate (Sigma-Aldrich, St. Louis, MO, USA), 2.5% (w/w) acrylamide (Sigma-Aldrich, St. Louis, MO, USA), 0.15% (w/w) N,N‘-methylenbisacrylamide (Sigma-Aldrich, St. Louis, MO,

USA), and 11.7% (w/w) sodium chloride (Sigma-Aldrich, St. Louis, MO, USA) in PBS was added at 4°C for 30 min. Gelation was performed after replacement with fresh monomer solution, additionally containing 0.2% (w/v) ammonium persulfate (Sigma-Aldrich, St. Louis, MO, USA), 0.2% (v/v) tetramethylethylenediamine (Sigma-Aldrich, St. Louis, MO, USA), and 0.01% 4-Hydroxy-TEMPO (w/v) (Sigma-Aldrich, St. Louis, MO, USA). Sections were first incubated at 4°C for 30 min followed by 2h at 37°C. A gelation chamber assembled with each two coverslip pieces No1 (R. Langenbrinck, Emmendingen, Germany) on the side as spacers and one on top, serving as a lid, in a humidified plastic chamber was used to enable uniform gelation. Gelated samples were digested in 4 U/ml proteinase K buffer (New England Biolabs, Ipswitch, MA, USA) with 50 mM Tris pH 8.0 (Serva, Heidelberg, Germany), 50 mM EDTA (Sigma-Aldrich, St. Louis, MO, USA), 0.5% (v/v) Triton X-100 (Thermo Fisher Scientific Scientific, MA, USA) and 0.8 M guanidine HCl (Sigma-Aldrich, St. Louis, MO, USA) for 2 h at 60°C. Subsequently, gels were washed 10 min at RT with PBS, then with 1:2,500 DAPI (Sigma Aldrich, St. Louise, MO, USA) in PBS for 20 min at RT and again 10 min in BPS at RT. Gels were transfer into a dark petri dish with 100x times final gel volume of sterile ddH_2O with a razor blade. Gels were expanded for at least 1 h at RT before direct post-expansion imaging or storage at 4°C.

Labeled sections were imaged both in pre-expansion and post-expansion state with an DMi8 inverse microscope via 20x dry objective HC PL FLUOTAR L 20x/0.40, 11506243, LAS X software, and DMC300G monochrome camera (all Leica Microsystems, Wetzlar, Germany) to determine the expansion factor via manual alignment in inkscape. Further, imaging was performed using the ELYRA S.1 SR-SIM with 63x water-immersion objective C-Apochromat, 63 x 1.2 NA, 441777-9970 (all Zeiss, Oberkochen, Germany), and a PCO Edge 5.5 sCMOS camera (PCO, Kelheim, Germany). Gels were imaged inside poly-D lysine (Sigma Aldrich, St. Louise, MO, USA) coated imaging chambers (Thermo Fisher Scientific, Waltham, ME, USA) to prevent

229 drifting. Non-computed (widefield) images were used. Min/Max values were processed via ImageJ
230 (version 1.51n, National Institute of Health, Bethesda, MD, USA) for visualization.
231
232 **Fully human co-culture system**
233 Human induced pluripotent stem cells (iPSC) derived from fibroblasts were differentiated
234 into sensory neurons of a healthy control cell line as previously described (Klein et al., submitted).
235 Co-culture chambers (ibidi, Gräfelfing, Germany) were attached to 12-mm BioCoat® Poly-D-
236 Lysine/Laminin coverslips (Corning, New York, NY, USA). Both inner chambers were
237 additionally coated with 1:50 matrigel growth factor reduced (Corning, Corning, New York, NY,
238 USA) at 37°C for 30 min. Four-week old neurons were detached via TrypLE (Thermo Fisher
239 Scientific, Waltham, MA, USA), transferred into falcon tubes containing DMEM/F12 (Dulbecco's
240 Modified Eagles Medium/Nutrient Mixture F-12; Thermo Fisher Scientific, Waltham, MA, USA)
241 at 37 °C, and centrifuged for 3 min with 500 x g at RT.
242 Conditioned neuronal medium, consisting of DMEM/F12 GlutaMAX + 1X B-27 Plus
243 Supplement + 1X N-2 Supplement + 100 U/ml 1% penicillin/ streptomycin (pen/strep; all Thermo
244 Fisher Scientific, Waltham, MA, USA) + 20 ng/ml BDNF + 20 ng/ml GDNF + 20 ng/ml NGFb
245 (all Peprotech, Rocky Hill, NJ, USA) + 200 ng/ml ascorbic acid (Sigma-Aldrich, St. Louis, MO,
246 USA), spiked with 10 µM floxuridine (Santa Cruz Biotechnology, Dallas, TX, USA), was
247 withdrawn prior to TrypLE treatment, filtrated via 0.2 µm syringe filters (Sarstedt, Nümbrecht,
248 Germany) and kept at 37°C. Neurons were resuspended in 70 µl of filtered conditioned neuronal
249 medium and seeded into one chamber compartment and acclimated for one week. Healthy control-
250 derived primary keratinocytes were acquired and cultured via routine methods (Karl *et al.*, 2019)
251 and seeded into the corresponding compartment. The chamber insert barrier separating the
252 associated chambers was removed after 24 h and medium exchanged either with fresh keratinocyte

medium, comprising of EpiLife Medium supplemented with 1% EpiLife defined growth supplement, and 1% pen/strep (all Thermo Fisher Scientific, Waltham, USA) or stored conditioned neuronal medium. After 6 days, co-cultures were fixed with 4% PFA (v/v) in PBS $^{Ca^{++}/Mg^{++}}$ (PBS^{++}) at RT for 15 min and washed three times 5 min in PBS. Briefly, coverslips were treated with10 µg/ml wheat germ agglutinin, conjugated with Alexa Fluor 647 (WGA-647; Thermo Fisher Scientific, Waltham, MA, USA) in PBS for 10 min at RT and washed two times with PBS. Subsequently cells were blocked 30 min with 10% FCS (v/v) and 0.1% (w/v) saponin in PBS^{++}, then labeled either 1:100 anti-Cx43, or 1:100 anti-synaptophysin antibodies for visualization of contact sites over night at 4°C. Antibody solution contained 10% FCS (v/v) and 0.1% saponin (w/v) in PBS. After washing, secondary antibodies, 1:10,000 DAPI, and 10 µg/ml cholera toxin subunit B, conjugated with Alexa Fluor 488 (Thermo Fisher Scientific Scientific, MA, USA) were applied for 30 min at RT in antibody solution without saponin. Coverslips were transferred onto object holders, embedded with mowiol 4-88 (Roth, Karlsruhe, Germany) and -stored at 4°C until further processing.

2D co-culture live imaging and fluorescence microscopy

Directly before barrier removal, the co-cultures were transferred into a Lab-Tek chamber system (Thermo Fisher Scientific, Waltham, MA, USA) with two-well compartments. The remaining well was filled with 500 µl PBS^{++}. After barrier removal and addition of conditioned neuronal medium, co-cultures were incubated for 2d. For live-imaging, the Lab-Tek slide was transferred to an inverse DMi8 microscope operated on LAS X software (Leica Microsystems, Wetzlar, Germany), equipped with a live imaging chamber (ibidi, Gräfelfing, Germany). Phase contrast images with 20x objective HC PL FLUOTAR L dry 20x/0.40, 11506243 were taken in 20 min intervals for 67 h with a DMC2900 color camera (both Leica Microsystems, Wetzlar,

Germany), with cells kept at 37°C, with 5% CO_2, and 20% O_2 (both v/v). Single regions were stitched together as overview via Fiji plugin MosaicJ (Thévenaz and Unser, 2007). Min/Max values were processed via ImageJ (version 1.51n, National Institute of Health, Bethesda, MD, USA) for visualization.

Fluorescently labeled co-cultures were imaged with an Axio Imager.M2 (Zeiss, Oberkochen, Germany), equipped with spinning disc-confocal system (X-light V1, CrestOptics, Rome Italy) and Spot Xplorer CCD camera (SPOT Imaging, Sterling Heights, MI, USA) operated on VisiView software (Visitron Systems, Puchheim, Germany) for overview and Lattice-SIM for detailed super-resolution analysis with 63x water immersion C-Apochromat 63x/1.2 W Korr UV-VIS-IR M27, 21787-9971-790 and ZEN (black edition) software (all Zeiss, Oberkochen, Germany), with two aligned PCO Edge 4.2 M sCMOS cameras (PCO, Kelheim, Germany). Min/Max values were processed via ImageJ (version 1.51n, National Institute of Health, Bethesda, MD, USA) for visualization. For 3D visualization, Min/Max values of complete z-stacks were adjusted per channel in ZEN (blue edition) software (Zeiss, Oberkochen, Germany) and depicted in 3D mode.

Results

Human intraepidermal nerve fiber segments are engulfed by keratinocytes

While many IENF were passing between neighboring keratinocytes, srAT revealed IENF ensheathed by keratinocytes in all three healthy subjects. This tunneling of fibers was observed both in the basal and upper epidermal layers for several consecutive 100-nm thin sections indicated via PGP9.5 labeling (Figure 1A). IENF intersected closely to either the lateral, posterior, or anterior boundary of the respective keratinocyte and was engulfed by the respective cell for several µm (Figure 1A, Video1). For advanced tracing of an IENF through the epidermis,

a representative site was reconstructed (Figure 1B, Video2). Whilst a major part of the respective nerve fiber grew in close contact to and in between keratinocytes, a substantial portion tunneled through one basal keratinocyte. Specificity of antibodies was examined by tracking the fluorophore signal within consecutive slices and negative control via omission of the primary antibody (Figure supplement 1). High pressure freezing and freeze substitution followed by LR-White embedding preserved the ultrastructure and antigenicity of the human skin tissue well, illustrated by identification of collagen fibrils, desmosomes, nuclei, and mitochondria (Figure 1C).

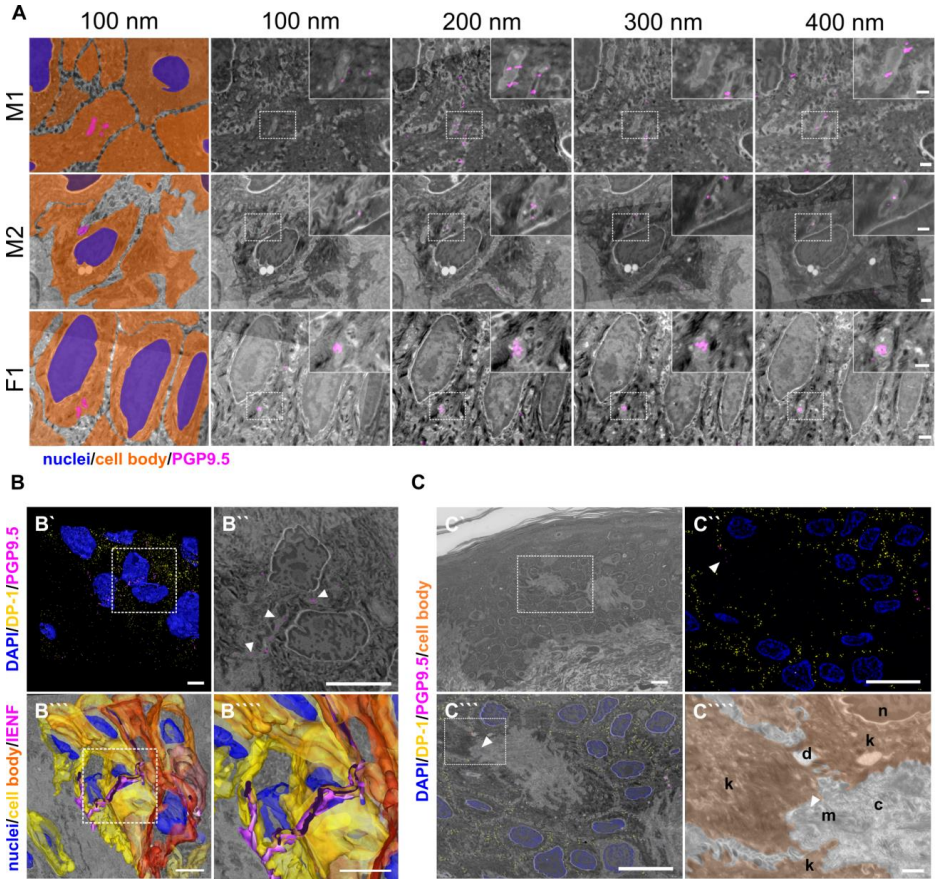

Figure 1. Epidermal nerve fiber ensheathment and srAT functionality.

(A) Ensheathment of IENF by keratinocytes. Nerve fibers projecting within keratinocytes in skin punch biopsy samples of two male (M1, M2) and one female subject (F1). First tile shows keratinocyte cell bodies (orange), nuclei (blue), and fiber (magenta) in pseudo color. Each row represents four consecutive sections with 100 nm thickness of correlated images, with PGP9.5 labeling for IENF (magenta), while dashed insets show higher magnification of the region of interest in inlay. See also Video1. Scale bar 1 µm, magnified insets 500 nm. (B) 3D

317 reconstruction of IENF processes traversing between and within keratinocytes. (B`) 3D
318 visualization of fluorescence signal from srAT approach, white rectangle indicates area in b``.
319 PGP9.5 (magenta) labeled nerve fiber processes between and in keratinocytes in close apposition
320 to nuclei (blue). DP-1 (yellow) marks intercellular desmosomal junctions as keratinocyte cell
321 boundaries. (B``) Single plane with overlay of PGP9.5 signal and EM. (B```) Extrapolation of
322 IENF trajectory in 3D, based on IF signal and EM ultrastructure with fiber (magenta),
323 keratinocyte cell bodies (yellow-orange), and nuclei (blue); see also Video2. Scale bars 5 µm. (C)
324 Preservation of antigenicity and cellular structure in LR-White embedded epidermal tissue with
325 Overview area from SEM (C`). Scale bar 10 µm. (C``) SIM image of 100-nm skin section with
326 DP-1 (yellow), PGP9.5 (magenta), and DAPI (blue) labeling. Arrowhead indicates PGP9.5-
327 positive IENF processes. Scale bar 10 µm. (C```) Correlated SIM and SEM image from dashed
328 rectangle in A. Scale bar 10 µm. (C````) Inset of c showing subcellular preservation of collagen
329 fibers (co), desmosomes (de), keratinocytes (k), mitochondria (m), and nucleus (n). Arrowhead
330 indicates IENF processes also observed via IF in a. Scale bar 1 µm. Abbreviations: DP-1,
331 desmoplakin 1; IENF, intraepidermal nerve fiber; IF, immunofluorescence; LR-White, London
332 Resin-White; PGP9.5, protein gene product-9.5; SEM, scanning electron microscopy; SIM,
333 structured illumination microscopy.

334 **srAT facilitates tracing of further skin cell populations**

335 The combination of cellular markers such as PGP9.5 or S100β with information on cell
336 morphology from EM scans allowed tracing of various cell populations via srAT in human skin.
337 S100β-positive Langerhans cells were visualized in the epidermis and their dendritic protrusions
338 were traced between keratinocytes (Figure 2A and B). Within the dermis, S100β-PGP9.5-co-
339 localized signal identified dermal Schwann cells enwrapping nerve fiber processes (Figure
340 2C-D).

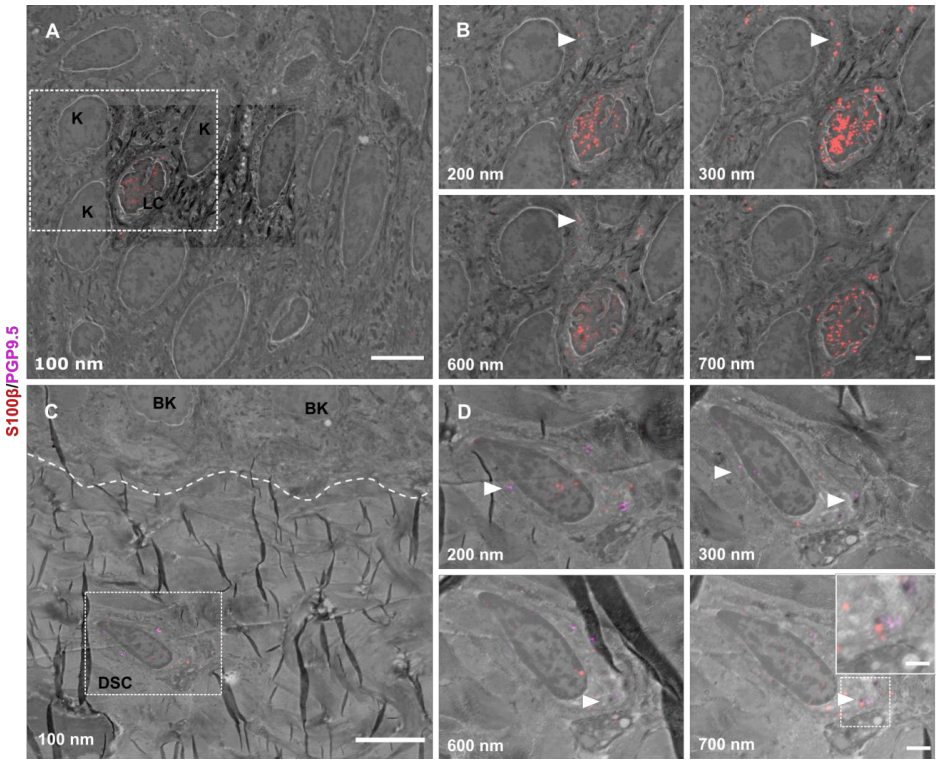

Figure 2. General utility of srAT for tracing skin cells.

(A) Epidermis with keratinocytes (K) and Langerhans cell (LC) (B) Single Z-sections of outlined areas. LC was identified via S100β (red). Arrowheads indicate LC protrusions in contact to K. (C) Upper dermis and basement membrane (dashed line) with basal keratinocytes (BK) and dermal Schwann cell (DSC). (D) Single Z-sections of outlined areas. DSC was identified via PGP9.5 (magenta) and S100β (red) labeling. Dermal fiber processes are enwrapped by CSC, indicated with arrowheads. Inset in last panel shows magnification of marked fiber. Scale bars 5 µm (A, C), 1 µm (B, D), and 500 nm (inset in D) Abbreviations: BK, basal keratinocyte; DSC, dermal Schwann cell; K, keratinocyte; LC, Langerhans cell; PGP9.5, protein product 9.5; S100β, S100 calcium binding protein B.

Nerve fiber ensheathment can be visualized by ExM in diagnostic skin samples

To visualize ensheathed nerve fibers also in thicker, diagnostically used skin punch biopsy sections, we applied ExM allowing super-resolution imaging with epifluorescence microscope setups. Expansion factor of samples fell between 4.3-4.4x and showed isotropic epidermal expansion as documented via pre and post-expansion acquired images (Figure 3). Actin filaments were used as a marker to outline epidermal cell bodies and IENF entry and exit points, while cytoplasmic PGP9.5 identified IENF. Nerve fibers were traced via ExM for their course through the epidermis, being ensheathed over several µm (Video3).

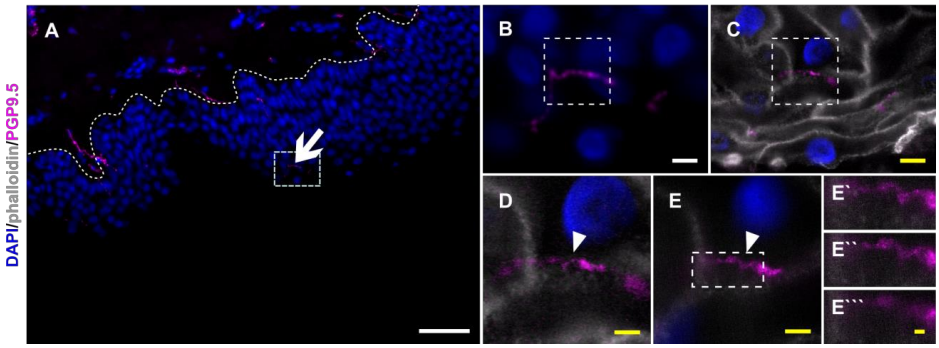

Figure 3. Resolving nerve fiber ensheathment in expanded skin tissue.

(A) Overview of skin section prior to expansion with PGP9.5-positive IENF (magenta) and nuclear DAPI (blue) signal; dotted line illustrated epidermis-dermis border and arrow indicates IENF. White rectangle marks inset enlarged in B. (B) Enlarged area prior to expansion and (C) matched area post-expansion at same magnification with addition of actin marker phalloidin (grey), white rectangles mark inset area of D and E.(D) enlarged IENF area at 20x magnification and (E) at 63x magnification with arrowheads indicating IENF passing through keratinocyte. Inset in E marks enlarged area in E`-E```. (E`) shows z-plane prior to E, (E``) same z-plane as E,

and E``` z-plane step after E. White scale bars indicate pre-expansion state, yellow scale bars were corrected for expansion factor. Scale bars: 50 µm (A), 5 µm (B, C), 2µm (d, e), 500 nm (E```). Z-step size of 1.2 µm translates to approximate 276 nm in expanded gel. Abbreviations: Cx43, connexin 43; DAPI, 4',6-diamidino-2-phenylindole; IENF, intraepidermal nerve fiber; PGP9.5, protein gene product-9.5

Cx43 plaques as potential keratinocyte-nerve fiber communication sites

Connexin hexamers can form hemichannels acting as small pores. In open state, small molecules can pass and be released from the cell, which was already shown for ATP and Cx43 (Weber *et al.*, 2004). This may allow purinergic signaling towards neighboring cells or nerve terminals in close proximity. For srAT, Cx43 labeling was assumed a *bona fide* signal, if ≥2 consecutive sections showed fluorescent staining, translating to 200-400 nm. These clusters were mostly found at keratinocyte-keratinocyte contact zones (Figure 4A), however, distinct Cx43 plaques were also identified in direct proximity to single IENF when growing between keratinocytes (Figure 4B).

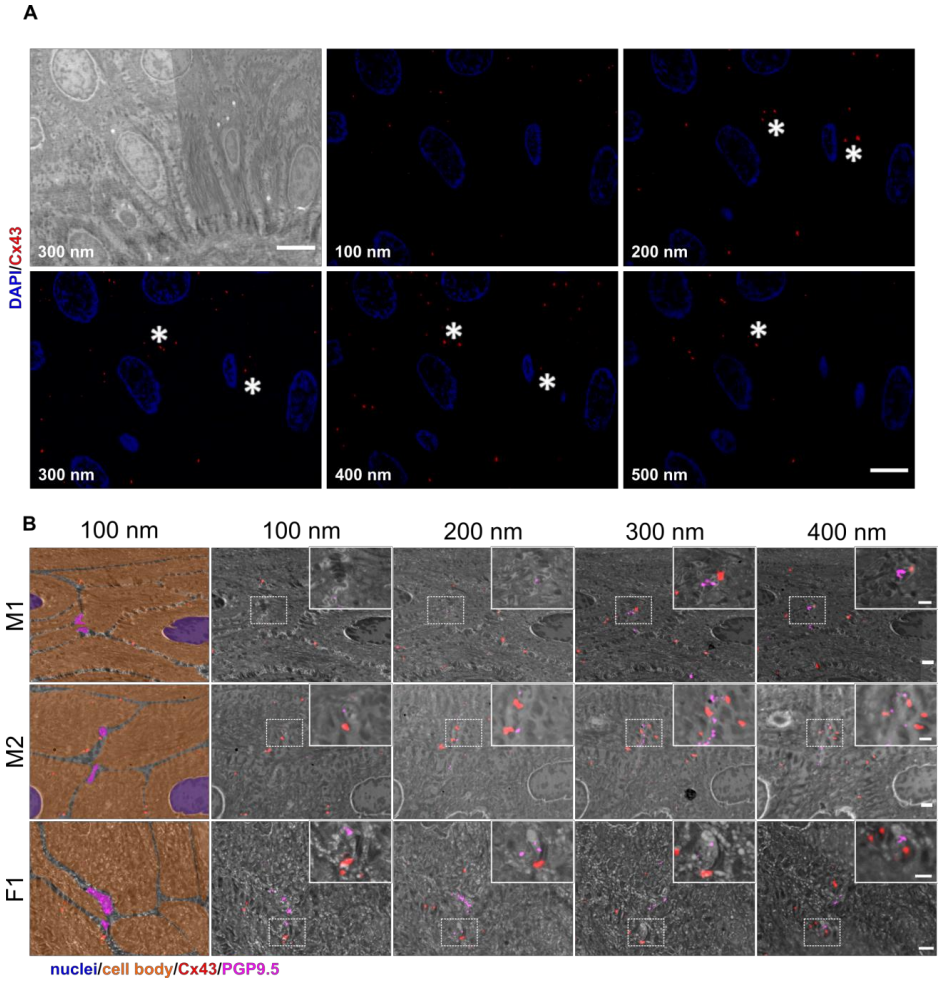

386

387 **Figure 4.** Identification of Cx43 plaques via srAT (A) Tracking of Cx43 plaques in epidermal

388 layers. First panel illustrates SEM overview of epidermal layers corresponding to five

389 consecutive sections of IF images showing Cx43 signal (red) and nuclei (blue). Asterisks show

390 examples of traced Cx43 plaques. (B) Cx43 plaques at keratinocyte-nerve fiber close contact

391 sites. Nerve fibers processing between keratinocytes in skin samples of two male subjects (M1,

392 M2) and one female subject (F1). Each row represents four consecutive sections of 100 nm

thickness. First tile shows keratinocyte cell bodies (orange), nuclei (blue) and fiber (magenta), in pseudo color with Cx43 signal (red). Correlated PGP9.5 labeling (magenta) locates at nerve fibers and Cx43 labeling (red) indicates Cx43 plaques. Insets show magnification of contact area. Scale bars: 5 µm (A), 1 µm (B), magnified insets 500 nm. Abbreviations: Cx43, connexin 43; IF, Immunofluorescence; PGP9.5, protein gene product-9.5; SEM, scanning electron microscopy.

In analogy to nerve fiber ensheathment, we investigated Cx43 accumulations also in expanded diagnostic skin samples. In pre-expansion state, the attribution of single Cx43 plaques to specific sites between keratinocytes or towards IENF was hardly possible, due to the compact structure of the epidermis. However, after expansion, specific Cx43-positive accumulations in direct contact to PGP9.5-positive IENF could be identified (Figure 5; Video3).

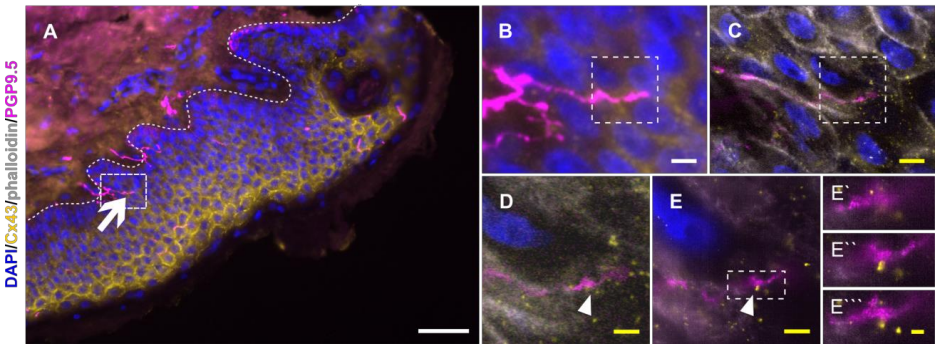

Figure 5. Cx43 accumulation at keratinocyte-nerve fiber contact site in expanded epidermis. (A) Overview of skin section prior to expansion with PGP9.5-labeled IENF (magenta), Cx43 (yellow), and nuclear DAPI (blue); dotted line illustrates epidermis-dermis border and arrow indicates IENF. White rectangle marks inset enlarged in B. (B) Enlarged area prior to expansion and (C) matched area post-expansion at same magnification with addition of actin marker phalloidin (grey), white rectangles mark inset area of D and E.(D) enlarged IENF area at 20x magnification and (E) at 63x magnification with arrowheads indicating Cx43 plaque at IENF.

411 Inset in e marks enlarged area in E`-E```. (E`) shows z-plane prior to E, (E``) same z-plane as E,
412 and E``` z-plane step after E. White scale bars indicate pre-expansion state, yellow scale bars are
413 corrected for expansion factor. Scale bars: 50 µm (A), 5 µm (B, C), 2µm (D, E), 500 nm (E`-
414 E```). Z-step size of 1.2 µm translates to approximate 274 nm in expanded gel. Abbreviations:
415 Cx43, connexin 43; IENF, intraepidermal nerve fiber; PGP9.5, protein gene product-9.5.
416

417 **Neurites establish contacts to keratinocytes in fully human co-culture system**

418 Sensory neurons and keratinocytes each formed clusters after seeding into two-comparted
419 chambers (Figure 6A-C). After barrier removal, neurites actively grew towards keratinocytes and
420 established contacts within few days (Figure 6C and D, Video4). Neurite-keratinocyte contacts
421 were apparent, both in conditioned neuronal medium and keratinocyte medium. However,
422 keratinocytes underwent terminal differentiation in neuronal medium, while predominantly
423 maintaining a basal state in keratinocyte medium (Figure supplement 2).

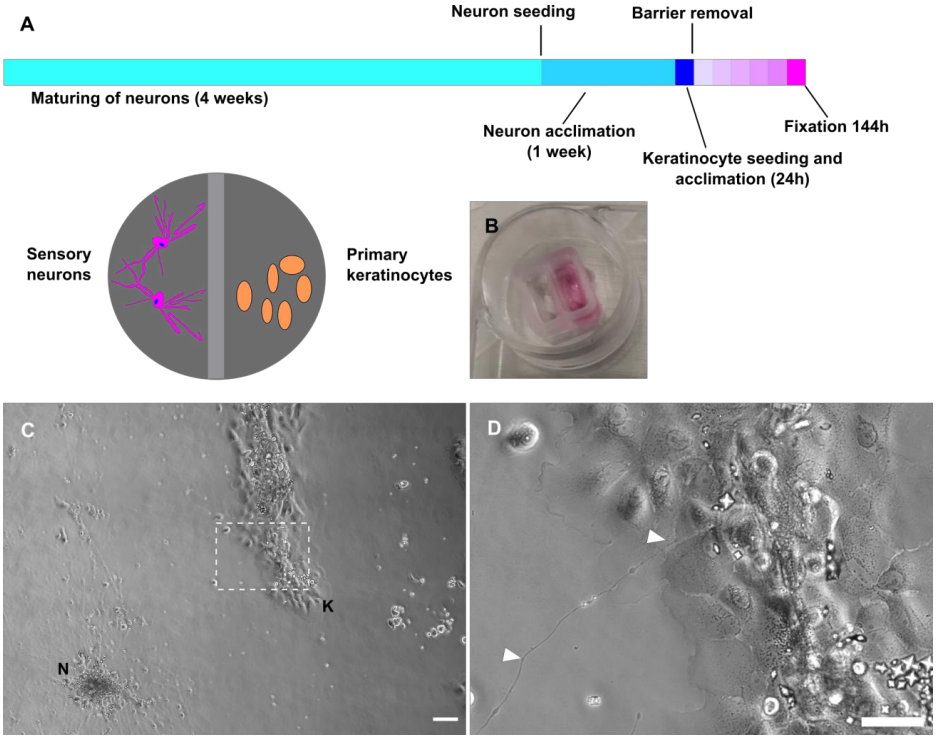

Figure 6. Fully human sensory neuron-keratinocyte co-culture model.

(A) Timeline of culturing protocol and compartment scheme. (B) Chamber system. (C) Overview of co-culture after 115h in conditioned neuronal medium with neuronal cluster (N) and keratinocyte colony (K). Inset (D) shows a single neurite in contact with keratinocytes (arrowheads). Co-culture kept in conditioned neuronal medium. Scale bars 100 µm (C), magnified inset 50 µm (D). See also Video4. Abbreviations: K, keratinocyte colony; N, neuronal cluster.

Ensheathment and Cx43 complexes are present in a fully human co-culture model

In order to distinguish the neurite versus keratinocyte membrane, we specifically labeled sensory neurons via cholera toxin subunit B (Ctx) targeting the ganglioside monosialotetrahexosylganglioside 1 (GM1) (Dederen *et al.*, 1994; Tong *et al.*, 1999). Conversely, the membrane of keratinocytes was targeted by wheat germ agglutinin (WGA) (Belleudi *et al.*, 2011; Watt, 1983). We identified neurite-keratinocyte contacts using confocal microscopy (Figure 7A and B) and observed ensheathment via lattice-SIM super-resolution microscopy (Figure 7 C-C``). Non-ensheathed neurites frequently passed in close proximity and over keratinocytes (Figure 7D). Intriguingly, Cx43 labeling revealed Cx43 plaques at those passing sites, distributed over several individual keratinocytes (Figure 7D-F```).

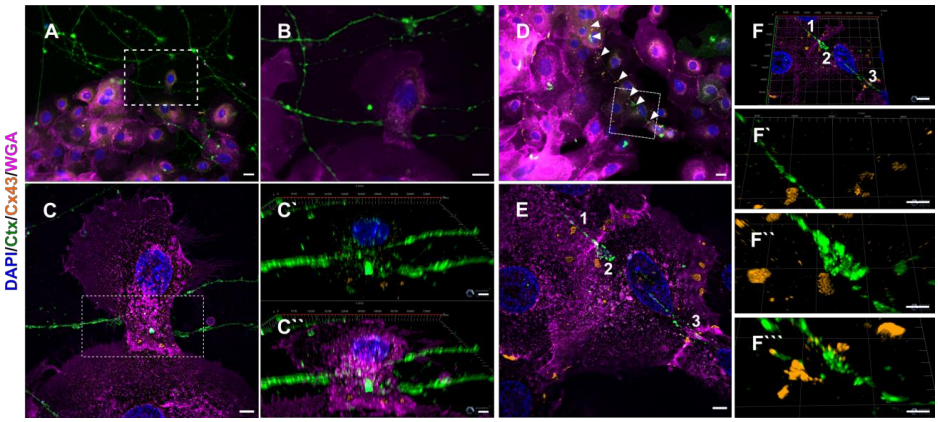

Figure 7. Neurite ensheathment and Cx43 plaques in full human co-culture model. (A) Confocal overview image of Ctx-positive sensory neurites (green), Cx43 positive (orange) keratinocytes with membrane labeling of keratinocytes via WGA (magenta) and nuclear DAPI (blue). (B) Inset of ensheathment area from A. (C) Single plane lattice SIM image and respective inset area with 3D visualization of z-stack (2.925 µm depth, 0.196 µm steps) showing nucleus, Cx43, and neurite signal (C`) and including WGA (C``). (D) Confocal overview image of Ctx-

positive sensory neurites (green), Cx43-positive (orange) keratinocytes with membrane labeling of keratinocytes via WGA (magenta) and nuclei (blue). Arrowheads indicate Cx43 - neurite contact areas. (E) Single plane lattice SIM image and respective inset area with 3D visualization, numbers represent single Cx43 plaques (F) of z-stack (2.925 µm depth, 0.196 µm steps). (F`-F```) detailed neurite - Cx43 contact areas. Co-culture kept in keratinocyte medium. Scale bars: 20 µm (A, D), 5 µm (C-C``, E, F`-F````), 10 µm (F). Abbreviations: Ctx, cholera toxin subunit B; Cx43, connexin 43; DAPI, 4',6-diamidino-2-phenylindole; SIM, structured illumination microscopy; WGA, wheat germ agglutinin.

We further found neurites growing in a gutter-like structure (Figure 8A), merging into the keratinocyte membrane (Figure 8B) and observed neurites that establish bouton-like contacts with keratinocytes (Figure 8C). We included SYP labeling as a marker for small synaptic vesicles, which might serve as another pathway of signal transduction between keratinocytes and IENF (Talagas *et al.*, 2020b). In our iPSC-derived neurons, SYP was distributed throughout the cytoplasm and not restricted to the cytoskeleton (Figure supplement 3). Conversely, only weak SYP labeling, not associated with neurite contact sites, was present in keratinocytes (Figure 8A-C).

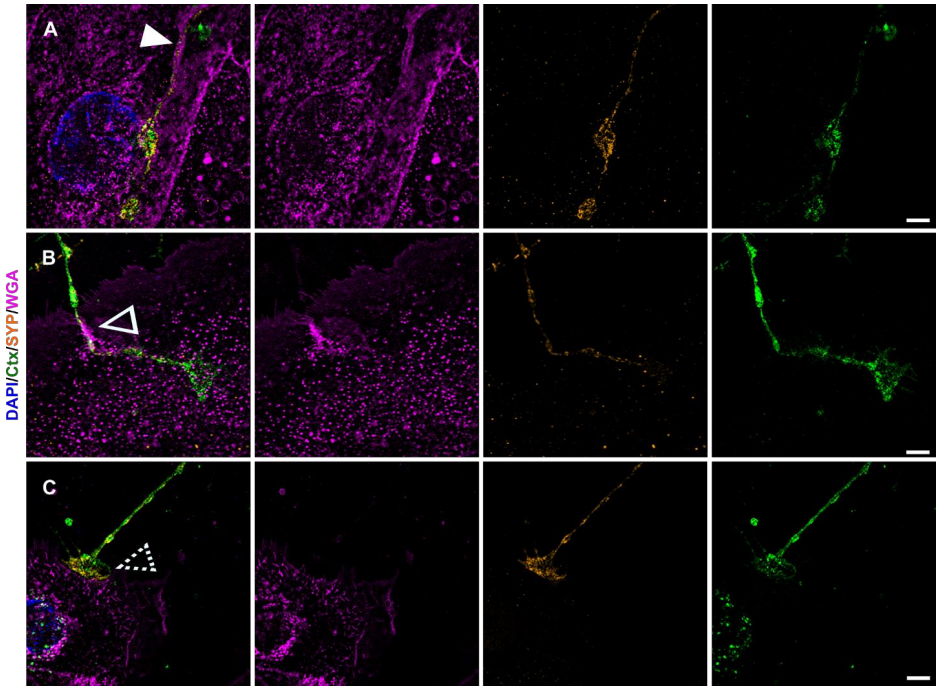

Figure 8. Further keratinocyte-neurite interactions and synaptic vesicular SYP distribution. Single plane lattice SIM images with overlay of nuclear DAPI (blue), WGA (magenta), SYP (yellow), and Ctx (green) signal as first panel, followed by single channel images of WGA, SYP, and Ctx. Distinct contact sites with gutter like structure (A) indicated by filled arrowhead, enwrapping (B) indicated via hollow arrowhead, and bouton-like contact (C) indicated via dashed arrowhead were observed in human co-culture. SYP signal in a-c is predominantly restricted to neurite with sparse dotted labeling in keratinocytes. Co-culture kept in keratinocyte medium. Scale bars: 5 µm. Abbreviations: Ctx, cholera toxin subunit B; DAPI, 4',6-diamidino-2-phenylindole, SIM, structured illumination microscopy; SYP, synaptophysin; WGA, wheat germ agglutinin.

Discussion

We have investigated the NCU in healthy human skin and provide evidence for crucial morphological phenomena, namely nerve fiber ensheathment by keratinocytes and Cx43 contact sites between keratinocytes and IENF. These findings may profoundly change the view on the role neuronal and non-neuronal cells play in the development and maintenance of neuropathy and neuropathic pain.

Ensheathment was previously described in model organisms with mono- or double-layered epidermis such as *Drosophila* and *Danio rerio* (Han *et al.*, 2012; O'Brien *et al.*, 2012). In multi-layered mammalian and human skin, only sparse data exist from early EM studies reporting conflicting observations. Given the small diameter of IENF (≤1 µm) within the dense tissue of the epidermis, application of super-resolution microscopy techniques is inevitably necessary to resolve the exact course of these neurites. Recently, "tunneling" of IENF within keratinocytes was proposed via confocal microscopy in human skin (Talagas *et al.*, 2020a) and via SEM in an heterologous rat-human co-culture model (Talagas *et al.*, 2020b). srAT and ExM techniques used in our study fortify these findings at ultrastructural level and ExM opens the avenue for detailed assessment in diagnostically relevant tissue sections. We further identified Cx43 plaques of keratinocytes in close proximity to IENF as potential components of the NCU exactly size-matching similar connexin and innexin plaques (Agullo-Pascual *et al.*, 2013; Markert *et al.*, 2016; Taki *et al.*, 2018). Keratinocyte-keratinocyte communication via calcium wave propagation and ATP release are canonical functions of Cx43, orchestrating proliferation, wound healing, and inflammatory processes (Martin *et al.*, 2014; Tsutsumi *et al.*, 2009). It is of note that ATP was also found to be a direct signal transducer from keratinocytes to sensory neurites (Cook and McCleskey, 2002; Sondersorg *et al.*, 2014).

Interactions at the NCU may have unprecedented implications for a wide range of somatosensory functions in health and disease. In *Drosophila* larvae, a bidirectional guidance mechanism stabilizing existing fibers and limiting fiber arborization was proposed maintaining sensory receptive fields. In this model, disturbance of ensheathment reduced nocifensive behavior (Jiang *et al.*, 2019). In human patients, small fiber pathology is characterized by functional and/or morphological impairment of IENF and is a common finding in a range of neurodegenerative, metabolic, and chronic pain-associated diseases (Ghasemi and Rajabally, 2020; Pittenger *et al.*, 2005; Vinik *et al.*, 2001). Skin punch biopsies are an easily accessible biomaterial of increasingly acknowledged diagnostic value (Evdokimov *et al.*, 2019; Lin *et al.*, 2016). Hence, studying the NCU may help understand the pathophysiology of diseases of the peripheral and central nervous system including dystrophic changes typically found in skin of patients with neuropathies (Hovaguimian and Gibbons, 2011).

It is pivotal to recognize and further investigate the active role of keratinocytes within the NCU. Keratinocytes communicate with IENF via ATP and facilitate normal and nociceptive sensory perception in mechanical and thermal modalities (Moehring *et al.*, 2018; Sadler *et al.*, 2020). Vesicles (Maruyama *et al.*, 2018), pannexins (Sondersorg *et al.*, 2014), and connexins (Barr *et al.*, 2013) are potential mediators of this ATP release and might be dependent on the evoking stimulus. Our observation of Cx43 plaques along the course of IENF in native skin and human co-culture model substantiates a morphological basis for keratinocyte hemichannels as signaling pathway towards IENF. A single cell RNA-sequencing approach of human epidermal cells determined “channel keratinocytes” with upregulated pore and intercellular communication transcripts, e.g. Cx26 and Cx30 (Cheng *et al.*, 2018). Hemichannel or even gap junctional communication between keratinocytes and IENF might hence not be restricted to Cx43 and differentially organized in varying specialized keratinocytes.

We successfully established a fully human co-culture model of sensory neurons and keratinocytes maintaining viability for at least six days and neurites growing towards and interacting with keratinocytes. The 2D culture system reduced the multilayered complexity of native skin, yet conserved ensheathment and Cx43 plaques as hallmarks of the NCU. Embryonic stem cell-derived human sensory neurons and human keratinocytes were successfully co-cultured before resulting in direct contacts and engulfed neurites (Krishnan-Kutty *et al.*, 2017). However, our model uses fibroblast-derived iPSC which can be generated from virtually any relevant group of patients. Recently, a heterologous model of rat DRG neurons and human keratinocytes showed neurites passing along a keratinocyte gutter or being ensheathed by keratinocytes, which matches our observations. Additionally, SYP, synaptotagmin, and syntaxin 1A were successfully labeled demonstrating synapse-like contacts together with cytokeratin 6 as a keratinocyte marker and pan-neurofilament as a neurite marker (Talagas *et al.*, 2020b). Neurofilaments represent intermediate filaments within the cytoplasm and may not encompass the whole neuronal outline compared to membrane labeling (see Figure supplement 3). In accordance with findings from native DRG neurons, our sensory iPSC neurons contained SYP accumulations within the cytoplasm (Chou *et al.*, 2002; Chung *et al.*, 2019), deeming a membranous labeling necessary to clearly localize SYP in a co-culture approach. Keratinocytes showed no clusters of SYP associated to passing neurites (Figure 8). Still, electrophysiological activity of neurons in contact with keratinocytes can be attenuated by blocking vesicular secretion of keratinocytes via botulinum neurotoxin type C, hinting towards a physiological role in signal transduction at the NCU (Talagas *et al.*, 2020b).

Our data further show that diagnostic interpretation of IENF density in skin punch biopsies solely based on PGP9.5 labeling deserves some caution. PGP9.5 is a cytoplasmic marker that may not be distributed homogenously along the whole fiber and omits the neurites membrane

(Figure 1), which will be important for localization and co-localization of involved proteins at super-resolution. Regarding *in vitro* approaches, our homologous model should minimize variability and potential artifacts of heterologous co-cultures, especially since profound differences in neuronal DRG subpopulations can be observed across mammalian species (Klein *et al.*, 2021; Kupari *et al.*, 2021; Shiers *et al.*, 2020).

Conclusion

Sophisticated cell culture and animal models along with super-resolution microscopy are barely beginning to unveil the complexity of the NCU. Epidermal keratinocytes show an astonishing set of interactions with sensory IENF including ensheathment and electrical and chemical synapse-like contacts to nerve fibers (Figure 9). Our morphological findings underline the significance of keratinocytes in somatosensorics and cutaneous nociception and add to the increasing change of textbook knowledge viewing sensory fibers as the sole transducers of environmental stimuli. Expanding investigations towards skin cell impairment in small fiber pathology will help to better understand the underlying mechanisms and open new avenues for targeted treatment.

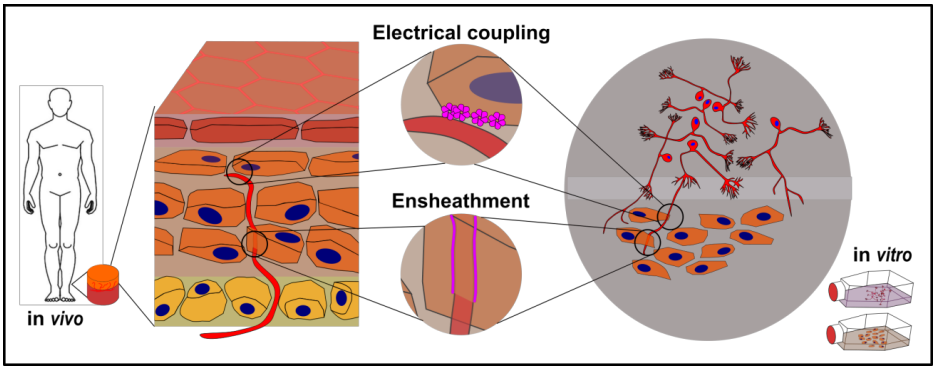

569 **Figure 9.** Keratinocyte-nerve fiber interactions in human epidermis and 2D model.
570 Proposed electrical synapses are potential transducers of sensory and nociceptive keratinocyte
571 adenosine triphosphate signaling towards intraepidermal nerve fibers. Ensheathment of fibers by
572 keratinocytes may orchestrate nerve fiber outgrowth and stabilization. Both observations are
573 conserved in human 2D co-culture model.
574

575 **Acknowledgements**
576 We thank Dr. Franziska Karl-Schöller for technical help in co-culture handling, Viktoria
577 Diesendorf, BSc for routine sensory neuron differentiation and Alexandra Gentschev, BSc for srAT
578 test runs (all Department of Neurology, University of Würzburg, Germany).
579 We also thank Daniela Bunsen, Claudia Gehrig-Höhn (Biocenter, Imaging Core Facility,
580 University of Würzburg, Germany), and Dr. Sebastian Markert (Department of Cell Biology, Johns
581 Hopkins University, Baltimore, USA) for expert technical help in srAT. We further thank Dr. Jan
582 Schlegel (Department of Biotechnology and Biophysics, University of Würzburg, Germany) for
583 the preparation of SeTau647 conjugated secondary antibody and Dr. Ralph Götz (Department of
584 Biotechnology and Biophysics, University of Würzburg, Germany) for the introduction into
585 expansion microscopy. The study was supported by the German Research Foundation (Deutsche
586 Forschungsgemeinschaft, DFG UE171/4-1). N.Ü. was supported by DFG UE171/15-1. M.S. was
587 supported by the grant ULTRARESOLUTION from the European Research Council.
588

589 **Author contributions**
590 C.E, N.Ü, and C.S. conceptualized the projects and experiments. C.E. performed all experiments.
591 T.K. established methodology for stem cell generation and neuronal differentiation. S.B. and P.D.

592 supported srAT sample generation and imaging. C.E. and N.Ü. wrote the manuscript with
593 contributions from S.B., M.S., and C.S. All authors read and approved the manuscript.

594

595 **Competing interests**

596 The authors declare no conflicts of interest.
597

598 **References:**

599 Agullo-Pascual, E., Reid, D.A., Keegan, S., Sidhu, M., Fenyö, D., Rothenberg, E., Delmar, M.,
600 2013. Super-resolution fluorescence microscopy of the cardiac connexome reveals
601 plakophilin-2 inside the connexin43 plaque. *Cardiovasc. Res.* 100**,** 231-240.
602 Barr, T.P., Albrecht, P.J., Hou, Q., Mongin, A.A., Strichartz, G.R., Rice, F.L., 2013. Air-
603 stimulated ATP release from keratinocytes occurs through connexin hemichannels. *PloS*
604 *one* 8**,** e56744.
605 Baumbauer, K.M., DeBerry, J.J., Adelman, P.C., Miller, R.H., Hachisuka, J., Lee, K.H., Ross,
606 S.E., Koerber, H.R., Davis, B.M., Albers, K.M., 2015. Keratinocytes can modulate and
607 directly initiate nociceptive responses. *eLife* 4.
608 Belleudi, F., Scrofani, C., Torrisi, M.R., Mancini, P., 2011. Polarized endocytosis of the
609 keratinocyte growth factor receptor in migrating cells: role of SRC-signaling and
610 cortactin. *PLoS One* 6**,** e29159.
611 Birklein, F., 2005. Complex regional pain syndrome. *J. Neurol.* 252**,** 131-138.
612 Cardona, A., Saalfeld, S., Schindelin, J., Arganda-Carreras, I., Preibisch, S., Longair, M.,
613 Tomancak, P., Hartenstein, V., Douglas, R.J., 2012. TrakEM2 software for neural circuit
614 reconstruction. *PloS one* 7**,** e38011.
615 Cheng, J.B., Sedgewick, A.J., Finnegan, A.I., Harirchian, P., Lee, J., Kwon, S., Fassett, M.S.,
616 Golovato, J., Gray, M., Ghadially, R., Liao, W., Perez White, B.E., Mauro, T.M., Mully,
617 T., Kim, E.A., Sbitany, H., Neuhaus, I.M., Grekin, R.C., Yu, S.S., Gray, J.W., Purdom,
618 E., Paus, R., Vaske, C.J., Benz, S.C., Song, J.S., Cho, R.J., 2018. Transcriptional
619 Programming of Normal and Inflamed Human Epidermis at Single-Cell Resolution. *Cell*
620 *Rep* 25**,** 871-883.
621 Chou, A.-K., Muhammad, R., Huang, S.-M., Chen, J.-T., Wu, C.-L., Lin, C.-R., Lee, T.-H., Lin,
622 S.-H., Lu, C.-Y., Yang, L.-C., 2002. Altered synaptophysin expression in the rat spinal
623 cord after chronic constriction injury of sciatic nerve. *Neurosci. Lett.* 333**,** 155-158.
624 Chung, J., Franklin, J.F., Lee, H.J., 2019. Central expression of synaptophysin and synaptoporin
625 in nociceptive afferent subtypes in the dorsal horn. *Sci. Rep.* 9**,** 1-11.
626 Cook, S., McCleskey, E., 2002. Cell damage excites nociceptors through release of cytosolic
627 ATP. *Pain* 95**,** 41-47.
628 Dederen, P.J., Gribnau, A.A., Curfs, M.H., 1994. Retrograde neuronal tracing with cholera toxin
629 B subunit: comparison of three different visualization methods. *J. Histochem. Cytochem.*
630 26**,** 856-862.

631 Evdokimov, D., Frank, J., Klitsch, A., Unterecker, S., Warrings, B., Serra, J., Papagianni, A.,
632 Saffer, N., Meyer zu Altenschildesche, C., Kampik, D., 2019. Reduction of skin
633 innervation is associated with a severe fibromyalgia phenotype. *Ann. Neurol.* 86**,** 504-516.
634 Ghasemi, M., Rajabally, Y.A., 2020. Small fiber neuropathy in unexpected clinical settings: a
635 review. *Muscle Nerve* 62**,** 167-175.
636 Han, C., Wang, D., Soba, P., Zhu, S., Lin, X., Jan, L.Y., Jan, Y.-N., 2012. Integrins regulate
637 repulsion-mediated dendritic patterning of drosophila sensory neurons by restricting
638 dendrites in a 2D space. *Neuron* 73**,** 64-78.
639 Hovaguimian, A., Gibbons, C.H., 2011. Diagnosis and treatment of pain in small-fiber
640 neuropathy. *Curr. Pain Headache Rep.* 15**,** 193-200.
641 Jiang, N., Rasmussen, J.P., Clanton, J.A., Rosenberg, M.F., Luedke, K.P., Cronan, M.R., Parker,
642 E.D., Kim, H.-J., Vaughan, J.C., Sagasti, A., 2019. A conserved morphogenetic
643 mechanism for epidermal ensheathment of nociceptive sensory neurites. *eLife* 8**,** e42455.
644 Karl, F., Wussmann, M., Kress, L., Malzacher, T., Fey, P., Groeber-Becker, F., Uceyler, N.,
645 2019. Patient-derived in vitro skin models for investigation of small fiber pathology. *Ann.*
646 *Clin. Transl. Neurol.* 6**,** 1797-1806.
647 Keppel Hesselink, J.M., Kopsky, D.J., Bhaskar, A.K., 2017. Skin matters! The role of
648 keratinocytes in nociception: a rational argument for the development of topical
649 analgesics. *J. Pain Res.* 10**,** 1-8.
650 Klein, A., Solinski, H.J., Malewicz, N.M., Ieong, H.F.-h., Sypek, E.I., Shimada, S.G., Hartke,
651 T.V., Wooten, M., Wu, G., Dong, X., 2021. Pruriception and neuronal coding in
652 nociceptor subtypes in human and nonhuman primates. *eLife* 10**,** e64506.
653 Klusch, A., Ponce, L., Gorzelanny, C., Schafer, I., Schneider, S.W., Ringkamp, M., Holloschi,
654 A., Schmelz, M., Hafner, M., Petersen, M., 2013. Coculture model of sensory neurites and
655 keratinocytes to investigate functional interaction: chemical stimulation and atomic force
656 microscope-transmitted mechanical stimulation combined with live-cell imaging. *J.*
657 *Invest. Dermatol.* 133**,** 1387-1390.
658 Kremer, J.R., Mastronarde, D.N., McIntosh, J.R., 1996. Computer visualization of three-
659 dimensional image data using IMOD. *J. Struct. Biol.* 116**,** 71-76.
660 Krishnan-Kutty, V., Bigliardi, P.L., Dykas, M.M., Pomp, O., Kyaw, H.M., Poddar, K.,
661 Venkatesan, T., Bigliardi-Qi, M., 2017. Peripheral nerve fibres form multifacet
662 interactions with keratinocytes in a novel complete human 2D culture model. *Exp.*
663 *Dermatol.* 26**,** 281-284.
664 Kupari, J., Usoskin, D., Parisien, M., Lou, D., Hu, Y., Fatt, M., Lönnerberg, P., Spångberg, M.,
665 Eriksson, B., Barkas, N., 2021. Single cell transcriptomics of primate sensory neurons
666 identifies cell types associated with chronic pain. *Nat. Commun.* 12**,** 1-15.
667 Lacomis, D., 2002. Small-fiber neuropathy. *Muscle Nerve* 26**,** 173-188.
668 Lin, C.-H., Chao, C.-C., Wu, S.-W., Hsieh, P.-C., Feng, F.-P., Lin, Y.-H., Chen, Y.-M., Wu, R.-
669 M., Hsieh, S.-T., 2016. Pathophysiology of small-fiber sensory system in Parkinson's
670 disease: skin innervation and contact heat evoked potential. *Medicine (Baltimore)* 95.
671 Lumpkin, E.A., Caterina, M.J., 2007. Mechanisms of sensory transduction in the skin. *Nature*
672 445**,** 858.
673 Mandadi, S., Sokabe, T., Shibasaki, K., Katanosaka, K., Mizuno, A., Moqrich, A., Patapoutian,
674 A., Fukumi-Tominaga, T., Mizumura, K., Tominaga, M., 2009. TRPV3 in keratinocytes
675 transmits temperature information to sensory neurons via ATP. *Pflugers. Arch.* 458**,** 1093-
676 1102.

677 Markert, S.M., Bauer, V., Muenz, T.S., Jones, N.G., Helmprobst, F., Britz, S., Sauer, M., Rössler,
678 W., Engstler, M., Stigloher, C. 2017. 3D subcellular localization with superresolution
679 array tomography on ultrathin sections of various species. In: *Methods Cell Biol.* pp. 21-
680 47. Elsevier.
681 Markert, S.M., Britz, S., Proppert, S., Lang, M., Witvliet, D., Mulcahy, B., Sauer, M., Zhen, M.,
682 Bessereau, J.-L., Stigloher, C., 2016. Filling the gap: adding super-resolution to array
683 tomography for correlated ultrastructural and molecular identification of electrical
684 synapses at the C. elegans connectome. *Neurophotonics* 3**,** 041802.
685 Martin, P.E., Easton, J.A., Hodgins, M.B., Wright, C.S., 2014. Connexins: sensors of epidermal
686 integrity that are therapeutic targets. *FEBS Lett.* 588**,** 1304-1314.
687 Maruyama, K., Takayama, Y., Sugisawa, E., Yamanoi, Y., Yokawa, T., Kondo, T., Ishibashi, K.-
688 i., Sahoo, B.R., Takemura, N., Mori, Y., 2018. The ATP transporter VNUT mediates
689 induction of Dectin-1-triggered Candida nociception. *iScience* 6**,** 306-318.
690 Moehring, F., Cowie, A.M., Menzel, A.D., Weyer, A.D., Grzybowski, M., Arzua, T., Geurts,
691 A.M., Palygin, O., Stucky, C.L., 2018. Keratinocytes mediate innocuous and noxious
692 touch via ATP-P2X4 signaling. *eLife* 7.
693 Nolano, M., Provitera, V., Estraneo, A., Selim, M.M., Caporaso, G., Stancanelli, A.,
694 Saltalamacchia, A.M., Lanzillo, B., Santoro, L., 2008. Sensory deficit in Parkinson's
695 disease: evidence of a cutaneous denervation. *Brain* 131**,** 1903-1911.
696 O'Brien, G.S., Rieger, S., Wang, F., Smolen, G.A., Gonzalez, R.E., Buchanan, J., Sagasti, A.,
697 2012. Coordinate development of skin cells and cutaneous sensory axons in zebrafish. *J.*
698 *Comp. Neurol.* 520**,** 816-831.
699 Pang, Z., Sakamoto, T., Tiwari, V., Kim, Y.S., Yang, F., Dong, X., Guler, A.D., Guan, Y.,
700 Caterina, M.J., 2015. Selective keratinocyte stimulation is sufficient to evoke nociception
701 in mice. *Pain* 156**,** 656-665.
702 Pittenger, G.L., Mehrabyan, A., Simmons, K., Dublin, C., Barlow, P., Vinik, A.I., 2005. Small
703 fiber neuropathy is associated with the metabolic syndrome. *Metab. Syndr. Relat. Disord.*
704 3**,** 113-121.
705 Reynolds, E.S., 1963. The use of lead citrate at high pH as an electron-opaque stain in electron
706 microscopy. *J. Cell Biol.* 17**,** 208-212.
707 Sadler, K.E., Moehring, F., Stucky, C.L., 2020. Keratinocytes contribute to normal cold and heat
708 sensation. *eLife* 9**,** e58625.
709 Schindelin, J., Arganda-Carreras, I., Frise, E., Kaynig, V., Longair, M., Pietzsch, T., Preibisch,
710 S., Rueden, C., Saalfeld, S., Schmid, B., 2012. Fiji: an open-source platform for
711 biological-image analysis. *Nature methods* 9**,** 676-682.
712 Shiers, S., Klein, R.M., Price, T.J., 2020. Quantitative differences in neuronal subpopulations
713 between mouse and human dorsal root ganglia demonstrated with RNAscope in situ
714 hybridization. *Pain* 161**,** 2410-2424.
715 Sondersorg, A.C., Busse, D., Kyereme, J., Rothermel, M., Neufang, G., Gisselmann, G., Hatt, H.,
716 Conrad, H., 2014. Chemosensory information processing between keratinocytes and
717 trigeminal neurons. *J. Biol. Chem.* 289**,** 17529-17540.
718 Stucky, C.L., Mikesell, A.R., 2021. Cutaneous pain in disorders affecting peripheral nerves.
719 *Neurosci. Lett.* 765**,** 136233.
720 Taki, T., Takeichi, T., Sugiura, K., Akiyama, M., 2018. Roles of aberrant hemichannel activities
721 due to mutant connexin26 in the pathogenesis of KID syndrome. *Sci. Rep.* 8**,** 1-11.

722 Talagas, M., Lebonvallet, N., Leschiera, R., Elies, P., Marcorelles, P., Misery, L., 2020a. Intra-
723 epidermal nerve endings progress within keratinocyte cytoplasmic tunnels in normal
724 human skin. *Exp. Dermatol.* 29**,** 387-392.
725 Talagas, M., Lebonvallet, N., Leschiera, R., Marcorelles, P., Misery, L., 2017. What about
726 physical contacts between epidermal keratinocytes and sensory neurons? *Exp. Dermatol.*
727 27**,** 9-13.
728 Talagas, M., Lebonvallet, N., Leschiera, R., Sinquin, G., Elies, P., Haftek, M., Pennec, J.P.,
729 Ressnikoff, D., La Padula, V., Le Garrec, R., 2020b. Keratinocytes Communicate with
730 Sensory Neurons via Synaptic-like Contacts. *Ann. Neurol.* 88**,** 1205-1219.
731 Thévenaz, P., Unser, M., 2007. User-friendly semiautomated assembly of accurate image
732 mosaics in microscopy. *Microsc. Res. Tech.* 70**,** 135-146.
733 Tillberg, P.W., Chen, F., Piatkevich, K.D., Zhao, Y., Yu, C.-C.J., English, B.P., Gao, L.,
734 Martorell, A., Suk, H.-J., Yoshida, F., DeGennaro, E.M., Roossien, D.H., Gong, G.,
735 Seneviratne, U., Tannenbaum, S.R., Desimone, R., Cai, D., Boyden, E.S., 2016. Protein-
736 retention expansion microscopy of cells and tissues labeled using standard fluorescent
737 proteins and antibodies. *Nat. Biotechnol.* 34**,** 987-992.
738 Tong, Y.G., Wang, H.F., Ju, G., Grant, G., Hökfelt, T., Zhang, X., 1999. Increased uptake and
739 transport of cholera toxin B-subunit in dorsal root ganglion neurons after peripheral
740 axotomy: Possible implications for sensory sprouting. *J. Comp. Neurol.* 404**,** 143-158.
741 Tsutsumi, M., Inoue, K., Denda, S., Ikeyama, K., Goto, M., Denda, M., 2009. Mechanical-
742 stimulation-evoked calcium waves in proliferating and differentiated human
743 keratinocytes. *Cell Tissue Res.* 338**,** 99-106.
744 Üçeyler, N., 2016. Small fiber pathology—a culprit for many painful disorders? *Pain* 157**,** S60-
745 S66.
746 Üçeyler, N., Kafke, W., Riediger, N., He, L., Necula, G., Toyka, K., Sommer, C., 2010. Elevated
747 proinflammatory cytokine expression in affected skin in small fiber neuropathy.
748 *Neurology* 74**,** 1806-1813.
749 Üçeyler, N., Zeller, D., Kahn, A.-K., Kewenig, S., Kittel-Schneider, S., Schmid, A., Casanova-
750 Molla, J., Reiners, K., Sommer, C., 2013. Small fibre pathology in patients with
751 fibromyalgia syndrome. *Brain* 136**,** 1857-1867.
752 Vinik, A., Erbas, T., Stansberry, K., Pittenger, G., 2001. Small fiber neuropathy and
753 neurovascular disturbances in diabetes mellitus. *Exp. Clin. Endocrinol. Diabetes* 109**,**
754 S451-S473.
755 Watt, F.M., 1983. Involucrin and other markers of keratinocyte terminal differentiation. *J. Invest.*
756 *Dermatol.* 81**,** S100-S103.
757 Weber, P.A., Chang, H.-C., Spaeth, K.E., Nitsche, J.M., Nicholson, B.J., 2004. The permeability
758 of gap junction channels to probes of different size is dependent on connexin composition
759 and permeant-pore affinities. *Biophys. J.* 87**,** 958-973.
760 Weis, J., Katona, I., Müller-Newen, G., Sommer, C., Necula, G., Hendrich, C., Ludolph, A.C.,
761 Sperfeld, A.-D., 2011. Small-fiber neuropathy in patients with ALS. *Neurology* 76**,** 2024-
762 2029.
763 Zhao, Y., Bucur, O., Irshad, H., Chen, F., Weins, A., Stancu, A.L., Oh, E.-Y., DiStasio, M.,
764 Torous, V., Glass, B., 2017. Nanoscale imaging of clinical specimens using pathology-
765 optimized expansion microscopy. *Nat. Biotechnol.* 35**,** 757.

766

767

768 **Supplementary Information**

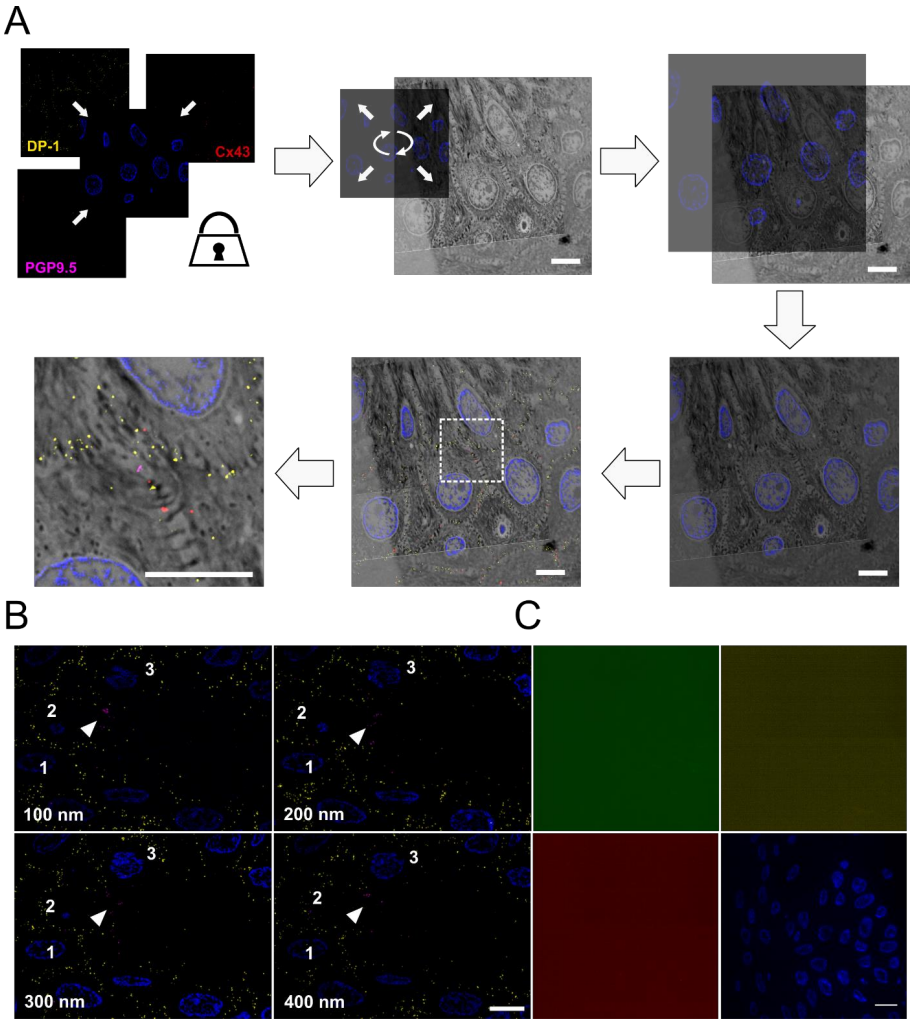

769

770 **Figure supplement 1:** CLEM principle and labeling verification. **(A)** Principle of unbiased

771 correlation using intrinsic landmarks. IF channels are locked and hidden behind nuclear DAPI

772 signal, which is used as only visible fluorescent channel, applied as landmark channel (blue).

773 DAPI signal and SEM nucleus texture are used to achieve unbiased correlation of IF and SEM

774 information. After optimization of the correlation, the channels of interest are made visible,
775 overlaid and regions of interest selected. No further changes of image locations were applied
776 afterwards. IF signal specificity. (B) Four consecutive tissue sections with nuclear DAPI (blue),
777 DP-1 (yellow), and PGP9.5 (magenta) labeling showing traceable persistent labeling. Arrowhead
778 indicates PGP9.5 positive nerve fiber and numbers show position of respective nuclei. Nucleus
779 number 2 is ceasing within the z-stack. Scale bar 5 µm. (C) Application of secondary antibodies
780 Al488-anti mouse (green), SeTau-647-anti rabbit (yellow), and Cy3-anti guinea pig (red) alone
781 showed no fluorescent signal. DAPI signal (blue) for orientation. Scale bar 10 µm.
782 Abbreviations: Al488, Alexa Fluor 488; Cy3, cyanine 3; DAPI, 4',6-diamidino-2-phenylindole ;
783 DP-1, desmoplakin 1; IF, immunofluorescence, PGP9.5, protein product 9.5 SEM, scanning
784 electron microscopy.
785

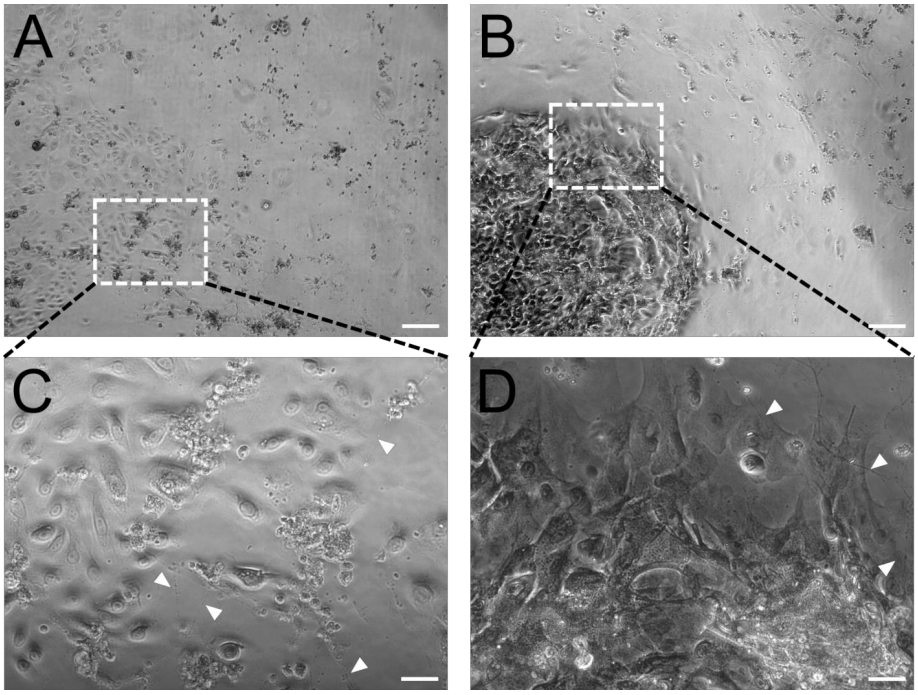

Figure supplement 2. Comparison of co-culture dependent on media condition. Overview of contrast imaged co-culture in keratinocyte medium (A) and conditioned neuronal medium (B) imaged with 5x objective. Insets represent enlarged areas in C and D at 20x objective. Single keratinocytes show basal or early differentiated state in keratinocyte medium (C), whereas differentiated and aggregated keratinocytes are predominant in conditioned neuronal medium (D) Arrowheads indicate passing neurites. Scale bars: 200 µm (A, B) and 50 µm (C, D).

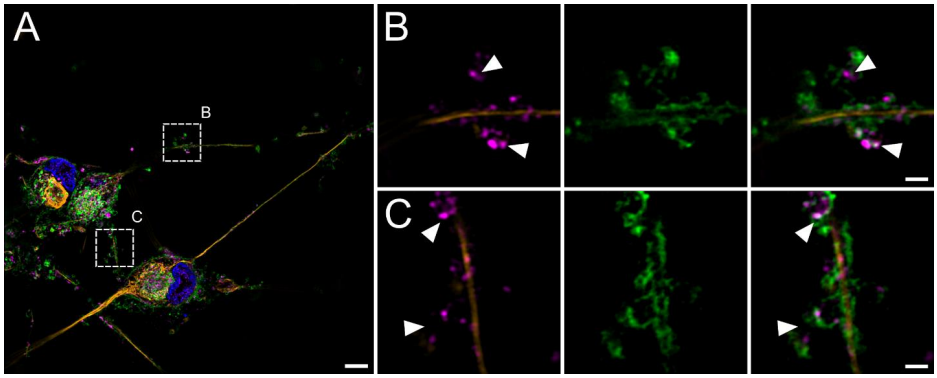

Figure supplement 3. Neurite outline and synaptic vesicular SYP localization. (A) Overview images of neuronal culture with DAPI (blue), Ctx (green), pan-NF (yellow), and SYP (magenta). Insets indicate enlarged areas in B and C. (B, C). First panel shows overlay of neurofilament marker pan-NF and SYP with apparent extra neuronal SYP accumulations (indicated via arrowheads). Second panel shows neurite membrane marker Ctx. Last panel depicts overlay, revealing SYP signal located within the outline of neurites. Scale bars: 5 µm (A), 1 µm (B, C). Abbreviations: Ctx, cholera toxin subunit B; DAPI, 4',6-diamidino-2-phenylindole, pan-NF, pan-neurofilament; SIM, structured illumination microscopy; SYP, synaptophysin.

Video 1: srAT with serial 100 nm sections with two frames per second. PGP9.5 (magenta) marks IENF ensheated in keratinocytes. Scale bar 5 µm. Abbreviations: IENF, intraepidermal nerve fiber; PGP9.5, protein product 9.5; srAT super-resolution array tomography.

Video 2. srAT with serial 100 nm SEM sections and 3D interpolation of keratinocyte nuclei (blue), keratinocyte cell bodies (yellow-orange), and IENF (magenta). Four sections per second.

Scale bar 5 µm. Abbreviations: IENF, intraepidermal nerve fiber; SEM, scanning electron microscopy; srAT super-resolution array tomography.

Video 3. Ensheathment and Cx43 plaque in expanded human epidermis. Magnification with filled arrowhead indicating part of an IENF, labeled via PGP9.5 (magenta), tunneling through a keratinocyte, labeled via phalloidin (grey). Additional hollow arrowhead showing a Cx43 plaque in contact with IENF. Physical 1.2 µm stack step size, translating to 276 nm biological step size. Framerate of two planes per second. Expansion factor corrected scale bar 1µm. Abbreviations: Cx43, connexin 43; IENF, intraepidermal nerve fiber; PGP9.5, protein gene product-9.5.

Video 4. Live imaging of fully human sensory neuron-keratinocyte co-culture with neurite establishing contact to keratinocyte colony. Arrowheads indicate outgrowing neurite. Framerate of eight time points per second with 20 min intervals per time point. Scale bar 50 µm.

8. Discussion

Within the three presented chapters, we aimed to decipher systemic and local mechanisms in FMS and their relation towards SFP. Heterogeneity of FMS symptoms and severity likely reflect various genetic, epigenetic, or acquired "hits" (D'Agnelli et al., 2019, Van Houdenhove and Egle, 2004). This may lead to similar phenotypic representations grouped as FMS along a spectrum (Borchers and Gershwin, 2015). Together with the heterogeneity of patients, alterations in diagnostic criteria over time and between countries hamper drawing conclusions on FMS pathophysiology and identification of biomarkers.

Hence, it is crucial to investigate clinically well characterized patient cohorts and minimize heterogeneity within patients and methods. We investigated affected women via application of the latest diagnostic criteria and used stabilized whole blood. Observed miR changes were linked to the peripheral cholinergic system, which modulates a broad range of immune processes. Accordingly, IL6ST and BMPR2 gene expression was suppressed in FMS patients. Interestingly, no CholinomiR signature was found in female PD patients, indicating specificity for FMS. This finding is of relevance for therapeutic treatment options with amitriptyline as one of three off-label pharmaceutical treatment options used e.g. in Germany that acts as an anti-cholinergic agent (Schiltenwolf et al., 2017). Pathway prediction of miR FMS signature highlighted the FoxO signaling pathway as a promising component in FMS pathophysiology. Hsa-miR-182-5p, upregulated in our FMS cohort, is both a CholinomiR and a regulator of FoxO signaling pathway and its role needs to be further investigated.

There is increasing evidence for the involvement of inflammation and immune-related mechanisms in FMS (Coskun Benlidayi, 2019, Goebel et al., 2021), however its extent may vary greatly within patients and between subgroups (O'Mahony et al., 2021). It can be speculated that immune cell activity and e.g. cytokine profiles and release may also be altered in patient subgroups without primary (auto-) immune origin of etiology. In a broader context, the profound impact of external factors like stress on the immune system (Padgett and Glaser, 2003) and vice versa of the immune system on psychosomatic symptoms and resilience are already recognized (Ménard et al., 2017).

TRFs add a new layer to cell regulation in FMS by targeting RNA processing, e.g., splicing pathways. Candidate transcripts like tRF-20-40KK5Y93 may either complement or substitute miRs as potential biomarkers in FMS. However, correlation of clinical parameter showed little association with tRFs compared to miRs, linked with WPI, GCPS, and FMS impact severity in blood. SFP represented by IENFD and NPSI was not well reflected in these correlations.

The major drawback of our whole blood approach is the lack of "cellular resolution". It will be highly important to investigate small RNAs within immune cell subtypes to detangle the multilayered pathway changes within certain blood immune cell populations and to stratify FMS patients with and without potential autoimmune involvement. The inclusion of disease controls illustrated the necessity for more extensive evaluation of biomarker candidates. Combining several individual small RNAs should increase specify and sensitivity for FMS. Novel techniques for absolute transcript quantification, e.g. by digital PCR can further improve reproducibility and usability of biomarker candidates, since more robust and precise total copy numbers are obtained (Campomenosi et al., 2016).

Beside systemic blood, we pioneer by describing changes of small RNAs in keratinocytes of FMS patients. SFP is apparent on functional and morphological level in FMS, however, its origin remains unclear. Transcriptomic shifts in keratinocytes could be the result of impairments in other cell types like immune cells, or sensory neurons and their neurites themself. Here, cultivation of primary keratinocytes in monoculture prior to RNA extraction should limit the impact of other skin resident cells on the identified small RNA signature.

Epithelial cell function pathways were predicted to be modulated by both aberrant miR and tRF expression in FMS keratinocytes with genes regulating cell-cell contacts (adherens junctions, focal adhesion, cell adhesion molecules). While identified miRs correlated predominantly with WPI, tRF-40-86J8WPMN1E8Y7Z2R, and tRF-30-JZOYJE22RRN3 positively correlated with severity of IENF loss. Out of three tested small RNA targets only TGFB1 was altered with approximately 50% reduction of gene expression in FMS. Interestingly, TGFB1 orchestrates extracellular matrix (EM) formation and remodeling, together with keratinocyte migration (Barrientos et al., 2008). Consequential shifts of the epidermal milieu could influence IENF function and innervation.

We further investigated cellular interactions between IENF and keratinocytes within the epidermis. Therefore, we applied super-resolution microscopy techniques, namely srAT and ExM in skin tissue sections and lattice SIM in a fully human co-culture model. This allowed

visualization of fibers and keratinocytes at ultrastructural resolution. We confirmed IENF ensheathment and discovered Cx43 plaques at the human neuro-cutaneous unit (NCU). In model organisms, initiation of ensheathment by neurites was shown and genetic ablation impaired normal sensory perceiption (Jiang et al., 2019). Recently, the impact of neurites on reorganizing epithelial membranes and intercellular contacts was highlighted (Rosa et al., 2021). This indicates that sensory nerve endings might be actively utilizing epidermal keratinocytes for anchoring, protection, and sensory perception. Aberrations of keratinocyte cell contacts and changes in the ECM may perturbate these processes. The ratio of ensheathment and frequency of Cx43 contacts need to be further investigated in clinical tissue sections to establish normative values and compare these in diseases with SFP. FMS patient subgroups comprising functional or morphological impairments of small fibers and presenting cutaneous pain are a promising cohort to assess these parameter. To link morphological findings with molecular and cellular processes siRNA injections mimicking the identified miRs and tRF might be used in keratinocyte-iPSC neuron CoC. Thereby, conclusions on whether small RNA deregulation represents a causal or at least contribution factor, in SFP, neurite ensheathment, and signal transduction at the NCU could be drawn.

It will be equally important to substantiate our morphological observation with functional assessments e.g. via dynamic live imaging experiments. Dye loading of keratinocytes in our CoC would, indicate, if direct small molecule transfer through Cx43 gap junction pores takes place (Meşe et al., 2007). Keratinocyte-specific stimulation, e.g., via the PIEZO1 agonist YODA1 or mechanical picking and simultaneous calcium imaging may help to unravel the effect on nociceptor sensitization and activation (Moehring et al., 2020, Shindo et al., 2021). Inclusion of hemichannel and gap junction inhibitors may help to further pin down exact release mechanisms (Sondersorg et al., 2014).

Taken together, we show systemic (whole blood) and peripheral (keratinocyte) alterations in small RNA levels of female FMS patients. Systemically, small RNAs were predicted to modulate immune pathways. In keratinocytes, cell-cell interactions might be altered via small RNA regulation of cell adherens and adhesion pathways. Since keratinocytes and IENF tightly interact at the NCU, these pathways may have a significant impact on SFP and cutaneous nociception. We propose two aspects of the NCU, namely ensheathment and Cx43 plaques, whose pathological role for SFP and nociceptive signaling in the skin needs to be assessed in more detail.

9. References

ABLIN, J. N., AMITAL, H., EHRENFELD, M., ALOUSH, V., ELKAYAM, O., LANGEVITZ, P., MEVORACH, D., MADER, R., SACHAR, T. & AMITAL, D. 2013. Guidelines for the diagnosis and treatment of the fibromyalgia syndrome. *Harefuah,* 152**,** 742-7, 751, 750.

ANNEMANS, L., LE LAY, K. & TAIEB, C. 2009. Societal and patient burden of fibromyalgia syndrome. *Pharmacoeconomics,* 27**,** 547-559.

ARIKAWA, E., SUN, Y., WANG, J., ZHOU, Q., NING, B., DIAL, S. L., GUO, L. & YANG, J. 2008. Cross-platform comparison of SYBR Green real-time PCR with TaqMan PCR, microarrays and other gene expression measurement technologies evaluated in the MicroArray Quality Control (MAQC) study. *BMC Genom.,* 9**,** 328.

ASTER, H. C., EVDOKIMOV, D., BRAUN, A., ÜÇEYLER, N., KAMPF, T., PHAM, M., HOMOLA, G. A. & SOMMER, C. 2022. CNS imaging characteristics in fibromyalgia patients with and without peripheral nerve involvement. *Sci. Rep.,* 12**,** 6707.

BAECHLER, E., BATLIWALLA, F., KARYPIS, G., GAFFNEY, P., MOSER, K., ORTMANN, W., ESPE, K., BALASUBRAMANIAN, S., HUGHES, K. & CHAN, J. 2004. Expression levels for many genes in human peripheral blood cells are highly sensitive to ex vivo incubation. *Genes Immun.,* 5**,** 347-353.

BANDAK, E., AMRIS, K., BLIDDAL, H., DANNESKIOLD-SAMSØE, B. & HENRIKSEN, M. 2013. Muscle fatigue in fibromyalgia is in the brain, not in the muscles: a case–control study of perceived versus objective muscle fatigue. *Ann. Rheum. Dis.,* 72**,** 963-966.

BANFI, G., DIANI, M., PIGATTO, P. D. & REALI, E. 2020. T cell subpopulations in the physiopathology of fibromyalgia: evidence and perspectives. *Int. J. Mol. Sci.,* 21**,** 1186.

BARR, T. P., ALBRECHT, P. J., HOU, Q., MONGIN, A. A., STRICHARTZ, G. R. & RICE, F. L. 2013. Air-stimulated ATP release from keratinocytes occurs through connexin hemichannels. *PloS One,* 8**,** e56744.

BARRIENTOS, S., STOJADINOVIC, O., GOLINKO, M. S., BREM, H. & TOMIC-CANIC, M. 2008. Growth factors and cytokines in wound healing. *Wound Repair Regen.,* 16**,** 585-601.

BAUCH, H. & SCHAFFER, J. 2006. Optical sections by means of "structured illumination": background and application in fluorescence microscopy. *Photonik Int.,* 5**,** 86-88.

BAUMBAUER, K. M., DEBERRY, J. J., ADELMAN, P. C., MILLER, R. H., HACHISUKA, J., LEE, K. H., ROSS, S. E., KOERBER, H. R., DAVIS, B. M. & ALBERS, K. M. 2015. Keratinocytes can modulate and directly initiate nociceptive responses. *eLife,* 4.

BEGEMANN, I. & GALIC, M. 2016. Correlative light electron microscopy: connecting synaptic structure and function. *Front. Synaptic Neurosci.,* 8**,** 28.

BENLIDAYI, I. C. 2019. Role of inflammation in the pathogenesis and treatment of fibromyalgia. *Rheumatol. Int.,* 39**,** 781-791.

BEUTNER, E. H. 1961. Immunofluorescent staining: the fluorescent antibody method. *Bacteriol. Rev.,* 25**,** 49-76.

BORCHERS, A. T. & GERSHWIN, M. E. 2015. Fibromyalgia: a critical and comprehensive review. *Clin. Rev. Allergy Immunol.,* 49**,** 100-151.

BRANCO, J. C., BANNWARTH, B., FAILDE, I., ABELLO CARBONELL, J., BLOTMAN, F., SPAETH, M., SARAIVA, F., NACCI, F., THOMAS, E., CAUBÈRE, J. P., LE LAY, K., TAIEB, C. & MATUCCI-CERINIC, M. 2010. Prevalence of fibromyalgia: a survey in five European countries. *Semin. Arthritis Rheum.,* 39**,** 448-53.

BRANDTZAEG, P. 1998. The increasing power of immunohistochemistry and immunocytochemistry. *J. Immunol. Methods,* 216**,** 49-67.

BRAUN, A., EVDOKIMOV, D., FRANK, J., SOMMER, C. & ÜÇEYLER, N. 2020. MiR103a-3p and miR107 are related to adaptive coping in a cluster of fibromyalgia patients. *PLoS One,* 15**,** e0239286.

BRONNER, I. F., QUAIL, M. A., TURNER, D. J. & SWERDLOW, H. 2014. Improved Protocols for Illumina Sequencing. *Curr. Protoc. Hum. Genet.,* 80**,** 18.2.1-42.

BURCH, C. & STOCK, J. 1942. Phase-contrast microscopy. *J. Sci. Instrum.,* 19**,** 71.

BUSHATI, N. & COHEN, S. M. 2007. microRNA functions. *Annu. Rev. Cell Dev. Biol.,* 23**,** 175-205.

BUSKILA, D. & SARZI-PUTTINI, P. 2008. Fibromyalgia and autoimmune diseases: the pain behind autoimmunity. *Isr. Med. Assoc. J. .* 10**,** 77.

CAMPOMENOSI, P., GINI, E., NOONAN, D. M., POLI, A., D'ANTONA, P., ROTOLO, N., DOMINIONI, L. & IMPERATORI, A. 2016. A comparison between quantitative PCR and droplet digital PCR technologies for circulating microRNA quantification in human lung cancer. *BMC Biotechnol.,* 16**,** 1-10.

CERDÁ-OLMEDO, G., MENA-DURÁN, A. V., MONSALVE, V. & OLTRA, E. 2015. Identification of a MicroRNA Signature for the Diagnosis of Fibromyalgia. *PloS One,* 10**,** e0121903.

COHEN, H. 2017. Controversies and challenges in fibromyalgia: a review and a proposal. *Ther. Adv. Musculoskelet. Dis.,* 9**,** 115-127.

COSKUN BENLIDAYI, I. 2019. Role of inflammation in the pathogenesis and treatment of fibromyalgia. *Rheumatol. Int.,* 39**,** 781-791.

D'AGNELLI, S., ARENDT-NIELSEN, L., GERRA, M. C., ZATORRI, K., BOGGIANI, L., BACIARELLO, M. & BIGNAMI, E. 2019. Fibromyalgia: genetics and epigenetics insights may provide the basis for the development of diagnostic biomarkers. *Mol. Pain,* 15**,** 1744806918819944.

DENDA, M., NAKATANI, M., IKEYAMA, K., TSUTSUMI, M. & DENDA, S. 2007. Epidermal keratinocytes as the forefront of the sensory system. *Exp. Dermatol.,* 16**,** 157-61.

DEVIGILI, G., RINALDO, S., LOMBARDI, R., CAZZATO, D., MARCHI, M., SALVI, E., ELEOPRA, R. & LAURIA, G. 2019. Diagnostic criteria for small fibre neuropathy in clinical practice and research. *Brain,* 142**,** 3728-3736.

DEVIGILI, G., TUGNOLI, V., PENZA, P., CAMOZZI, F., LOMBARDI, R., MELLI, G., BROGLIO, L., GRANIERI, E. & LAURIA, G. 2008. The diagnostic criteria for small fibre neuropathy: from symptoms to neuropathology. *Brain,* 131**,** 1912-1925.

DUALE, N., LIPKIN, W. I., BRIESE, T., AAREM, J., RØNNINGEN, K. S., AAS, K. K., MAGNUS, P., HARBAK, K., SUSSER, E. & BRUNBORG, G. 2014. Long-term storage of blood RNA collected in RNA stabilizing Tempus tubes in a large biobank--evaluation of RNA quality and stability. *BMC Res. Notes,* 7**,** 633.

EGENOLF, N., MEYER ZU ALTENSCHILDESCHE, C., KREß, L., EGGERMANN, K., NAMER, B., GROSS, F., KLITSCH, A., MALZACHER, T., KAMPIK, D., MALIK, R. A., KURTH, I., SOMMER, C. & ÜÇEYLER, N. 2021. Diagnosing small fiber neuropathy in clinical practice: A deep phenotyping study. *Ther. Adv. Neurol. Disord.*

EICH, W., BÄR, K.-J., BERNATECK, M., BURGMER, M., DEXL, C., PETZKE, F., SOMMER, C., WINKELMANN, A. & HÄUSER, W. 2017. Definition, Klassifikation, klinische Diagnose und Prognose des Fibromyalgiesyndroms. *Der Schmerz,* 31**,** 231-238.

EVDOKIMOV, D., FRANK, J., KLITSCH, A., UNTERECKER, S., WARRINGS, B., SERRA, J., PAPAGIANNI, A., SAFFER, N., MEYER ZU ALTENSCHILDESCHE, C. & KAMPIK, D. 2019. Reduction of skin innervation is associated with a severe fibromyalgia phenotype. *Ann. Neurol.,* 86**,** 504-516.

EVDOKIMOV, D., KREß, L., DINKEL, P., FRANK, J., SOMMER, C. & ÜÇEYLER, N. 2020. Pain-associated mediators and axon pathfinders in fibromyalgia skin cells. *J. Rheumatol.,* 47**,** 140-148.

FAULKNER, E. L., THOMAS, S. G. & NEELY, R. K. 2020. An introduction to the methodology of expansion microscopy. *Int. J. Biochem. Cell Biol.,* 124**,** 105764.

FITZCHARLES, M.-A., STE-MARIE, P. A., GOLDENBERG, D. L., PEREIRA, J. X., ABBEY, S., CHOINIÈRE, M., KO, G., MOULIN, D. E., PANOPALIS, P. & PROULX, J. 2013. 2012 Canadian guidelines for the diagnosis and management of fibromyalgia syndrome: executive summary. *Pain Res. Manag.,* 18**,** 119-126.

GHASEMI, M. & RAJABALLY, Y. A. 2020. Small fiber neuropathy in unexpected clinical settings: a review. *Muscle Nerve,* 62**,** 167-175.

GIRALDEZ, M. D., SPENGLER, R. M., ETHERIDGE, A., GODOY, P. M., BARCZAK, A. J., SRINIVASAN, S., DE HOFF, P. L., TANRIVERDI, K., COURTRIGHT, A., LU, S., KHOORY, J., RUBIO, R., BAXTER, D., DRIEDONKS, T. A. P., BUERMANS, H. P. J., NOLTE-'T HOEN, E. N. M., JIANG, H., WANG, K., GHIRAN, I., WANG, Y. E., VAN KEUREN-JENSEN, K., FREEDMAN, J. E., WOODRUFF, P. G., LAURENT, L. C., ERLE, D. J., GALAS, D. J. & TEWARI, M. 2018. Comprehensive multi-center assessment of small RNA-seq methods for quantitative miRNA profiling. *Nat. Biotechnol.,* 36**,** 746-757.

GOEBEL, A., KROCK, E., GENTRY, C., ISRAEL, M. R., JURCZAK, A., URBINA, C. M., SANDOR, K., VASTANI, N., MAURER, M. & CUHADAR, U. 2021. Passive transfer of fibromyalgia symptoms from patients to mice. *J. Clin. Invest.,* 131.

GRAYSTON, R., CZANNER, G., ELHADD, K., GOEBEL, A., FRANK, B., ÜÇEYLER, N., MALIK, R. A. & ALAM, U. A systematic review and meta-analysis of the prevalence of small fiber pathology in fibromyalgia: Implications for a new paradigm in fibromyalgia etiopathogenesis. Semin. Arthritis Rheum., 2019. Elsevier, 933-940.

HÄUSER, W., ZIMMER, C., FELDE, E. & KÖLLNER, V. 2008. What are the key symptoms of fibromyalgia? Results of a survey of the German Fibromyalgia Association. *Schmerz (Berlin, Germany),* 22**,** 176-183.

HOMBACH, S. & KRETZ, M. 2016. Non-coding RNAs: classification, biology and functioning. *Non-coding RNAs in colorectal cancer***,** 3-17.

JIANG, N., RASMUSSEN, J. P., CLANTON, J. A., ROSENBERG, M. F., LUEDKE, K. P., CRONAN, M. R., PARKER, E. D., KIM, H.-J., VAUGHAN, J. C. & SAGASTI, A. 2019. A conserved morphogenetic mechanism for epidermal ensheathment of nociceptive sensory neurites. *eLife,* 8**,** e42455.

KARADAGLIĆ, D. & WILSON, T. 2008. Image formation in structured illumination wide-field fluorescence microscopy. *Micron,* 39**,** 808-818.

KARL, F., WUSSMANN, M., KRESS, L., MALZACHER, T., FEY, P., GROEBER-BECKER, F. & UCEYLER, N. 2019. Patient-derived in vitro skin models for investigation of small fiber pathology. *Ann. Clin. Transl. Neurol.,* 6**,** 1797-1806.

KIA, S. & CHOY, E. 2017. Update on treatment guideline in fibromyalgia syndrome with focus on pharmacology. *Biomedicines,* 5**,** 20.

KIM, M. E., SHRESTHA, B. R., BLAZESKI, R., MASON, C. A. & GRUEBER, W. B. 2012. Integrins establish dendrite-substrate relationships that promote dendritic self-avoidance and patterning in Drosophila sensory neurons. *Neuron,* 73**,** 79-91.

KOIZUMI, S., FUJISHITA, K., INOUE, K., SHIGEMOTO-MOGAMI, Y., TSUDA, M. & INOUE, K. 2004. Ca2+ waves in keratinocytes are transmitted to sensory neurons: the involvement of extracellular ATP and P2Y2 receptor activation. *Biochem. J.,* 380**,** 329-38.

KOROSCHETZ, J., REHM, S. E., GOCKEL, U., BROSZ, M., FREYNHAGEN, R., TÖLLE, T. R. & BARON, R. 2011. Fibromyalgia and neuropathic pain-differences and similarities. A comparison of 3057 patients with diabetic painful neuropathy and fibromyalgia. *BMC Neurol.,* 11**,** 1-8.

KÖTTER, I., NEUSCHELER, D., GÜNAYDIN, I., WERNET, D. & KLEIN, R. 2007. Is there a predisposition for the development of autoimmune diseases in patients with fibromyalgia? Retrospective analysis with long term follow-up. *Rheumatol. Int.,* 27**,** 1031-1039.

KRESS, L., HOFMANN, L., KLEIN, T., KLUG, K., SAFFER, N., SPITZEL, M., BAR, F., SOMMER, C., KARL, F. & UCEYLER, N. 2021. Differential impact of keratinocytes and fibroblasts on nociceptor degeneration and sensitization in small fiber neuropathy. *Pain,* 162**,** 1262-1272.

KRISHNA, S., RAGHAVAN, S., DASGUPTA, R. & PALAKODETI, D. 2021. tRNA-derived fragments (tRFs): establishing their turf in post-transcriptional gene regulation. *Cell. Mol. Life Sci.,* 78**,** 2607-2619.

KUZMENKOV, A. I. & VASSILEVSKI, A. A. 2018. Labelled animal toxins as selective molecular markers of ion channels: Applications in neurobiology and beyond. *Neurosci. Lett.,* 679**,** 15-23.

LACOMIS, D. 2002. Small-fiber neuropathy. *Muscle Nerve,* 26**,** 173-188.

LANGHORST, M. F., SCHAFFER, J. & GOETZE, B. 2009. Structure brings clarity: structured illumination microscopy in cell biology. *Biotechnol. J.,* 4**,** 858-865.

LAURIA, G., MERKIES, I. S. & FABER, C. G. 2012. Small fibre neuropathy. *Curr. Opin. Neurol.,* 25**,** 542-549.

LEE, R. C., FEINBAUM, R. L. & AMBROS, V. 1993. The C. elegans heterochronic gene lin-4 encodes small RNAs with antisense complementarity to lin-14. *cell,* 75**,** 843-854.

LICHTMAN, J. W. & CONCHELLO, J.-A. 2005. Fluorescence microscopy. *Nat. Methods,* 2**,** 910-919.

LIU, J., JENNINGS, S. F., TONG, W. & HONG, H. 2011. Next generation sequencing for profiling expression of miRNAs: technical progress and applications in drug development. *Journal of biomedical science and engineering,* 4**,** 666.

LOHER, P., TELONIS, A. G. & RIGOUTSOS, I. 2017. MINTmap: fast and exhaustive profiling of nuclear and mitochondrial tRNA fragments from short RNA-seq data. *Sci. Rep.,* 7**,** 1-20.

LU, M., ZHANG, Q., DENG, M., MIAO, J., GUO, Y., GAO, W. & CUI, Q. 2008. An analysis of human microRNA and disease associations. *PLoS One,* 3**,** e3420.

LUMPKIN, E. A. & CATERINA, M. J. 2007. Mechanisms of sensory transduction in the skin. *Nature,* 445**,** 858.

MANDADI, S., SOKABE, T., SHIBASAKI, K., KATANOSAKA, K., MIZUNO, A., MOQRICH, A., PATAPOUTIAN, A., FUKUMI-TOMINAGA, T., MIZUMURA, K. & TOMINAGA, M. 2009. TRPV3 in keratinocytes transmits temperature information to sensory neurons via ATP. *Pflugers. Arch.,* 458**,** 1093-1102.

MANGUS, L. M., RAO, D. B. & EBENEZER, G. J. 2020. Intraepidermal nerve fiber analysis in human patients and animal models of peripheral neuropathy: a comparative review. *Toxicol. Pathol.,* 48**,** 59-70.

MARKERT, S. M., BRITZ, S., PROPPERT, S., LANG, M., WITVLIET, D., MULCAHY, B., SAUER, M., ZHEN, M., BESSEREAU, J.-L. & STIGLOHER, C. 2016. Filling the gap: adding super-resolution to array tomography for correlated ultrastructural and molecular identification of electrical synapses at the C. elegans connectome. *Neurophotonics,* 3**,** 041802.

MARUYAMA, K., TAKAYAMA, Y., SUGISAWA, E., YAMANOI, Y., YOKAWA, T., KONDO, T., ISHIBASHI, K.-I., SAHOO, B. R., TAKEMURA, N. & MORI, Y. 2018. The ATP transporter VNUT mediates induction of Dectin-1-triggered Candida nociception. *iScience,* 6**,** 306-318.

MASOTTI, A., BALDASSARRE, A., GUZZO, M. P., IANNUCCELLI, C., BARBATO, C. & DI FRANCO, M. 2017. Circulating microRNA profiles as liquid biopsies for the characterization and diagnosis of fibromyalgia syndrome. *Mol. Neurobiol.,* 54**,** 7129-7136.

MAY, A. 2011. Structural brain imaging: a window into chronic pain. *Neuroscientist,* 17**,** 209-220.

MÉNARD, C., PFAU, M. L., HODES, G. E. & RUSSO, S. J. 2017. Immune and neuroendocrine mechanisms of stress vulnerability and resilience. *Neuropsychopharmacology,* 42**,** 62-80.

MERRIWETHER, E. N., AGALAVE, N. M., DAILEY, D. L., RAKEL, B. A., KOLKER, S. J., LENERT, M. E., SPAGNOLA, W. H., LU, Y., GEASLAND, K. M. & ALLEN, L.-A. H. 2021. IL-5 mediates monocyte phenotype and pain outcomes in fibromyalgia. *Pain,* 162**,** 1468-1482.

MEŞE, G., RICHARD, G. & WHITE, T. W. 2007. Gap junctions: basic structure and function. *J. Invest. Dermatol.,* 127**,** 2516-2524.

MICHEVA, K. D. & SMITH, S. J. 2007. Array tomography: a new tool for imaging the molecular architecture and ultrastructure of neural circuits. *Neuron,* 55**,** 25-36.

MOEHRING, F., COWIE, A. M., MENZEL, A. D., WEYER, A. D., GRZYBOWSKI, M., ARZUA, T., GEURTS, A. M., PALYGIN, O. & STUCKY, C. L. 2018. Keratinocytes mediate innocuous and noxious touch via ATP-P2X4 signaling. *eLife,* 7.

MOEHRING, F., MIKESELL, A. R., SADLER, K. E., MENZEL, A. D. & STUCKY, C. L. 2020. Piezo1 mediates keratinocyte mechanotransduction. *bioRxiv*.

MURALEETHARAN, D., FADICH, A., STEPHENSON, C. & GARNEY, W. 2018. Understanding the Impact of Fibromyalgia on Men: Findings From a Nationwide Survey. *Am. J. Men's Health.***,** 1557988317753242.

NORMAND, J. & KARASEK, M. A. 1995. A method for the isolation and serial propagation of keratinocytes, endothelial cells, and fibroblasts from a single punch biopsy of human skin. *In Vitro Cell. Dev. Biol. Anim.,* 31**,** 447-55.

O'BRIEN, G. S., RIEGER, S., WANG, F., SMOLEN, G. A., GONZALEZ, R. E., BUCHANAN, J. & SAGASTI, A. 2012. Coordinate development of skin cells and cutaneous sensory axons in zebrafish. *J. Comp. Neurol.,* 520**,** 816-831.

O'MAHONY, L. F., SRIVASTAVA, A., MEHTA, P. & CIURTIN, C. 2021. Is fibromyalgia associated with a unique cytokine profile? A systematic review and meta-analysis. *Rheumatology,* 60**,** 2602-2614.

OAKLANDER, A. L., HERZOG, Z. D., DOWNS, H. M. & KLEIN, M. M. 2013. Objective evidence that small-fiber polyneuropathy underlies some illnesses currently labeled as fibromyalgia. *Pain,* 154**,** 2310-6.

PADGETT, D. A. & GLASER, R. 2003. How stress influences the immune response. *Trends Immunol.,* 24**,** 444-448.

PAIVA, E. S., MARIANO DA COSTA, E. D. G. & SCHEINBERG, M. 2008. Fibromyalgia: an update and immunological aspects. *Curr. Pain Headache Rep.,* 12**,** 321-326.

PANG, Z., SAKAMOTO, T., TIWARI, V., KIM, Y. S., YANG, F., DONG, X., GULER, A. D., GUAN, Y. & CATERINA, M. J. 2015. Selective keratinocyte stimulation is sufficient to evoke nociception in mice. *Pain,* 156**,** 656-65.

PEDERSON, T. 2010. Regulatory RNAs derived from transfer RNA? *Rna,* 16**,** 1865-1869.

PERROT, S. 2012. If fibromyalgia did not exist, we should have invented it. A short history of a controversial syndrome. *Reumatismo,* 64**,** 186-193.

PFAFFL, M. W. 2007. Relative quantification. *Real-time PCR.* Taylor & Francis.

PODNAR, J., DEIDERICK, H., HUERTA, G. & HUNICKE-SMITH, S. 2014. Next-Generation Sequencing RNA-Seq Library Construction. *Curr. Protoc. Mol. Biol.,* 106**,** 4.21.1-19.

QUEIROZ, L. P. 2013. Worldwide epidemiology of fibromyalgia. *Curr. Pain Headache Rep.,* 17**,** 356.

ROSA, J. B., NASSMAN, K. Y. & SAGASTI, A. 2021. Sensory axons induce epithelial lipid microdomain remodeling and determine the distribution of junctions in the epidermis. *bioRxiv*.

RUSSELL, I. J. 1996. Neurochemical pathogenesis of fibromyalgia syndrome. *J. Musculoskelet. Pain,* 4**,** 61-92.

SADLER, K. E., MOEHRING, F. & STUCKY, C. L. 2020. Keratinocytes contribute to normal cold and heat sensation. *eLife,* 9**,** e58625.

SCHILTENWOLF, M., EIDMANN, U., KÖLLNER, V., KÜHN, T., OFFENBÄCHER, M., PETZKE, F., SARHOLZ, M., WEIGL, M., WOLF, B. & HÄUSER, W. 2017. Multimodale Therapie des Fibromyalgiesyndroms. *Der Schmerz,* 31**,** 285-288.

SCHMIDT-WILCKE, T. & DIERS, M. 2017. New insights into the pathophysiology and treatment of fibromyalgia. *Biomedicines,* 5**,** 22.

SCHWEINHARDT, P., SAURO, K. M. & BUSHNELL, M. C. 2008. Fibromyalgia: a disorder of the brain? *Neuroscientist,* 14**,** 415-421.

SERRA, J., COLLADO, A., SOLÀ, R., ANTONELLI, F., TORRES, X., SALGUEIRO, M., QUILES, C. & BOSTOCK, H. 2014. Hyperexcitable C nociceptors in fibromyalgia. *Ann. Neurol.,* 75**,** 196-208.

SHIGEMATSU, M., HONDA, S. & KIRINO, Y. 2014. Transfer RNA as a source of small functional RNA. *J. Mol. Biol. Mol. Imaging,* 1.

SHINDO, Y., FUJITA, K., TANAKA, M., FUJIO, H., HOTTA, K. & OKA, K. 2021. Mechanical stimulus-evoked signal transduction between keratinocytes and sensory neurons via extracellular ATP. *Biochem. Biophys. Res. Commun.,* 582**,** 131-136.

SIMMS, R. W. 1998. Fibromyalgia is not a muscle disorder. *Am. J. M. Sc.,* 315**,** 346-350.

SIMMS, R. W., ROY, S. H., HROVAT, M., ANDERSON, J. J., SKRINAR, G., LEPOOLE, S. R., ZERBINI, C. A., LUCA, C. D. & JOLESZ, F. 1994. Lack of association between fibromyalgia syndrome and abnormalities in muscle energy metabolism. *Arthritis Rheum.,* 37**,** 794-800.

SONDERSORG, A. C., BUSSE, D., KYEREME, J., ROTHERMEL, M., NEUFANG, G., GISSELMANN, G., HATT, H. & CONRAD, H. 2014. Chemosensory information processing between keratinocytes and trigeminal neurons. *J. Biol. Chem.,* 289**,** 17529-40.

SPAETH, M. 2009. Epidemiology, costs, and the economic burden of fibromyalgia. Arthritis Research and Therapy.

STUCKY, C. L. & MIKESELL, A. R. 2021. Cutaneous pain in disorders affecting peripheral nerves. *Neurosci. Lett.,* 765**,** 136233.

SU, Z., NING, B., FANG, H., HONG, H., PERKINS, R., TONG, W. & SHI, L. 2011. Next-generation sequencing and its applications in molecular diagnostics. *Expert Rev. Mol. Diagn.,* 11**,** 333-43.

SU, Z., WILSON, B., KUMAR, P. & DUTTA, A. 2020. Noncanonical roles of tRNAs: tRNA fragments and beyond. *Annu. Rev. Genet.,* 54**,** 47-69.

SUK, J., LEE, J. & KIM, J. 2012. Association between thyroid autoimmunity and fibromyalgia. *Exp. Clin. Endocrinol. Diabetes,* 120**,** 401-404.

SUNDERMANN, B., DEHGHAN NAYYERI, M., PFLEIDERER, B., STAHLBERG, K., JÜNKE, L., BAIE, L., DIECKMANN, R., LIEM, D., HAPPE, T. & BURGMER, M. 2019. Subtle changes of gray matter volume in fibromyalgia reflect chronic musculoskeletal pain rather than disease-specific effects. *Eur. J. Neurosci.,* 50**,** 3958-3967.

TALAGAS, M., LEBONVALLET, N., LESCHIERA, R., ELIES, P., MARCORELLES, P. & MISERY, L. 2020a. Intra-epidermal nerve endings progress within keratinocyte cytoplasmic tunnels in normal human skin. *Exp. Dermatol.,* 29**,** 387-392.

TALAGAS, M., LEBONVALLET, N., LESCHIERA, R., SINQUIN, G., ELIES, P., HAFTEK, M., PENNEC, J. P., RESSNIKOFF, D., LA PADULA, V. & LE GARREC, R. 2020b. Keratinocytes Communicate with Sensory Neurons via Synaptic-like Contacts. *Ann. Neurol.,* 88**,** 1205-1219.

ÜÇEYLER, N., HÄUSER, W. & SOMMER, C. 2011. Systematic review with meta-analysis: cytokines in fibromyalgia syndrome. *BMC Musculoskelet. Disord.,* 12**,** 245.

ÜÇEYLER, N., ZELLER, D., KAHN, A.-K., KEWENIG, S., KITTEL-SCHNEIDER, S., SCHMID, A., CASANOVA-MOLLA, J., REINERS, K. & SOMMER, C. 2013. Small fibre pathology in patients with fibromyalgia syndrome. *Brain,* 136**,** 1857-1867.

VAN HOUDENHOVE, B. & EGLE, U. T. 2004. Fibromyalgia: A stress disorder? *Psychother. Psychosom.,* 73**,** 267-275.

VANGUILDER, H. D., VRANA, K. E. & FREEMAN, W. M. 2008. Twenty-five years of quantitative PCR for gene expression analysis. *Biotechniques,* 44**,** 619-26.

VISHNOI, A. & RANI, S. 2017. MiRNA biogenesis and regulation of diseases: an overview. *MicroRNA Profiling***,** 1-10.

WANG, S.-M., HAN, C., LEE, S.-J., PATKAR, A. A., MASAND, P. S. & PAE, C.-U. 2015. Fibromyalgia diagnosis: a review of the past, present and future. *Expert Rev. Neurother.,* 15**,** 667-679.

WASSIE, A. T., ZHAO, Y. & BOYDEN, E. S. 2019. Expansion microscopy: principles and uses in biological research. *Nat. Methods,* 16**,** 33-41.

WINTER, J., JUNG, S., KELLER, S., GREGORY, R. I. & DIEDERICHS, S. 2009. Many roads to maturity: microRNA biogenesis pathways and their regulation. *Nat. Cell Biol.,* 11**,** 228-234.

WOLFE, F., CLAUW, D. J., FITZCHARLES, M.-A., GOLDENBERG, D. L., HÄUSER, W., KATZ, R. L., MEASE, P. J., RUSSELL, A. S., RUSSELL, I. J. & WALITT, B. 2016 Revisions to the 2010/2011 fibromyalgia diagnostic criteria. Semin. Arthritis Rheum., 2016. Elsevier, 319-329.

WOLFE, F., CLAUW, D. J., FITZCHARLES, M. A., GOLDENBERG, D. L., KATZ, R. S., MEASE, P., RUSSELL, A. S., RUSSELL, I. J., WINFIELD, J. B. & YUNUS, M. B. 2010. The American College of Rheumatology preliminary diagnostic criteria for fibromyalgia and measurement of symptom severity. *Arthritis Care Res.,* 62**,** 600-610.

WOLFE, F., SMYTHE, H. A., YUNUS, M. B., BENNETT, R. M., BOMBARDIER, C., GOLDENBERG, D. L., TUGWELL, P., CAMPBELL, S. M., ABELES, M. & CLARK, P. 1990. The American College of Rheumatology 1990 criteria for the classification of fibromyalgia. *Arthritis Rheum.,* 33**,** 160-172.

WU, Y. & SHROFF, H. 2018. Faster, sharper, and deeper: structured illumination microscopy for biological imaging. *Nat. Methods,* 15**,** 1011-1019.

10. Statement of individual author contributions and of legal second publication rights to manuscripts included in the dissertation

Manuscript 1 (complete reference): Erbacher, C., Vaknine, S., Moshitzky, G., Lobentanzer, S., Eisenberg, L., Evdokimov, D., Sommer, C., Greenberg, D.S., Soreq, H., Üçeyler, N. (2022). "Distinct CholinomiR Blood Cell Signature as a Potential Modulator of the Cholinergic System in Women with Fibromyalgia Syndrome." Cells 11(8): 1276.					
Participated in	Author Initials, Responsibility decreasing from left to right				
Study Design	N.Ü.	H.S.	D.S.G	C.S.	
Methods Development	C.E	S.V.	G.M.	D.S.G.	S.L.
Data Collection	C.E.	S.V.	G.M.	L.E.	
Data Analysis and Interpretation	C.E.	S.V.	G.M.	N.Ü.	H.S.
Manuscript Writing					
Writing of Introduction	C.E.	N.Ü.	H.S.		
Writing of Materials & Methods	C.E.	S.V.	N.Ü.	H.S.	
Writing of Discussion	C.E.	N.Ü.	H.S	S.V.	
Writing of First Draft	C.E.	S.V.	N.Ü.	H.S.	

Explanations (if applicable): All authors have read and agreed to the published version of the manuscript.

Manuscript 2 (complete reference): Erbacher, C., Madrer, N., Moshitzky, G., Weinbender, S., Prtvar, D., Evdokimov, D., Unterecker, S., Sommer, C., Greenberg, D.S., Soreq, H., Üçeyler, N (2022). “Systemic up- and peripheral downregulation of microRNAs and transfer RNA fragments in fibromyalgia syndrome”. In preparation					
Participated in	Author Initials, Responsibility decreasing from left to right				
Study Design	N.Ü.	H.S.	D.S.G	C.S.	
Methods Development	C.E	N.M.	G.M.	S.W.	D.S.G.
Data Collection	C.E.	G.M.	D.P.	S.W.	
Data Analysis and Interpretation	C.E.	N.M.	G.M.	N.Ü.	H.S.
Manuscript Writing					
Writing of Introduction	C.E.	N.Ü.			
Writing of Materials & Methods	C.E.	N.Ü.	N.M.		
Writing of Discussion	C.E.	N.Ü.			
Writing of First Draft	C.E.	N.Ü.			

Explanations (if applicable): All authors have read and agreed to the published version of the manuscript.

Manuscript 3 (complete reference): Erbacher, C., Britz, S., Dinkel, P., Klein, T., Sauer, M., Stigloher, C., Üçeyler, N. (2022). "Interaction of human keratinocytes and nerve fiber terminals at the neuro-cutaneous unit." bioRxiv. https://doi.org/10.1101/2022.02.23.481592					
Participated in	Author Initials, Responsibility decreasing from left to right				
Study Design	C.E.	N.Ü.	C.S.		
Methods Development	C.E.	S.B.	T.K.	P.D.	
Data Collection	C.E.				

Data Analysis and Interpretation	C.E.	N.Ü.	S.B.	C.S.	
Manuscript Writing					
Writing of Introduction	C.E.	N.Ü.			
Writing of Materials & Methods	C.E.	N.Ü.	S.B	C.S.	
Writing of Discussion	C.E.	N.Ü.	S.B.	C.S.	
Writing of First Draft	C.E.	N.Ü.			

Explanations (if applicable): All authors agreed to the current version of the manuscript.

If applicable, the doctoral researcher confirms that she/he has obtained permission from both the publishers (copyright) and the co-authors for legal second publication.

The doctoral researcher and the primary supervisor confirm the correctness of the above-mentioned assessment.

Christoph Erbacher

_____

Doctoral Researcher's Name Date Place Signature

Prof. Nurcan Üçeyler

_____

Primary Supervisor's Name Date Place Signature

11. Statement of individual author contributions to figures/tables of manuscripts included in the dissertation

Manuscript 1 (complete reference): Erbacher, C., Vaknine, S., Moshitzky, G., Lobentanzer, S., Eisenberg, L., Evdokimov, D., Sommer, C., Greenberg, D.S., Soreq, H., Üçeyler, N.

(2022). "Distinct CholinomiR Blood Cell Signature as a Potential Modulator of the Cholinergic System in Women with Fibromyalgia Syndrome." Cells 11(8): 1276.					
Figure	Author Initials, Responsibility decreasing from left to right				
1	C.E.	N.Ü.			
2	C.E.				
3	C.E.	S.V.			
4	C.E.	S.V.			
5	C.E.				
6	C.E.				
7	C.E.				
8	C.E.				
Table	Author Initials, Responsibility decreasing from left to right				
1	CE				
2	CE				

Explanations (if applicable):

Manuscript 2 (complete reference): Erbacher, C., Madrer, N., Moshitzky, G., Weinbender, S., Prtvar, D., Evdokimov, D., Unterecker, S., Sommer, C., Greenberg, D.S., Soreq, H., Üçeyler, N (2022). “Systemic up- and peripheral downregulation of microRNAs and transfer RNA fragments in fibromyalgia syndrome”. In preparation

Figure	Author Initials, Responsibility decreasing from left to right				
1	N.M.	C.E.			
2	C.E.				
3	C.E.				
4	N.M.	C.E.			
5	C.E.				
6	C.E.				
7	C.E.				
Table	Author Initials, Responsibility decreasing from left to right				
1	C.E.				
2	C.E.				
3	C.E.				
4	C.E.	N.Ü.			

Explanations (if applicable):

Manuscript 3 (complete reference): Erbacher, C., Britz, S., Dinkel, P., Klein, T., Sauer, M., Stigloher, C., Üçeyler, N. (2022). "Interaction of human keratinocytes and nerve fiber terminals at the neuro-cutaneous unit." bioRxiv. https://doi.org/10.1101/2022.02.23.481592

Figure	Author Initials, Responsibility decreasing from left to right				
1	C.E.	S.B.			
2	C.E.				
3	C.E.				
4	C.E.				
5	C.E.				
6	C.E.				
7	C.E.				
8	C.E.				
9	C.E.	N.Ü.			
S1	C.E				
S2	C.E				
S3	C.E				
Table	Author Initials, Responsibility decreasing from left to right				
1	C.E.				

Explanations (if applicable):

I also confirm my primary supervisor's acceptance.

Doctoral Researcher's Name Date Place Signature

12. Curriculum vitae

13. Publications

Peer reviewed journals; original articles:

Erbacher, C., Vaknine, S., Moshitzky, G., Lobentanzer, S., Eisenberg, L., Evdokimov, D., Sommer, C., Greenberg, D.S., Soreq, H., Üçeyler, N. Distinct CholinomiR Blood Cell Signature as a Potential Modulator of the Cholinergic System in Women with Fibromyalgia Syndrome. Cells 2022, 11, 1276. https://doi.org/10.3390/cells11081276

Seifert, R., Markert, S. M., Britz, S., Perschin, V., Erbacher, C., Stigloher, C., Kollmannsberger, P. (2020). DeepCLEM: automated registration for correlative light and electron microscopy using deep learning. *F1000Research*, *9*(1275), 1275.

Thölken, C., Thamm, M., Erbacher, C. Lechner, M. 2019. Sequence and structural properties of circular RNAs in the brain of nurse and forager honeybees (Apis mellifera). BMC Genom., 20, 88.

Preprints:

Erbacher, C., Britz, S., Dinkel, P., Klein, T., Sauer, M., Stigloher, C., Üçeyler, N. (2022). Interaction of human keratinocytes and nerve fiber terminals at the neuro-cutaneous unit. bioRxiv.

Poster presentations at international conferences:

Erbacher, C., Birklein, F., Üçeyler, N. (2018). Studying the role of potential pain mediator within the skin of fibromyalgia patients. 13th International GSLS Student Symposium (EUREKA!)

Erbacher, C., Dinkel, P., Gentschev, A., Britz, S., Stigloher, C., Üçeyler, N. (2019). Correlative light and electron microscopy (CLEM) for investigating keratinocyte-nerve fiber contact zones in human skin. 13th Göttingen Meeting of the German Neuroscience Society.

Erbacher C., Moshitzky, G., Sommer, C., Greenberg, D.S., Soreq, H., Üçeyler N. (2019). Investigating cholinergic contributions to the fibromyalgia syndrome. XVIth International Symposium on Cholinergic Mechanisms.

Erbacher C., Moshitzky, G., Greenberg, D.S., Sommer, C., Soreq, H., Üçeyler N. (2021). Tracing small RNA Signatures in Fibromyalgia Syndrome. EMBL Symposium: The Non-Coding Genome.

Erbacher, C., Diesendorf, V., Klein, T., Üçeyler, N. (2022). A fully human sensory neuron – keratinocyte co-culture model for investigating the neuro-cutaneous unit. Clinical Neurophysiology, 137, e49.

14. Danksagung

Ich will mich herzlich bei allen, die mich bis hierher begleitet und unterstützt haben bedanken! Insbesondere gilt mein Dank:
Prof. Nurcan Üçeyler für die Möglichkeit meine Doktorarbeit in ihrer Arbeitsgruppe zu diesem Thema schreiben zu dürfen. Es waren sehr prägende Jahre, in denen ich viel gelernt habe. Ich bedanke mich vor allem die Freiheit eigene Fragen und Methoden einzubringen, das große Vertrauen, und ihre Geduld.
Meinen BetreuerInnen Prof. Christian Wegener, Prof. Christian Stigloher, und Prof. Claudia Sommer im Promotionskomitee für die produktiven Diskussionen. Ein zusätzlicher Dank gilt Prof. Christian Stigloher, der mich in die Welt der höchstauflösenden Mikroskopie eingeführt hat und stets eine offene Labortüre für mich und meine Proben hatte.
Meinen Büro- und DoktorandenkollegInnen Maximilian Breyer, Julia Grüner, Katharina Klug, Patricia Garcia Fernandez, Luisa Kreß, und Nicole Schottmann und ehemaligen KollegInnen Thomas Klein, Franziska Karl-Schöller, Dimitar Evdokimov, und Lukas Hofmann für die tolle Arbeitsatmosphäre und moralische und wissenschaftliche Hilfe. Das gilt auch für alle weiteren Mitstreiter in „Schmackofatz“ und „Escalated“.
Den von mir mitbetreuten StudentInnen Philine Dinkel, Alexandra Gentschev, Dorothea Tsounis, Danilo Prtvar, und Sophia Weinbender, bei denen ich die Ehre und das Vergnügen hatte, sie ein Stück auf ihren wissenschaftlichen Weg zu begleiten. Ich hoffe ich konnte ein wenig Wissen weitergeben und ihre Neugier für die Wissenschaft stärken.
Allen TAs der AG Üçeyler/AG Sommer/AG Stigloher, die mich in viele Methoden eingeführt haben und mir im Laboralltag geholfen haben, insbesondere Daniela Urlaub für Ihre Hilfe bei den Zellkulturen und qRT-PCRs.
Unseren Kooperationspartnern, für die Bereitstellung ihrer Expertise, Geräte, und die bereichernden Diskussionen. Vor allem möchte ich mich bei Frau Prof. Hermona Soreq bedanken, die mich virtuell und physisch bei meinem Laborbesuch 2019 sehr herzlich in ihre AG aufgenommen hat. Ihren Doktoranden Gilli Moshitzky, Shani Vakine, und Nimrod Madrer gilt ein großer Dank für die Unterstützung. Sebastian Britz aus der AG Stigloher danke ich aus dem gleichen Grund.
Nicht zuletzt, sondern vor allem meiner Familie. Ohne eure Unterstützung, Fürsorge, und Verständnis wäre mein Weg bis hin zur Doktorarbeit nicht möglich gewesen! Und meinen Freunden, ohne deren Rückhalt und Unterstützung dieser Weg nicht so schön und erträglich gewesen wäre.